Superimposed training for channel estimation in next-generation wireless multicarrier techniques

by

Juan Carlos Estrada Jiménez

A dissertation submitted by in partial fulfillment of the requirements for the degree of Doctor of Philosophy in

Multimedia and Communications interuniversity program

Universidad Carlos III de Madrid

Advisor:

María Julia Fernández-Getino García

November, 2019

This thesis is distributed under license "Creative Commons **Attribution - Non Commercial - Non Derivatives**".

Dedico este trabajo en especial a mis padres Antonio y Laura, a mi abuela Celia, a mis hermanos José, María y Luis, y a Diana por estar siempre a mi lado.

Agradecimientos

A mi familia por sus consejos y soporte con los que, a lo largo de los años, he logrado formarme.

A Dianita, quien ha sido mi compañera en esta aventura.

A Julia, mi tutora, quien con una increíble paciencia ha sabido guiarme en este periodo de aprendizaje.

A mis compañeros y amigos de despacho, Borja, Kun, Estefanía, Alejandro, Gema, Alberto, quienes con sus comentarios y discusiones contribuyeron para la finalización de este proyecto.

A Ana y Víctor por sus contribuciones a través de ideas y propuestas que ayudaron a conseguir los objetivos de esta tesis.

Finalmente, y no menos importante, quiero expresar mi especial agradecimiento al programa de becas de la Secretaría de Educación Superior Ciencia, Tecnología e Innovación (SENESCYT) y al Instituto de Fomento al Talento Humano (IFTH) del Ecuador, quienes a través del programa de Becas "Convocatoria Abierta 2013" ayudaron a la financiación de este proyecto.

0.1 Published and submitted content

Conferences

- J. C. Estrada Jiménez, B. Genovés Guzmán, M. Julia Fernández-Getino García and V. P. Gil Jiménez, "Superimposed training-based channel estimation for Visible Light Communications," 2017 13th International Wireless Communications and Mobile Computing Conference (IWCMC), Valencia, 2017, pp. 240-245. doi: 10.1109/IWCMC.2017.7986293. It is partially included in the chapter 5 of the thesis. The material from this source included in the thesis is not singled out with typographic means and references.

- K. Chen-Hu, J. C. Estrada-Jiménez, M. Julia Fernández-Getino García and A. García Armada, "Superimposed Training for Channel Estimation in FBMC-OQAM," 2017 IEEE 86th Vehicular Technology Conference (VTC-Fall), Toronto, ON, 2017, pp. 1-5, *Invited paper*. doi: 10.1109/VTCFall.2017.8287938. It is partially included in the chapter 4 of the thesis. The material from this source included in the thesis is not singled out with typographic means and references.

- J. C. Estrada-Jiménez, B. Genovés Guzmán, M. Julia Fernández-Getino García, V. P. Gil Jiménez, "Comparativa de técnicas de estimación de canal para VLC en interiores," 2018, Proc. of XXXII Simposio de la Unión Científica de Radio (URSI), Granada, Spain, Sept. 2018. It is partially included in the chapter 5 of the thesis. The material from this source included in the thesis is not singled out with typographic means and references.

Journals

- J. C. Estrada-Jiménez and M. Julia Fernández-Getino García, "Partial-Data Superimposed Training With Data Precoding for OFDM Systems," in IEEE Transactions on Broadcasting, vol. 65, no. 2, pp. 234-244, June 2019. doi: 10.1109/TBC.2018.2874542. It is totally included in the chapter 3 of the thesis. The material from this source included in the thesis is not singled out with typographic means and references.

- J. C. Estrada-Jiménez, K. Chen-Hu, M. Julia Fernández-Getino García and A. García Armada, "Power Allocation and Capacity Analysis for FBMC-OQAM With Superimposed Training," in IEEE Access, vol. 7, pp. 46968-46976, 2019. doi: 10.1109/ACCESS.2019.2909405. It is totally included in the chapter 4 of the thesis. The material from this source included in the thesis is not singled out with typographic means and references.

- J. C. Estrada Jiménez, B. Genovés Guzmán, M. Julia Fernández-Getino García and V. P. Gil Jiménez, "Superimposed Training-based Channel Estimation for MISO Optical-OFDM VLC," in IEEE Transactions on Vehicular Technology. doi: 10.1109/TVT.2019.2909428. It is totally included in the chapter 5 of the thesis. The material from this source included in the thesis is not singled out with typographic means and references.

Book chapter

- J. C. Estrada-Jiménez, M. Julia Fernández-Getino García and Diego Méndez-Romero, “Superimposed Training and Blind Channel Estimation” in WILEY 5G REF: The Essential 5G Reference Online, Section 1: Radio Technologies, accepted, Ed. John Wiley & Sons, 2019. It is partially included in the chapter 2 of the thesis. The material from this source included in the thesis is not singled out with typographic means and references.

0.2 Other research merit

Journal

- K. Chen-Hu, J. C. Estrada-Jiménez, M. Julia Fernández-Getino García and A. García Armada, "Continuous and Burst Pilot Sequences for Channel Estimation in FBMC-OQAM," in IEEE Transactions on Vehicular Technology, vol. 67, no. 10, pp. 9711-9720, Oct. 2018.

  doi: 10.1109/TVT.2018.2861995

0.3 Abstract

In this thesis, we propose novel superimposed training (ST) techniques for channel estimation for future wireless systems for 5G and beyond. ST is a promising technique that permits to obtain channel state information in a way that it can provide higher spectral efficiency compared with dedicated pilot proposals at the cost of increasing the channel estimation error. In this context, a new proposal called partial-data superimposed training (PDST) is addressed for orthogonal frequency division multiplexing (OFDM) systems. The novelty of PDST is that incorporates an additional power control factor that, unlike previous proposals, allows to improve performance with an accurate control of data and pilot interference. Based on this proposal the channel estimation error is derived. The signal-to-interference and noise ratio (SINR) and average channel capacity are later introduced. The partial superimposition can overcome classical overlay schemes reducing the number of resources affected by the superimposition.

Secondly, the channel estimation performance of a promising multicarrier technique known as filterbank multicarrier offset quadrature amplitude modulation (FBMC-OQAM) is evaluated. In this contribution, we model the introduction of a superimposed training sequence in an FBMC-OQAM system. Due to the superimposition new parameters appear in the formulation known as intrinsic interference and data interference. An analytical expression for the channel estimation error, which fits with the simulation results, is depicted. Then, the SINR and its average channel capacity expressions are presented. Furthermore, the power allocation factor that maximizes the spectral efficiency is found. It is shown that this proposal overcomes the performance of FBMC-OQAM with pilot symbol assisted modulation (PSAM) and other multicarrier techniques as OFDM with PSAM and ST.

Finally, the channel estimation in a promising technology known as visible light communication (VLC) is analyzed. In this proposal, we model a VLC scenario where ST is used for channel estimation. The multicarrier technique DC-offset OFDM is taken into account to adapt the electrical signal to the optical one. Then, multiple

input single output (MISO) is considered to be used as the most adequate spatial multiplexing technique to work with VLC. In this novel technique an extensive analysis is done for deduction of the channel estimation error, SINR and spectral efficiency. Simulation results validate the performance of each proposal in a quasi stationary environment compared with PSAM-based channel estimation techniques.

High spectral efficiency and data rate can be expected of implementing these proposals which successfully could satisfy the new data-rate requirements. All of these proposals consider multicarrier techniques and novel technologies to be used in 5G and beyond systems thus offering new lines of investigation.

Contents

0.1 Published and submitted content 5

0.2 Other research merit 7

0.3 Abstract 8

1 Introduction **21**

1.1 Problem overview 21

1.2 Scientific contributions and structure of the thesis 24

2 Principles of multicarrier techniques **27**

2.1 OFDM 28

2.1.1 At the transmitter 28

2.1.2 At the receiver 29

2.2 FBMC-OQAM 30

2.2.1 At the transmitter 30

2.2.2 At the receiver 31

2.3 DCO-OFDM 33

2.3.1 At the transmitter 34

2.3.2 At the receiver 34

2.4 GFDM 35

2.4.1 At the transmitter 36

2.4.2 At the receiver 37

2.5 UFMC 37

2.5.1 At the transmitter 38

2.5.2 At the receiver 38

3 Partial-data superimposed training (PDST) 41

3.1 State of the art 41

3.2 System model 44

3.3 Channel Estimation 48

3.4 Data Detection 49

3.5 Analysis of the average system capacity 52

3.6 Complexity analysis of algorithms 54

3.6.1 Transmitter 54

3.6.2 Receiver 54

3.7 Simulation results 55

3.7.1 Channel estimator performance 56

3.7.2 Average capacity performance 57

3.7.3 Symbol error rate performance 61

3.7.4 Throughput Analysis 66

3.7.5 PAR performance 68

4 Superimposed training in FBMC-based systems 71

4.1 State of the art 72

4.2 System model 72

4.2.1 FBMC-OQAM with superimposed training 76

4.3 Channel estimation error for ST in FBMC-OQAM multicarrier technique 77

4.4 Analysis of the average system capacity 81

4.4.1 Average channel capacity for PSAM-FBMC 83

4.4.2 Average channel capacity for ST-FBMC 84

4.5 Analysis of the power allocation 85

4.5.1 FBMC using PSAM 85

4.5.2 FBMC using ST 86

4.6 Simulation results 87

5 Superimposed training in VLC scenarios based on DCO-OFDM 91

5.1 State of the art 91

5.2 System model 92
5.3 Channel estimation 96
5.3.1 LS channel estimation 96
5.3.2 Description of the pilot sequences and pilot tones 98
5.4 Analysis of the spectral efficiency 98
5.5 Simulation results 102

6 Conclusions and future lines of research 109

6.1 Conclusions 109
6.2 Future lines 110

List of Figures

2-1 Architecture of the OFDM system. 29

2-2 Architecture of the FBMC-OQAM system transmitter. 32

2-3 Architecture of the FBMC-OQAM system receiver. 33

2-4 Hermitian transpose operation in DCO-OFDM. 35

2-5 Architecture of the DCO-OFDM transmitter. 35

2-6 Architecture of the DCO-OFDM receiver. 36

2-7 Architecture of the GFDM transmitter. 36

2-8 Architecture of the GFDM receiver. 37

2-9 Architecture of the UFMC transmitter. 38

2-10 Architecture of the UFMC receiver. 39

3-1 System architecture of partial-data superimposed training (PDST). . 42

3-2 Symbol-blanking superimposed training 42

3-3 Data-nulling superimposed training 43

3-4 MSE for ST and PSAM schemes. 55

3-5 Average system capacity and symbol error rate as a function of α_{d} using QPSK and a SNR=10dB. 56

3-6 Evolution of the interference control factor (α_{d}) as a function of the power allocation factor (β) for different K. 57

3-7 Interference control factor (α_{d}) as a function of K averaged multicarrier symbols 58

3-8 Average channel capacity of ST and PSAM considering channels with i.i.d. PDP with $N = 64$ (SNR= $10dB$, $K = 10$ and $K = 20$). 58

3-9 Symbol error rate using QPSK modulation and K=10 OFDM symbols with $N = 64$ and $N_{\mathrm{P}} = 8$. The value of $\alpha_{\mathrm{d}} = 0.71$ maximizes the average channel capacity. 59
3-10 Symbol error rate using QPSK modulation and K=20 OFDM symbols with $N = 64$ and $N_{\mathrm{P}} = 8$. The value of $\alpha_{\mathrm{d}} = 0.54$ maximizes the average channel capacity. 60
3-11 Symbol error rate using 16QAM modulation and K=20 OFDM symbols with $N = 64$ and $N_{\mathrm{P}} = 8$. The value of $\alpha_{\mathrm{d}} = 0.64$ maximizes the average channel capacity. 61
3-12 Symbol error rate using QPSK modulation and K=20 OFDM symbols with $N = 128$ and $N_{\mathrm{P}} = 8$. The value of $\alpha_{\mathrm{d}} = 0.55$ maximizes the average channel capacity. 62
3-13 Symbol error rate using 16QAM modulation and K=20 OFDM symbols with $N = 128$ and $N_{\mathrm{P}} = 8$. The value of $\alpha_{\mathrm{d}} = 0.65$ maximizes the average channel capacity. 62
3-14 Symbol error rate using QPSK modulation and K=20 OFDM symbols with $N = 128$ and $N_{\mathrm{P}} = 16$. The value of $\alpha_{\mathrm{d}} = 0.38$ maximizes the average channel capacity. 63
3-15 Symbol error rate using QPSK modulation and K=20 OFDM symbols with $N = 256$ and $N_{\mathrm{P}} = 8$. The value of $\alpha_{\mathrm{d}} = 0.54$ maximizes the average channel capacity. 64
3-16 Symbol error rate using 16QAM modulation and K=20 OFDM symbols with $N = 256$ and $N_{\mathrm{P}} = 8$. The value of $\alpha_{\mathrm{d}} = 0.65$ maximizes the average channel capacity. 65
3-17 Symbol error rate using QPSK modulation and K=20 OFDM symbols with $N = 256$ and $N_{\mathrm{P}} = 32$. The value of $\alpha_{\mathrm{d}} = 0.24$ maximizes the average channel capacity. 65
3-18 Throughput analysis using PSAM and PDST. 66
3-19 Comparison of the PAR performance using its CCDF of ST techniques with $N = 128$ and $N_{\mathrm{P}} = 8$. 67

3-20 Comparison of the PAR performance using its CCDF of ST techniques with $N = 256$ and $N_{\mathrm{P}} = 8$. 67
3-21 Comparison of the PAR performance for PDST using its CCDF changing α_{d} and β with $N = 128$ and $N_{\mathrm{P}} = 8$. 68
3-22 Comparison of the PAR performance for PDST using its CCDF changing α_{d} and β with $N = 256$ and $N_{\mathrm{P}} = 8$. 69

4-1 Average mean squared error as a function of K multicarrier symbols using γ_{SNR}=$\{0, 10, 20\}$ $[dB]$. 82
4-2 Average capacity for OFDM using PSAM (dashed) and ST (dot dashed), and FBMC using AuP (dotted) and ST (solid-line) as a function of the power allocation factor α. 85
4-3 Average capacity of OFDM and FBMC multicarrier techniques using ST and PSAM as a function of SNR. 86
4-4 Average capacity of OFDM and FBMC multicarrier techniques using ST and PSAM as a function of K with a fixed SNR=10 dB. 87

5-1 VLC scenario. (Coordinates in meters.) 103
5-2 CIR for three different user locations. 103
5-3 MSE using ST as a function of the number of averaged OFDM symbols, SNR $\overline{\gamma} = 10$ dB and $\alpha = 0.8$. 104
5-4 Spectral efficiency as a function of the data power allocation α for ST (solid line) and PSAM (dashed line), for $K = 200$ and several SNR $\overline{\gamma}$. 105
5-5 Spectral efficiency (ideal, ST and PSAM) as a function of SNR for a range of α values and a $K = 200$. 105
5-6 Spectral efficiency (ideal, ST and PSAM) as a function of K for a fixed α=α_{opt} and $\overline{\gamma}$=10 dB. 106
5-7 Spectral efficiency (ideal, ST and PSAM) as a function of the number of channel taps L for a fixed SNR $\overline{\gamma}$=10 dB, K=200 and α=α_{opt}. . . . 107

List of Tables

3.1 Channel estimation (CE) error for ST and PSAM techniques 48

3.2 Complexity of the receiver 50

3.3 Detection algorithms used in ST 51

3.4 System Parameters 53

4.1 Intrinsic self-interference that affects the data at $[k_0, m_0]$ position using a PHYDYAS prototype filter. 89

5.1 Optical parameters 101

5.2 CPU time (s) in MSE computation 102

Chapter 1

Introduction

In this chapter, we present a general overview of the research topic to be analyzed. Then, some literature of the state of the art aiming the research topic is reviewed. At the end, the thesis structure and some scientific notation are presented.

1.1 Problem overview

The wireless communications have evolved continuously in last decades. The number of users, new applications and their requirements have been increased with the evolution of the mobile phone technologies. The bandwidth required to support these trends has exponentially raised. Thus, the academy community have shown great interest to respond to these needs where several generations of wireless communications have been developed adding new solutions to these new requirements. The first generation (1G) of mobile communications based its functionality in the transmission of voice. The 1G analog standard was introduced in the 80s and 90s. Two of the most important 1G technologies were advanced mobile phone system (AMPS) and total access communication systems (TACS).

The second generation (2G) of mobile communications appears at the beginning of the 90s and offers digital voice and several services as text and picture messaging at low data rates. The 2.5G provides improved throughput using general packet data rate (GPRS) technology. Its data rate can reach up to 144 kbps. 2.5G provides

services as phone calls, instant messaging, and applications as web browsing and email transmission.

The third generation (3G) begins to work at 2000's and it offers web services, TV, roaming with data rates that reach up to 2Mbps. The smart phones appear here allowing large capabilities of video transmission using bandwidths of 5 to 20 MHz [1].

4G offers data rates up to 100 Mbps multimedia messaging, broadband and broadcasting services [2]. The access technology is provided through code division multiple access (CDMA) or orthogonal frequency division multiple access (OFDMA). The bandwidth varies from 5 to 20 MHz.

In 5G, it is expected that the mobile communication provides more than 500 Mbps with a latency of 1 mS. Some signal processing techniques as massive multiple input multiple output (MIMO) [3], edge computing, small cells, beamforming, non-orthogonal multiple access (NOMA) [4], have been researched to offer high data rates that can face the new users demands. Other proposals are in literature are related to the millimeter waves (mmWave) technology [5]. In this case ultra-high frequency (UHF) bands are used to transmit information at very high frequencies [6].

The multicarrier techniques increase the bandwidth availability for data transmission using narrow band channels, and, therefore, allowing to work with frequency flat channels. Here, the signals can be transmitted ideally without interference by overlapping with nearby signals thanks to the orthogonality provided. One of the most common techniques is orthogonal frequency division multiplexing (OFDM) that was implemented in 4G.

OFDM is the most widely employed multicarrier technique and it is going to be considered as part of 5G mainly because it offers compatibility with previous OFDM-like standards [7]. It uses a cyclic prefix (CP) to eliminate the interference provoked by the nearby OFDM symbols in time-domain [8] [9]. Other multicarrier technique that has been studied in the literature is filterbank multicarrier offset quadrature amplitude modulation (FBMC-OQAM) which can eliminate the use of CP increasing the spectral efficiency compared to OFDM [10]. This technique reduces the inter-symbol interference (ISI) utilizing greater symbol lengths and certain level of overlapping.

One of its drawbacks is the intrinsic interference caused by the surrounding symbols due to the lack of subcarrier orthogonality.

Another popular way to increase the bandwidth to meet the users demand is using a promising technique known as visible light communication (VLC) which conveys information at the visible light spectrum [11]. This technique assures greater data rates and bandwidth thanks to the lack of interference and the frequency band where it works. VLC uses DCO-OFDM (DC offset OFDM) as a multicarrier technique to provide to the light emitting diode (LED) with a real-valued signal.

In coherent communications, channel estimation is a necessary step to recover the transmitted information. Pilot symbol amplitude modulation (PSAM) is a very popular technique which uses dedicated resources to transmit pilot signals to estimate the channel. This technique obtains good channel estimation error at the cost of spending dedicated resources in the transmission of pilots. Another attractive channel estimation technique is superimposed training (ST) [12] [13] [14], which can be used for 5G and beyond, because it increases the spectral efficiency which is highly desirable in current and future standards. This technique improves the spectral efficiency due to the fact that no dedicated pilot subcarriers are used at the cost of a reduced quality of channel estimation error. The literature of ST has been extended to relay networks as can be seen in [15] [16], and using MIMO systems [17] [18] [19] [20] [21]. Also, some investigations for the analysis of peak-to-average power ratio have been presented for ST in [22] [23] and [24].

In this thesis, we present novel channel estimation techniques using ST. We analyze the proposal, first introduced in [25], using OFDM where a channel estimation technique called partial-data superimposed training (PDST) is presented. Here, a pilot training sequence is added to previously precoded data taking control of the level of interference generated. The closed form expression of the channel estimation error is deduced. Then, the analytical expression for the average channel capacity is derived. Simulation results validate the analysis of the results.

Secondly, a novel technique considering FBMC-OQAM with ST-based channel estimation, firstly proposed in our paper [26], is analyzed against PSAM-like methods.

Considering the self-interference and the data interference generated, the analytical expression of the channel estimation error is introduced. Then, the average channel capacity is denoted. Simulations results are presented to validate the analysis,

Finally, the channel estimation is evaluated in a VLC scenario. A superimposed training sequence is tested to estimate the channel within the optical band. Analytical expressions are obtained for the channel estimation error, signal-to-noise ratio (SNR) and average channel capacity. Simulation results are depicted to show the performance of this proposal as it can be seen in [27] and [28].

1.2 Scientific contributions and structure of the thesis

In this thesis, we explain the main results obtained during last years related to the novel channel estimation technique based on ST. These results include an analysis of the expressions analytically deduced for different scenarios and its evaluation using simulation results. The scientific contributions that we obtained in this topic are listed as follows.

In [25], a journal paper, we propose a technique called "Partial-Data Superimposed Training With Data Precoding for OFDM Systems" for channel estimation in an OFDM scenario. In [29], a conference paper called "Superimposed Training for Channel Estimation in FBMC-OQAM", we proposed to use ST in a FBMC-OQAM scenario. In [26], in a journal paper called "Power Allocation and Capacity Analysis for FBMC-OQAM With Superimposed Training" a ST scheme for channel estimation is analyzed in an FBMC-OQAM scenario. In [27], in a conference paper called "Superimposed training-based channel estimation for Visible Light Communications" we proposed to use ST as channel estimation method in VLC. In [30], in a conference paper called "Comparativa de técnicas de estimación de canal para VLC en interiores" we proposed a comparative scheme of channel estimation techniques in indoor scenarios. In [28], in a journal paper called "Superimposed Training-based Channel

Estimation for MISO Optical-OFDM VLC" the use of ST for channel estimation in a MISO VLC scheme is proposed.

In the rest of this thesis, the chapters are organized as follows:

In chapter 2, relevant information is introduced explaining the state of the art of multicarrier techniques that later, in the following chapters, will be used for analysis. In chapter 3, a new channel estimation technique, called partial data superimposed training (PDST), is explained. Then, the channel estimation error in PDST is analytically deduced, and with this information the SINR and average channel capacity are obtained. Simulation results validate the analysis. In chapter 4, the ST-based channel estimation applied to FBMC-OQAM systems is analyzed. The channel estimation error, which includes the intrinsic self-interference of FBMC-OQAM, is deduced. Then, the SINR and the average channel capacity expressions are obtained. Simulation results validate this analysis. In chapter 5, the channel estimation is analyzed using ST over VLC. The channel estimation error considering intrinsic VLC parameters is obtained. Then, the SINR and spectral efficiency expressions are deduced. Simulation results validate the analysis. Finally, in chapter 6, the conclusions and future lines of research are provided.

Chapter 2

Principles of multicarrier techniques

The multicarrier techniques are used to guarantee high data rates in communications. This concept implies conveying data signals over multiple subcarriers relatively close, between them, using narrow bands. One of the main advantages of the multicarrier transmission is that these techniques make the system resistant to interference, multipath and fading channels. Thus, they can offer greater spectral efficiency than single carrier.

Multicarrier techniques have been proposed to be used in broadband communications. The most relevant is orthogonal frequency division multiplexing (OFDM) which is widely employed in current standards. Others such as filterbank multicarrier (FBMC) [31] [32], universal filtered multicarrier (UFMC) [33] [34], and generalized frequency division multiplexing (GFDM) [35] [36] have been considered to be the future waveform for 5G and beyond thanks of their own characteristics that allow to obtain greater spectral efficiency. Some other variants are devoted to optical wireless systems in visible-range, such as DC-biased optical OFDM (DCO-OFDM) [37] and asymmetrically clipped optical OFDM (ACO-OFDM) [38] [39]. These multicarrier transmission techniques will be described in the following sections.

2.1 OFDM

OFDM is a very popular multicarrier technique that has been used within the current mobile wireless technologies and it is also proposed for 5G. Different wireless technologies such as Wi-Fi [40] and long term evolution (LTE) [41] have chosen OFDM [42] [43] as their multicarrier waveform. This technique is robust against interference signals and fading channels. The channels can be divided in narrow-band flat fading channels what permits the designer to implement simple signal processing techniques at the receiver.

One of the most important characteristics is the orthogonality of the subcarriers, which implies that any interference provoked by a neighbor transmitted signal should not affect the actual one [44]. In practice, the orthogonality cannot be reached easily, thus, cyclic prefix (CP) or frequency sub-bands are used to make the system robust against inter-symbol and the inter-carrier (ISI/ICI) interference [45].

2.1.1 At the transmitter

The data symbols are introduced into an OFDM modulator where N corresponds to the number of OFDM subcarriers and M to the time-domain slots. The OFDM modulator is implemented using an inverse discrete Fourier transform (IDFT) implementation known as inverse fast Fourier transform (IFFT) module. The IFFT allows to decompose the available bandwidth into narrowband subcarriers and transform the frequency-domain signal into time-domain.

Then, the signal vector resulting from the IDFT operation can be represented as $\mathbf{x}_t = \mathbf{F}^H\mathbf{x}$ where $\mathbf{F}^{m,n} = e^{-2j\pi mn/N}$ at the m-th row and n-th column, where $\mathbf{x}$ corresponds to the signal to be transmitted in frequency-domain and $[\cdot]^H$ is the Hermitian operation.

A CP is introduced to eliminate the ISI/ICI interferences. This one consists in an interval of N_{CP} samples in time-domain copied from the N-th sample of an OFDM symbol (N_{CP} samples) and it is collocated at the beginning of the OFDM symbol. The transmitted signal after the CP insertion can be written as $\mathbf{x}_t^{cp} = [[\mathbf{x}_t(N -$

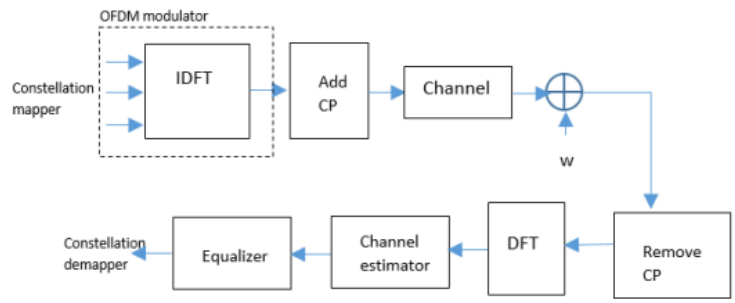

Figure 2-1: Architecture of the OFDM system.

$N_{CP})...\mathbf{x}_t(N)] \quad \mathbf{x}_t]^T$. Thus, the CP insertion transforms a linear convolution between the channel and transmitted signal into a circular one simplifying the recovering process at the receiver. This can be seen in Fig. 2-1.

2.1.2 At the receiver

The conveyed signal is received in time-domain. Then, the CP is eliminated, whereby, after DFT transformation the signal is represented as

$$\mathbf{r} = \mathbf{H}\mathbf{x} + \mathbf{w} \tag{2.1.1}$$

where the channel in frequency-domain $\mathbf{H}$ is represented by the $N \times N$ matrix $\mathbf{H} = \mathbf{F}_L\mathbf{h}$ and $\mathbf{F}_L$ is the $N \times L$ front submatrix of $\mathbf{F}$ where L indicates the number of channel taps. The channel impulse response is represented by the $L \times 1$ vector $\mathbf{h}$. The $N \times 1$ vector $\mathbf{w}$ is the additive white Gaussian noise (AWGN). Then, the channel is estimated making use of pilots and next with this information the received signal is equalized.

Next, data-detection is performed to approximate the demodulated and equalized signal to the most likelihood constellation symbol. Depending on the complexity, iterative processes and complex algorithms can be implemented to improve the performance of data-detection.

2.2 FBMC-OQAM

Filter bank multicarrier offset quadrature amplitude modulation (FBMC-OQAM) [46] [47] is a recently studied multicarrier waveform that has been considered as candidate for 5G and beyond communication networks. FBMC-OQAM offers lower out-of-band emissions implementing well-designed prototype filters. This allows avoiding the use of frequency guard bands for interference protection and therefore it improves the spectral efficiency compared with OFDM.

The multicarrier symbols used in FBMC-OQAM are longer than those in OFDM to minimize the interference effects caused by not using CP. Several FBMC symbols can overlap, since in this technique subcarriers are not required to be orthogonal to each other. Considering sufficiently large FBMC-OQAM symbols, the ISI can be ignored when compared with the channel estimation error and noise.

2.2.1 At the transmitter

In FBMC-OQAM, QAM symbols grouped in $N \times M/2$ QAM symbols matrix $\mathbf{S}$ are introduced in the transmitter, where N represents the number of subcarriers and $M/2$ is the number of QAM symbols. Then, the QAM symbols are divided into real and imaginary parts (OQAM) and delivered with a time-delay to the prototype filter with the corresponding phase. The $N \times M$ OQAM symbols matrix is represented as $\mathbf{S}_o$ where

$$S_o[n, m = 2m'] = \Re(S[n, m']), \tag{2.2.2}$$

$$S_o[n, m = 2m' + 1] = \Im(S[n, m']), \tag{2.2.3}$$

where $\Re\{\cdot\}$ and $\Im\{\cdot\}$ represents the real and imaginary parts, respectively, $n = 0 \cdots N-1$, $m' = 0 \cdots M/2 - 1$ and m ranges up to $M-1$.

Assuming a discrete-time system model being $T_S = \frac{T}{N}$ the sampling period, where N corresponds to the number of symbols conveyed in a transmission time T. Thus,

the transmitted signal is

$$x[n_s]=\sum_{m=0}^{M-1}\sum_{n=0}^{N-1} S_o\left[n,m\right] e^{j\phi[n,m]} g\left[n_s-m\frac{N}{2}\right] e^{j\frac{2\pi}{N}\Delta f n\left(n_s-m\frac{N}{2}\right)}, \tag{2.2.4}$$

where $g[n]$ corresponds to the real-valued prototype filter, $\Delta f=\frac{1}{T}$ is the subcarrier spacing, n_s corresponds to the time delay, and the phase $\phi[n,m]$ is given by

$$\phi[n,m] = \left\{ \begin{array}{ll} 0, & n+m \text{ even} \\ \frac{\pi}{2}, & n+m \text{ odd} \end{array} \right\}. \tag{2.2.5}$$

The time-frequency shifted version of $g[n_s]$ can be defined as $g_n[n_s] = g[n_s]e^{j\frac{2\pi}{N}\Delta f n_s}$. Then, $x[n_s]$ is represented as

$$x[n_s]=\sum_{m=-\infty}^{M-1}\sum_{n=0}^{N-1} S_o[n,m]e^{j\phi[n,m]} g_k\left[n_s-n\frac{N}{2}\right]. \tag{2.2.6}$$

In the literature, this process is also known as synthesis filter bank (SFB). Note that $g[n_s]$ and $\phi[n,m]$ are designed so that $g_n[n_s]$ is orthogonal in the real field satisfying

$$\Re\left\{< g_n[n_s], g_{n'}[n_s] >\right\} = \left\{ \begin{array}{ll} 1, & n=n' \text{ and } n_s=n'_s \\ 0 & \text{otherwise} \end{array} \right\}. \tag{2.2.7}$$

Thus, the signal is transmitted through the channel. The architecture of the FBMC-OQAM transmitter can be seen in the Fig. 2-2.

2.2.2 At the receiver

To recover the conveyed information, the inverse process applied at the transmitter is taken. The received signal, represented by the $N \times M$ matrix $\mathbf{R}_o$, consists in a composition of the desired signal summed with the interference provoked by the surrounding symbols around the transmitted one when the prototype filter is applied

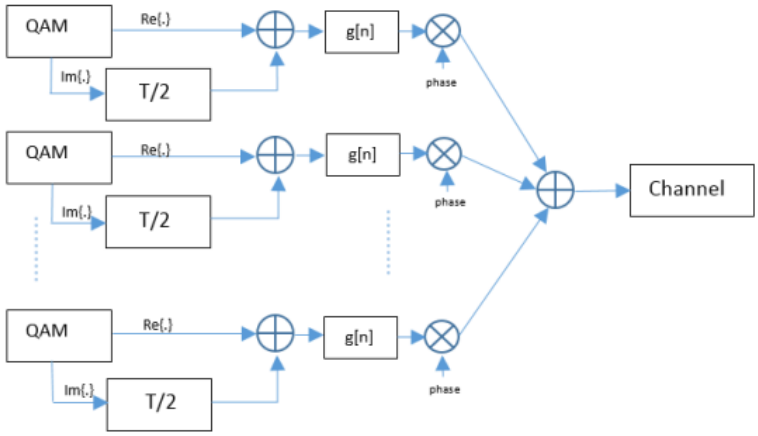

Figure 2-2: Architecture of the FBMC-OQAM system transmitter.

as it can be seen in Fig. 2-3.

$$
\begin{aligned}
&R_o[n_0, m_0] = \\
&= H[n_0, m_0] S_o[n_0, m_0] + \sum_{(n,m) \neq (n_0,m_0)} \sum H[n, m] S_o[n, m] v_{n_0,m_0}[n, m]
\end{aligned}
\tag{2.2.8}
$$

If the channel is quasi-stationary in K multicarrier symbols, the received signal can be expressed as

$$
\begin{aligned}
&R_o[n_0, m_0] = \\
&= H[n_0, m_0] \Big[\underbrace{S_o[n_0, m_0]}_{\text{desired signal}} + \underbrace{\sum_{(n,m) \neq (n_0,m_0)} \sum S_o[n, m] v_{n_0,m_0}[n, m]}_{\text{self-interference}} \Big] \\
&= S_o[n_0, m_0] + jB[n_0, m_0],
\end{aligned}
\tag{2.2.9}
$$

where the interference caused in $[n_0, m_0]$ is represented by $v_{n_0,m_0}[n, m]$ produced by the surrounding symbols placed at $[n, m]$, due to the joint effect of the residual components of the prototype filter $g(t)$ and additional phase rotation $\phi[n, m]$. Thus, $B[n_0, m_0]$ denotes the whole self-interference amplitude at $[n_0, m_0]$.

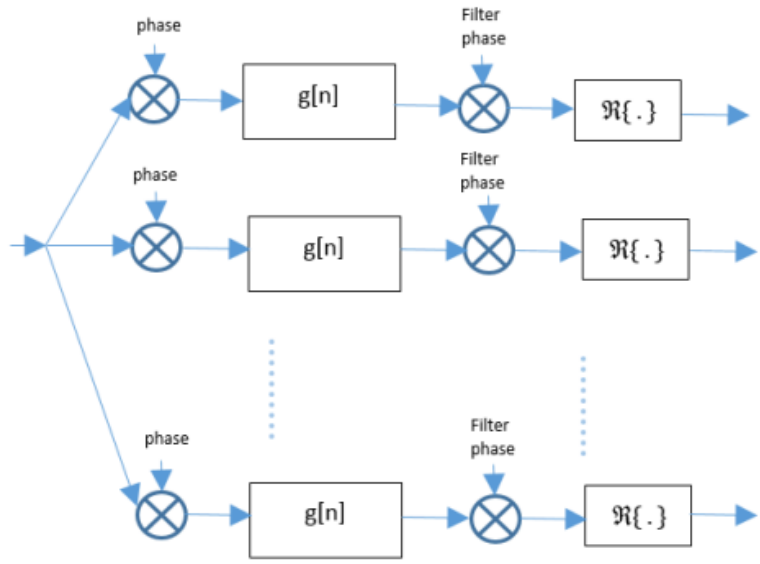

Figure 2-3: Architecture of the FBMC-OQAM system receiver.

Finally, the transmitted symbols represented by **S** are recovered using

$$\begin{aligned} S[n_0, m_0'] =& \Re\left(R_o[n_0, m_0 = 2m_0']\right) + \\ &+ j\Re\left(R_o[n_0, m_0 = 2m_0' + 1]\right). \end{aligned} \tag{2.2.10}$$

Then, special mechanisms have been proposed in the literature for channel estimation as it can be seen in [48] [49] [50] taking into account the self-interference generated. After the filter and channel effects have been counteracted, the equalization is performed. Thus, QAM symbols are recovered. The architecture of the FBMC-OQAM receiver can be seen in Fig. 2-3.

2.3 DCO-OFDM

Direct current biased optical OFDM (DCO-OFDM), [51] [52], is a multicarrier modulation technique commonly proposed in VLC thanks to its spectral efficiency and flexibility. This technique generates a real valued signal composed by a set of symbols to be transmitted and by its Hermitian symmetric operation as it can be seen in Fig. 2-4. This multicarrier technique takes advantage of the FFT capability to create real valued signals needed to power the transmitter light emitting diode (LED).

2.3.1 At the transmitter

A communication system with N subcarriers is taken into account, where the transmitted signal in frequency-domain is represented by the $(N-2)\times 1$ vector $\mathbf{x}$ with $x(k)$ values.

The OFDM symbol is divided in two segments; the first subcarrier index set is $\{1, ..., N/2-1\}$ which consists in the pilot and signal symbols that are going to be transmitted through the channel. Then, the second subcarrier index set $\{N/2+1, ..., N-1\}$ transmits the Hermitian symmetric of the first segment. This operation can be seen in Fig. 2-4. Additionally, the 0-th and $N/2$-th subcarriers do not transmit information in such a way that a real-valued signal can be guaranteed at the output of the IFFT. The construction of a DCO-OFDM symbol can be described as follows

$$\mathbf{x}=\begin{bmatrix}0 & \mathbf{x}_{\mathrm{C}}^{\mathrm{T}}[1, ..., N/2-1] & 0 & \mathbf{x}_{\mathrm{C}}^{\mathrm{T}}[N/2, ..., N-2]\end{bmatrix}^{\mathrm{T}} \tag{2.3.11}$$

where $\mathbf{x}_{\mathrm{C}}$ is an $(N/2-1)\times 1$ vector and $\mathbf{x}_{\mathrm{C}}[N/2, ..., N-2]=\left\{\mathbf{x}_{\mathrm{C}}^{\mathrm{T}}[1, ..., N/2-1]\right\}^{\mathrm{H}}=\mathbf{x}_{\mathrm{half}}$.

The 0-th index subcarrier value is set to 0 given that a DC value is introduced to the system which changes as a function of the requirements of the system. In Fig. 2-5, it is possible to see the architecture of the DCO-OFDM transmitter where the Hermitian symmetry operation is represented followed by the IFFT, CP, and the digital to analog converter (DAC).

2.3.2 At the receiver

The received signal can be represented by the following expression

$$y(k) = H(k)x(k) + w(k), \tag{2.3.12}$$

where $H(k)$ corresponds to the frequency-domain channel at k-th subcarrier, k is the subcarrier index and $w(k)$ is the AWGN noise at the k-th subcarrier. The received time-domain signal is demodulated via DFT and the information is taken from the

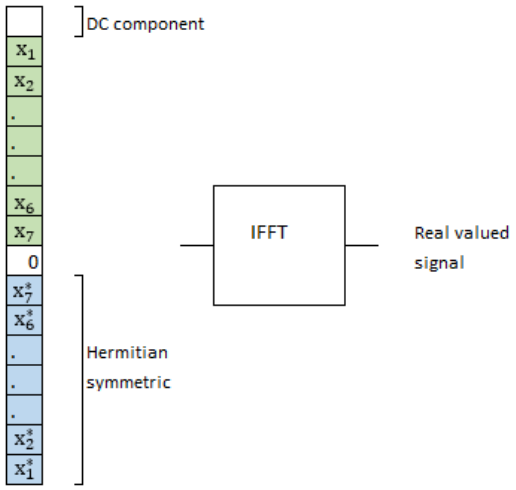

Figure 2-4: Hermitian transpose operation in DCO-OFDM.

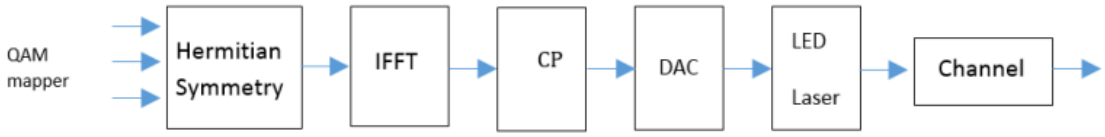

Figure 2-5: Architecture of the DCO-OFDM transmitter.

corresponding subcarriers. The channel is estimated and then the information is recovered. The architecture of the receiver can be seen in Fig. 2-6

As it can be seen in Fig. 2-6, an analog to digital converter (ADC) is necessary at the receiver.

2.4 GFDM

Generalized frequency division multiplexing (GFDM) is a promising multicarrier technique that works with block filtering. This technique allows to convey several subsymbols per subcarrier and per block working similarly as in FBMC applying a pulse shape for each subcarrier. To face multipath selective channel effects, the CP and the frequency equalization are permitted [53] [54]. GFDM uses non-orthogonal pulse shapes with well-localized filters to avoid out of band interference emissions. This technique presents a high degree of spectrum fragmentation, which exploits unused

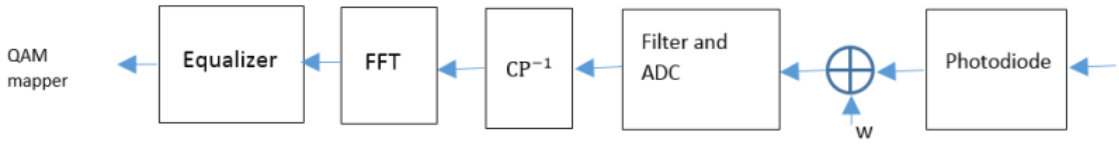

Figure 2-6: Architecture of the DCO-OFDM receiver.

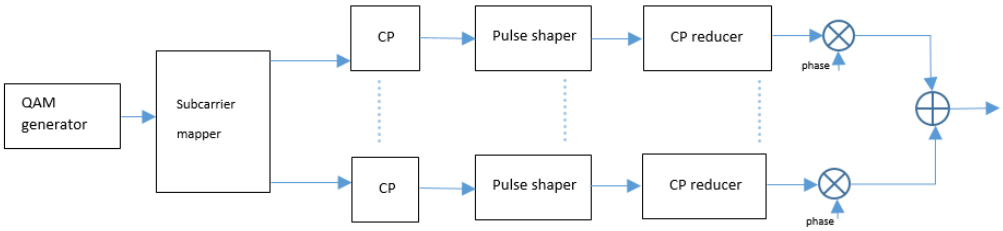

Figure 2-7: Architecture of the GFDM transmitter.

spaces close to the assigned spectrum.

In the case where no CP is used, intrinsic self-interference between the conveyed symbols will be present. Then, long symbol frames can be implemented to face this problem and to increase the spectral efficiency.

In GFDM [55], similarly as in FBMC, each subcarrier is filtered independently. Every transmitted data per subcarrier is upsampled and convolved with the pulse shaping prototype filters.

2.4.1 At the transmitter

The QAM mapper at the transmitter, [53], generates a vector of N QAM symbols which are split to be transmitted in M subcarriers and N/M sub-symbols by the subcarrier mapper. Then, a CP is inserted to avoid interferences and a pulse shaper is applied per each individual subcarrier. Then, a technique called tail biting is introduced to reduce the size of the CP. Finally, the signal is shifted to the corresponding carrier and summed to each other to be transmitted. In Fig. 2-7, the architecture of the transmitter is depicted.

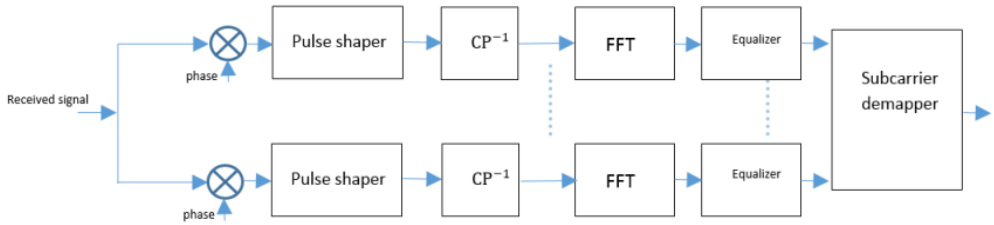

Figure 2-8: Architecture of the GFDM receiver.

2.4.2 At the receiver

An individual single-carrier demodulation per subcarrier is necessary. The received signal is the result of the convolution of the transmitted signal with the channel and the noise. This signal is shifted to the base-band signal and filtered following the inverse process of the transmitter. This filtering is used to eliminate the interference signal of the neighboring subcarriers. Then, the CP is retired, and the resulting signal is DFT transformed. Then, the signal can be equalized in frequency-domain per subcarrier. Each signal is IDFT modulated and conducted to a subcarrier demapper. Finally, the signal is detected. In Fig. 2-8, the architecture of the receiver can be observed.

2.5 UFMC

Universal filtered multicarrier (UFMC) is an emerging technology considered for the next generation of mobile communications. This waveform offers higher bandwidths than OFDM, then, it can overcome the intrinsic limitations of OFDM. It can be considered as a variant of OFDM where the assignment of a filtered sub-band allows a better spectral localization. In this technique, some subcarriers are grouped in a sub-band and managed as an available resource which can be assigned to users. This operation mode allows the communication systems to obtain a better spectral localization than in OFDM, and, offers better services associated with different cases of use for 5G and beyond. This technique is robust against misalignments in time and frequency which allows to transmit small size and low latency packages. Several

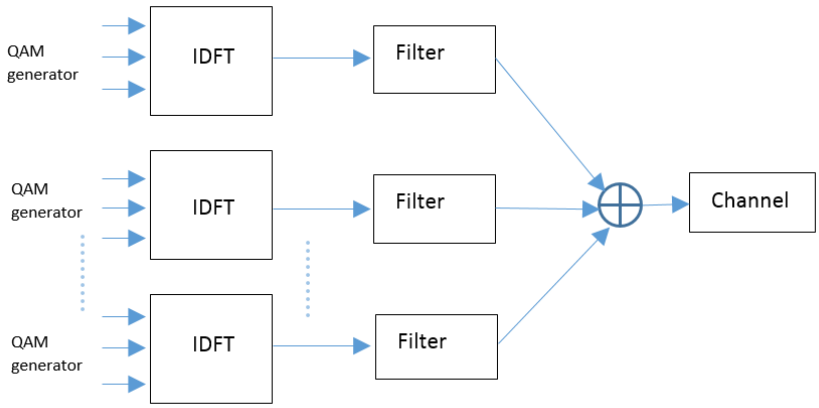

Figure 2-9: Architecture of the UFMC transmitter.

technologies as machine type communications (MTC) can be compatible with UFMC [56]. Note that being a variant of OFDM then the CP and a zero pos-fix (ZP) are permitted.

2.5.1 At the transmitter

At the transmitter, the whole band is divided in some sub-bands where each one has several subcarriers assigned. The generated information is transformed to time-domain via IDFT and then filtered using an FFT matrix. Thus, the filtered signals are summed with the filtered sub-bands to be transmitted to the channel. Finally, zeros are introduced to avoid ISI/ICI interference. The architecture of the UFMC transmitter can be observed in Fig. 2-9.

2.5.2 At the receiver

At the receiver side, the transmitted zeros are eliminated and the received signal is introduced into a DFT to de-filter the information. Then, the frequency-domain signal is equalized. The architecture of the UFMC receiver can be seen in Fig. 2-10.

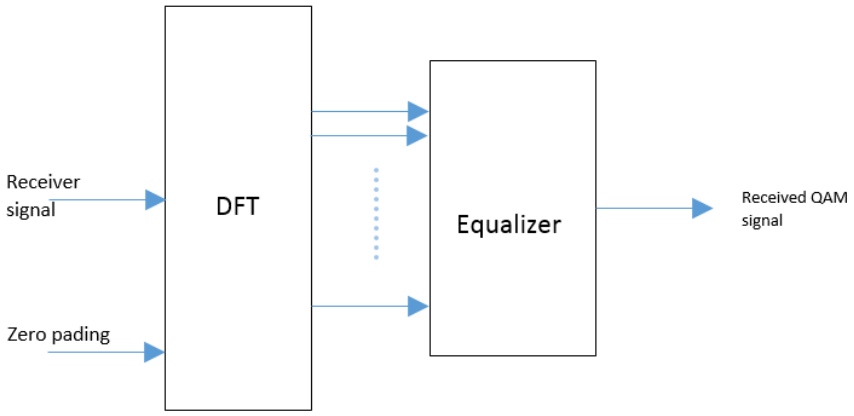

Figure 2-10: Architecture of the UFMC receiver.

Chapter 3

Partial-data superimposed training (PDST)

In this chapter, a new superimposed training technique called partial-data superimposed training (PDST) is described. Here, the generated interference signal is analyzed and a power control factor is introduced for the adequate pilot and data power assignment. Some expressions are deduced to describe the data interference signal, the channel estimation error and the average channel capacity. Finally, simulation results are presented at the end to evaluate the performance of the systems and to show that with the appropriate value of the power allocation factor, PDST overcomes the rest of the proposals presented in literature.

3.1 State of the art

ST methods have attracted much attention because of the advantages obtained in spectral efficiency compared with PSAM techniques. This one arithmetically sums the information signal with the pilot signal that later is used for estimating the channel. ST do not waste bandwidth, unlike PSAM, due to no subcarrier is used exclusively for pilot transmission. ST schemes are promising technologies especially for next-generation 5G wireless networks where higher demands of data rates are expected. These techniques have been proposed in 5G to exceed the existing limits like pilot

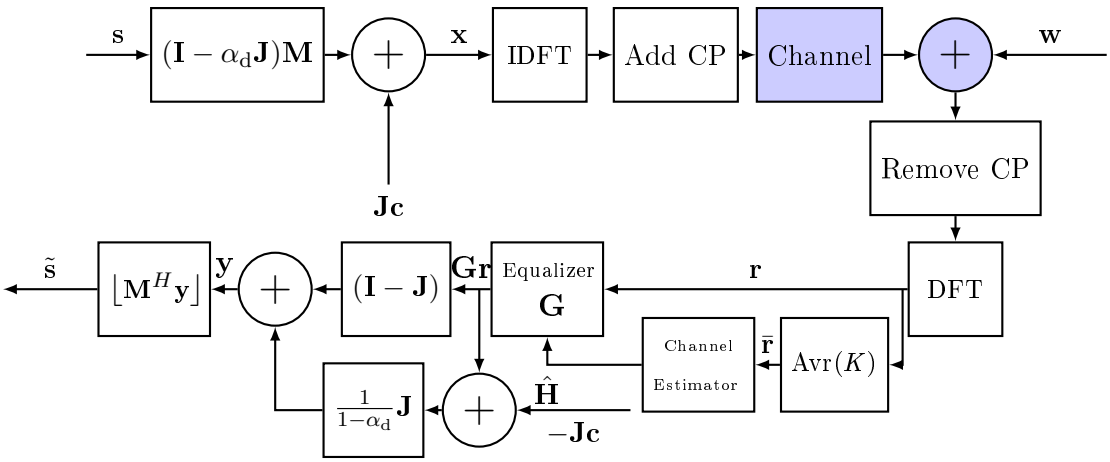

Figure 3-1: System architecture of partial-data superimposed training (PDST).

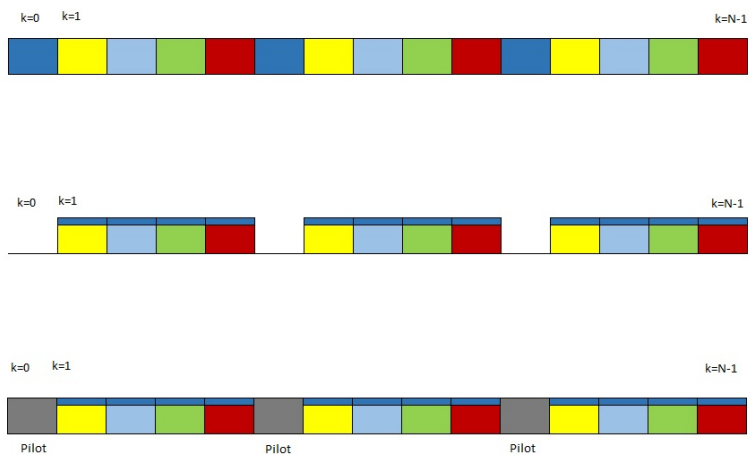

Figure 3-2: Symbol-blanking superimposed training

contamination interference in massive multiple input multiple output (MIMO) [3] or combined with modern proposals such as non-orthogonal multiple access (NOMA) [4] but using only simple methods of superimposition.

Some ST schemes have been proposed for single carrier schemes as it can be seen in [57] and [58] where a method called data-dependent superimposed training (DDST) is presented. DDST removes some periodical pilot symbols to leave spaces free to introduce a pilot training signal for channel estimation.

Several ST schemes are proposed to be used in orthogonal frequency division multiplexing (OFDM) as it can be seen in [59]. Here, a technique called symbol-blanking superimposed training (SBST) retires data symbols where pilot symbols

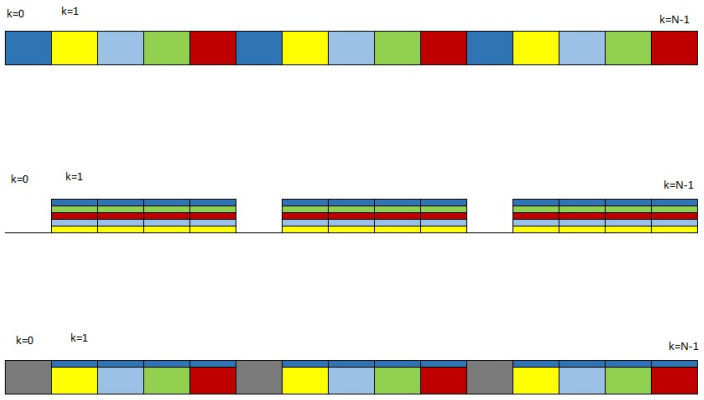

Figure 3-3: Data-nulling superimposed training

will be transmitted, as can be seen in Fig. 3-2. Then, the retired data symbols are spread over a group of data symbols next to them, inducing interference and degradation in the system performance.

In [60] and [61], in an OFDM transmission, the authors proposed to precode the information and then to null data in the subcarrier positions where the pilots are going to be transmitted as can be seen in Fig. 3-3. Then, a channel estimation error like in PSAM is reached, but with a reduction of the symbol error rate (SER) performance. This effect can be seen specially in high order constellations. Some iterative mechanisms have been proposed to recover the system from the nulling process.

Comparing both methods, [59] and [60], it is possible to see that they are similar in the sense that the pilots of the training sequence are placed at subcarriers where no data-interference is present. Then, in practice, there is no superimposition. The objective of both methods is to obtain a channel estimation error as reduced as possible, comparable to PSAM techniques. However, in [59] and [60], a better quality of the channel estimation is obtained at the cost of a reduction in the data detection performance.

Some hybrid mechanisms have been proposed in the literature for OFDM, where a data detection and channel estimation mechanism are combined in an iterative loop as it can be seen in [62] for DNST. Here, a bit interleaved coded modulation (BICM)

coder accompanied with an interference cancellation technique are used to improve the data detection performance but with a prohibitive complexity.

3.2 System model

The system architecture is depicted in Fig. 3-1 and is composed by transmission and reception blocks. The data information is conveyed to the OFDM modulator, then, the signal is transmitted, and it goes through the channel and the additive white Gaussian noise (AWGN) is added. At the receiver the signal is OFDM demodulated, then, the channel is estimated, the signal is equalized and data is finally detected.

Considering an OFDM multicarrier system in a frequency selective channel, the number of subcarriers and pilots are represented by N and N_{P}, respectively, where $(N_{\mathrm{P}} < N)$ and $k = 0, ..., N-1$ is the subcarrier index. The transmitted signal in frequency-domain is represented by $\mathbf{x}$ of size $N \times 1$ which is the result of following process

$$\mathbf{x} = (\mathbf{I} - \alpha_{\mathrm{d}}\mathbf{J})\mathbf{M}\mathbf{s} + \mathbf{J}\mathbf{c}. \tag{3.2.1}$$

Note that α_{d} consists in the data interference control factor, $0 < \alpha_{\mathrm{d}} < 1$, $\mathbf{s}$ is the data symbol vector of size $N \times 1$ in frequency-domain, $\mathbf{M}$ corresponds to the precoding matrix of size $N \times N$, $\mathbf{J}$ is a diagonal matrix with ones at N_{P} pilot positions, $\mathbf{I}$ represents an identity matrix of size $N \times N$ and $\mathbf{c}$ corresponds to the $N \times 1$ known pilot training sequence with N_{P} pilots where zeros are filled in the remaining $(N - N_{\mathrm{P}})$ positions.

The precoding matrix, named $\mathbf{M}$, is composed of several orthogonal codes satisfying $\mathbf{M}^H\mathbf{M} = \mathbf{I}$, e.g. Hadamard. In (3.2.1), each data symbol is spread over N subcarriers similarly as in [60].

Note that to simplify the analysis, $(\mathbf{I} - \alpha_{\mathrm{d}}\mathbf{J})$ can be extended to $(\mathbf{I} - \mathbf{J}) + (1 - \alpha_{\mathrm{d}})\mathbf{J}$. Thus, (3.2.1) is seen as

$$\mathbf{x} = (\mathbf{I} - \mathbf{J})\mathbf{M}\mathbf{s} + (1 - \alpha_{\mathrm{d}})\mathbf{J}\mathbf{M}\mathbf{s} + \mathbf{J}\mathbf{c}. \tag{3.2.2}$$

As can be seen in (3.2.2), in the first segment, the subcarrier positions indicated by $(\mathbf{I} - \mathbf{J})$ will convey the *non-superimposed information signal*. These ones will be called *data* subcarriers.

In (3.2.2), the positions in the second term indicated by $\mathbf{J}$ subcarriers convey *superimposed information signal*, whose power is controlled by the $(1 - \alpha_{\mathrm{d}})$ factor which multiplies $\mathbf{Ms}$. The information signal is arithmetically summed to a pilot vector $\mathbf{Jc}$. Consequently, the data and pilots are transmitted simultaneously using the *pilot-data* subcarriers.

The power used to transmit one multicarrier symbol (composed by N subcarriers), $\mathcal{P}$, can be divided in the information signal power $\mathcal{P}_{\mathbf{s}}$ and training pilot signal power $\mathcal{P}_{\mathbf{c}}$. Both powers can be expressed as

$$\mathcal{P} = \mathcal{P}_{\mathbf{s}} + \mathcal{P}_{\mathbf{c}}, \tag{3.2.3}$$

$$\mathcal{P}_{\mathbf{s}} = (1 - \beta)\mathcal{P}, \tag{3.2.4}$$

$$\mathcal{P}_{\mathbf{c}} = \beta\mathcal{P}. \tag{3.2.5}$$

β is the ratio between the powers $\mathcal{P}_{\mathbf{c}}$ and $\mathcal{P}$ which is called the power allocation factor. The power assigned to the information signal can be split into

$$\mathcal{P}_{\mathbf{s}} = \mathcal{P}_{s1} + \mathcal{P}_{s2} \tag{3.2.6}$$

where $\mathcal{P}_{s1}$ and $\mathcal{P}_{s2}$ consist in the *non-superimposed information signal* and the *superimposed information signal* power, respectively. In this chapter, we denote that $\tilde{\mathbf{x}} = (\mathbf{I} - \alpha_{\mathrm{d}}\mathbf{J})\mathbf{Ms}$ and it is assumed that the power $\mathcal{P}_{s1}$ over the $N - N_{\mathrm{P}}$ subcarriers is equally distributed,

$$E[|\tilde{\mathbf{x}}|^2]_k = \frac{\mathcal{P}_{s1}}{N - N_{\mathrm{P}}}, k \in \mathcal{I}_0, \tag{3.2.7}$$

and, the power $\mathcal{P}_{s2}$ over P subcarriers is equally distributed,

$$E[|\tilde{\mathbf{x}}|^2]_k = \frac{\mathcal{P}_{s2}}{N_\mathrm{P}}, k \in \mathcal{I}_0^\perp. \tag{3.2.8}$$

Here, the expectation is represented by $E[.]$, the index set that points to the *data* subcarriers is denoted by $\mathcal{I}_0$ being $\mathcal{I}_0^\perp$ its complementary index set which points to the *pilot-data* subcarriers. Note that data symbols at *pilot-data* subcarriers are scaled powered by $(1-\alpha_\mathrm{d})$. Then, the ratios between data and pilot powers are:

$$E[|\tilde{\mathbf{x}}|^2]_k = (1-\alpha_\mathrm{d})^2 E[|\mathbf{Ms}|^2]_k, k \in \mathcal{I}_0^\perp. \tag{3.2.9}$$

In the case of *data* subcarriers,

$$E[|\tilde{\mathbf{x}}|^2]_k = E[|\mathbf{Ms}|^2]_k, k \in \mathcal{I}_0. \tag{3.2.10}$$

Considering (3.2.8), it is possible to obtain

$$\frac{\mathcal{P}_{s2}}{N_\mathrm{P}} = (1-\alpha_\mathrm{d})^2 E[|\mathbf{Ms}|^2]_k, k \in \mathcal{I}_0^\perp, \tag{3.2.11}$$

and taking into account (3.2.7)

$$\mathcal{P}_{s1} = (N - N_\mathrm{P}) E[|\mathbf{Ms}|^2]_k, k \in \mathcal{I}_0. \tag{3.2.12}$$

Finally, replacing (3.2.11) and (3.2.12) into (3.2.6),

$$\mathcal{P}_s = [(N - N_\mathrm{P} + N_\mathrm{P}(1-\alpha_\mathrm{d})^2)] E[|\mathbf{Ms}|^2]_k. \tag{3.2.13}$$

Simpler expressions can be deduced depending on $\mathcal{P}_s$, N, N_P, and α_d. For *pilot-data* subcarriers, using (3.2.9) and (3.2.13)

$$E[|\tilde{\mathbf{x}}|^2]_k = \frac{\mathcal{P}_s(1-\alpha_\mathrm{d})^2}{N - N_\mathrm{P} + N_\mathrm{P}(1-\alpha_\mathrm{d})^2}, k \in \mathcal{I}_0^\perp, \tag{3.2.14}$$

and for *data* subcarriers, using (3.2.10) and (3.2.13) it is possible to obtain that

$$E[|\tilde{\mathbf{x}}|^2]_k = \frac{\mathcal{P}_s}{N - N_{\mathrm{P}} + N_{\mathrm{P}}(1-\alpha_{\mathrm{d}})^2}, k \in \mathcal{I}_0. \tag{3.2.15}$$

The $N\times 1$ $\mathbf{x}$ vector is Inverse Discrete Fourier Transform (IDFT) modulated obtaining $\mathbf{x}_t = \frac{1}{\sqrt{N}}\mathbf{F}^H\mathbf{x}$. The $N\times 1$ $\mathbf{x}_t$ vector is the time-domain conveyed signal and the $N \times N$ matrix $\mathbf{F}$ corresponds to the normalized DFT where each element can be denoted as $[\mathbf{F}]_{p,q} = \mathrm{e}^{\frac{-j2\pi pq}{N}}$. To avoid the inter-block interference (IBI) a cyclic prefix (CP) has to be inserted . It is assumed the presence of a discrete channel impulse response represented by the $L\times 1$ vector $\mathbf{h}$ where L represents the channel coefficients, $\{h_\ell\}_{\ell=0}^{L-1}$. The channel is assumed to be Rayleigh with variance of ${\sigma_{h_\ell}}^2$ and zero mean. To reduce the interpolation error of the channel estimation at pilot positions, the condition $N_{\mathrm{P}} \geq L$ must be satisfied. The channel is assumed to be quasi-stationary which implies that it only changes each K multicarrier symbols. The CP is removed at the receiver assuming perfect synchronization. Then, the received signal will be expressed as

$$\mathbf{r} = \mathbf{H}\mathbf{x} + \mathbf{w}, \tag{3.2.16}$$

$$\mathbf{r} = \mathbf{H}(\mathbf{I} - \alpha_{\mathrm{d}}\mathbf{J})\mathbf{M}\mathbf{s} + \mathbf{H}\mathbf{J}\mathbf{c} + \mathbf{w}. \tag{3.2.17}$$

Note that $\mathbf{H}$ is a diagonal matrix of dimensions $N\times N$ where the diagonal vector is the channel frequency response $\mathbf{h}_f = \mathbf{F}_L\mathbf{h}$ ($\mathbf{F}_L$ consists in the left $N\times L$ submatrix of $\mathbf{F}$), and the additive white Gaussian noise (AWGN) is represented by the $N\times 1$ $\mathbf{w}$ vector $\mathbf{w} \sim (0, \sigma_W^2)$. $\mathbf{h}_f$ is composed of random variables with zero mean and a variance of $\sigma_H^2 = \sum_{\ell=0}^{L-1} \sigma_{h_\ell}^2$. The signal-to-noise ratio (SNR) at the receiver can be denoted as

$$\rho_{snr} = \frac{\mathcal{P}}{N}\frac{\sigma_H^2}{\sigma_W^2}. \tag{3.2.18}$$

Table 3.1: Channel estimation (CE) error for ST and PSAM techniques

CE OFDM technique	CE	$\sigma^2_{\Delta_h}$
Huang *et. al.* [63]	LS	$\frac{L}{K\beta\mathcal{P}}\left(\frac{\mathcal{P}_S\sigma_H^2}{N}+\sigma_W^2\right)$
Dou *et. al.* [60]	LS	$\frac{L\sigma_W^2}{K\beta\mathcal{P}}$
Gayosso *et. al.* [59]	LS	$\frac{L\sigma_W^2}{K\beta\mathcal{P}}$
PDST	LS	$\frac{L}{K\beta\mathcal{P}}\left[\frac{\mathcal{P}_{\mathbf{s}}(1-\alpha_{\mathrm{d}})^2\sigma_H^2}{N-N_{\mathrm{P}}+N_{\mathrm{P}}(1-\alpha_{\mathrm{d}})^2}+\sigma_{\mathbf{w}}^2\right]$
PSAM	LS	$\frac{L\sigma_W^2}{K\beta\mathcal{P}}$

3.3 Channel Estimation

Taking into account the least squares (LS) channel estimator deduced in [63], it is possible to say that

$$\begin{aligned}\hat{\mathbf{h}}_{LS} =&(\tilde{\mathbf{F}}_L^H\tilde{\mathbf{F}}_L)^{-1}\tilde{\mathbf{F}}_L^H\mathbf{\Lambda}\mathbf{r}_{\mathcal{I}_0^\perp}\\ =&\frac{1}{N_{\mathrm{P}}}\tilde{\mathbf{F}}_L^H\mathbf{\Lambda}\mathbf{r}_{\mathcal{I}_0^\perp}\end{aligned} \tag{3.3.19}$$

where $\tilde{\mathbf{F}}_L$ corresponds to a submatrix of size $N_{\mathrm{P}}\times L$ from $\mathbf{F}_L$ (N_{P}-pilot rows of $\mathbf{F}_L$). $\mathbf{\Lambda}$ corresponds to a diagonal matrix of size $N_{\mathrm{P}}\times N_{\mathrm{P}}$, composed by the inversion of each non zero value of the pilot vector ($\mathbf{c}_{\mathcal{I}_0^\perp}$), $\mathrm{diag}\{\mathbf{\Lambda}\} = [\mathbf{c}_{\mathcal{I}_0^\perp}]^{-1}$, where the vector $\mathbf{r}_{\mathcal{I}_0^\perp}$ is the $N_{\mathrm{P}}\times 1$ array composed of the *pilot-data* symbols of $\mathbf{r}$. Taking into account the quasi-stationary condition, the channel estimation can be improved through the averaging over K multicarrier symbols. Now,

$$\hat{\mathbf{h}}_{LS} = \frac{1}{N_{\mathrm{P}}}\tilde{\mathbf{F}}_L{}^H\mathbf{\Lambda}\frac{1}{K}\sum_{t=0}^{K-1}\mathbf{r}^t_{\mathcal{I}_0^\perp} \tag{3.3.20}$$

where the signal received at tth OFDM symbol is denoted as $\mathbf{r}^t_{\mathcal{I}_0^\perp}$. Then, substituting $\bar{\mathbf{r}} = \sum_{t=0}^{K-1}\mathbf{r}^t_{\mathcal{I}_0^\perp}$ on (3.3.20) the time-domain channel impulse response estimation can be represented as

$$\hat{\mathbf{h}}_{LS} = \frac{1}{N_{\mathrm{P}}}\frac{1}{K}\tilde{\mathbf{F}}_L{}^H\mathbf{\Lambda}\bar{\mathbf{r}}. \tag{3.3.21}$$

Note that from (3.2.17), we can say that $\bar{\mathbf{r}} = \mathbf{H}_{\mathcal{I}_0^\perp}(1-\alpha_{\mathrm{d}})\overline{\mathbf{Ms}}+\mathbf{H}_{\mathcal{I}_0^\perp}\overline{\mathbf{c}}+\overline{\mathbf{w}}$. Here, $\mathbf{H}_{\mathcal{I}_0^\perp}$ consists in a diagonal matrix of size $N_{\mathrm{P}}\times N_{\mathrm{P}}$ which is a submatrix of $\mathbf{H}$ containing

in its diagonal the N_{P} elements indicated in the $\mathcal{I}_0^{\perp}$ index set; the vectors $\overline{\mathbf{Ms}}$, $\overline{\mathbf{c}}$ and $\overline{\mathbf{w}}$ of size $N_{\mathrm{P}}\times 1$ are similarly defined as $\overline{\mathbf{r}}$. Now, expanding (3.3.21), it is possible to say that

$$\hat{\mathbf{h}}_{LS} = \mathbf{h} + \frac{1}{N_{\mathrm{P}}}\frac{1}{K}\tilde{\mathbf{F}}_L^H \mathbf{\Lambda}\left[(1-\alpha_{\mathrm{d}})\mathbf{H}_{\mathcal{I}_0^{\perp}}\overline{\mathbf{Ms}} + \overline{\mathbf{w}}\right]. \tag{3.3.22}$$

The precoding scheme and the factor $(1-\alpha_{\mathrm{d}})$ can be seen in this last expression which can help to reduce the data-interference. Now, it is possible to observe that the quality of the channel estimation is dependent on α_{d} and K. Let us call $\mathbf{v} = \frac{1}{K}[(1-\alpha_{\mathrm{d}})\mathbf{H}_{\mathcal{I}_0^{\perp}}\overline{\mathbf{Ms}} + \overline{\mathbf{w}}]$ as the data interference and noise vector in frequency-domain with zero mean and a covariance matrix $\mathbf{R}_{\mathbf{v}} = E[\mathbf{v}\mathbf{v}^H]$, where $E[\cdot]$ denotes the expected value, with the following form:

$$\mathbf{R}_{\mathbf{v}} = \frac{1}{K}\left[\frac{\mathcal{P}_{\mathbf{s}}(1-\alpha_{\mathrm{d}})^2\sigma_H^2}{N - N_{\mathrm{P}} + N_{\mathrm{P}}(1-\alpha_{\mathrm{d}})^2} + \sigma_{\mathbf{w}}^2\right]\mathbf{I}_P \tag{3.3.23}$$

with $\mathbf{I}_P$ being a $N_{\mathrm{P}} \times N_{\mathrm{P}}$ identity matrix. Considering that $\mathbf{R}_{\mathbf{v}}$ is zero mean, it is possible to conclude that the channel estimator is unbiased [64]. The LS channel estimator variance could be denoted as $\sigma_{\hat{h}_{LS}} = L\frac{\sigma_{\mathbf{v}}^2}{\beta\mathcal{P}}$. Note that the channel estimation errors for different techniques can be seen in Table 3.1.

3.4 Data Detection

In this chapter, an LS and minimum mean squared error (MMSE) equalizers are constructed for *pilot-data* and *data* subcarriers, in the same way as done in [60]. The equalizer matrix consists in a diagonal matrix $\mathrm{diag}\{\mathbf{G}\} = [g_0, ..., g_{N-1}]$ whose diagonal is composed of elements of LS technique $g_k = \frac{1}{([\hat{\mathbf{h}}_f]_k)}, k \in \mathcal{I}_0^{\perp}$ for *pilot-data* subcarriers, and an MMSE technique $g_k = \frac{([\hat{\mathbf{h}}_f]_k)}{([\hat{\mathbf{h}}_f]_k)^2 + \sigma_{\mathbf{w}}^2}, k \in \mathcal{I}_0$ for *data* subcarriers, where $\hat{\mathbf{h}}_f$ is the frequency-domain channel estimation $\hat{\mathbf{h}}_f = \mathbf{F}_L\hat{\mathbf{h}}$.

The equalization can be expressed as

$$\mathbf{Gr} = \mathbf{GH}(\mathbf{I} - \alpha_{\mathrm{d}}\mathbf{J})\mathbf{Ms} + \mathbf{GHJc} + \mathbf{Gw}. \tag{3.4.24}$$

Table 3.2: Complexity of the receiver

Operation	Expression	Times	CM$^+$
Op. 1	$\mathbf{G}$	1	N
Op. 2	$\mathbf{M}^H(\mathbf{I}-\mathbf{J})\mathbf{y}$, where $\mathbf{y}=(\mathbf{I}-\mathbf{J})\mathbf{G}\mathbf{r}+\frac{1}{1-\alpha_\mathrm{d}}\mathbf{J}(\mathbf{G}\mathbf{r}-\mathbf{J}\mathbf{c})$	1	N^2
Op. 3	$\mathbf{M}^H\mathbf{J}\mathbf{M}\hat{\mathbf{s}}^{i-1}$	#it	0

$^+$ A similar analysis was done in [62]. CM means complex multiplications.

For simpler analysis of the technique, it is assumed that $\mathbf{GH}\cong\mathbf{I}$. Then, taking into account the expansion of $(\mathbf{I}-\alpha_\mathrm{d}\mathbf{J})\mathbf{M}\mathbf{s}$ to $(\mathbf{I}-\mathbf{J})\mathbf{M}\mathbf{s}+(1-\alpha_\mathrm{d})\mathbf{J}\mathbf{M}\mathbf{s}$, it is possible to obtain

$$\mathbf{G}\mathbf{r}=(\mathbf{I}-\mathbf{J})\mathbf{M}\mathbf{s}+(1-\alpha_\mathrm{d})\mathbf{J}\mathbf{M}\mathbf{s}+\mathbf{J}\mathbf{c}+\mathbf{w} \tag{3.4.25}$$

and sorting the elements of the previous equation, we can say that

$$\mathbf{G}\mathbf{r}-\mathbf{J}\mathbf{c}=(\mathbf{I}-\mathbf{J})\mathbf{M}\mathbf{s}+(1-\alpha_\mathrm{d})\mathbf{J}\mathbf{M}\mathbf{s}+\mathbf{w}. \tag{3.4.26}$$

The power of data symbols, that overlays N_P pilots, is controlled by $(1-\alpha_\mathrm{d})$. To obtain the original data signal, $\frac{\mathbf{J}}{1-\alpha_\mathrm{d}}$ is incorporated to (3.4.26). Now, considering $\mathbf{J}^2=\mathbf{J}$ and $\mathbf{J}(\mathbf{I}-\mathbf{J})=\mathbf{0}_{N\times N}$

$$\frac{1}{1-\alpha_\mathrm{d}}\mathbf{J}(\mathbf{G}\mathbf{r}-\mathbf{J}\mathbf{c})=\mathbf{J}\mathbf{M}\mathbf{s}+\frac{\mathbf{J}}{1-\alpha_\mathrm{d}}\mathbf{w}. \tag{3.4.27}$$

Then, using (3.4.27), it is possible to recover the *superimposed information*. Furthermore, the *non-superimposed one* is obtained including the factor $(\mathbf{I}-\mathbf{J})$ in (3.4.25)

$$\begin{aligned}(\mathbf{I}-\mathbf{J})\mathbf{G}\mathbf{r}=&(\mathbf{I}-\mathbf{J})(\mathbf{I}-\mathbf{J})\mathbf{M}\mathbf{s}+(\mathbf{I}-\mathbf{J})(1-\alpha_\mathrm{d})\mathbf{J}\mathbf{M}\mathbf{s}\\&+(\mathbf{I}-\mathbf{J})\mathbf{J}\mathbf{c}+(\mathbf{I}-\mathbf{J})\mathbf{w}.\end{aligned} \tag{3.4.28}$$

Knowing that $(\mathbf{I}-\mathbf{J})^2=(\mathbf{I}-\mathbf{J})$,

$$(\mathbf{I}-\mathbf{J})\mathbf{G}\mathbf{r}=(\mathbf{I}-\mathbf{J})\mathbf{M}\mathbf{s}+(\mathbf{I}-\mathbf{J})\mathbf{w}. \tag{3.4.29}$$

Table 3.3: Detection algorithms used in ST

ST OFDM technique	Data detection	Rec. complexity
Dou *et. al.* [60]	see (10) (11) from [60]	$N+N(N-N_{\mathrm{P}})$
Gayosso *et. al.* [59]	see (19)-(22) from [59]	N^2
PDST	$\hat{\mathbf{s}}^i=\lfloor \mathbf{M}^H(\mathbf{I}-\mathbf{J})\mathbf{y}+\mathbf{M}^H\mathbf{J}\mathbf{M}\hat{\mathbf{s}}^{i-1}\rfloor$	$N+N^2$

Summing the equations (3.4.27) and (3.4.29), it is possible to obtain that

$$(\mathbf{I}-\mathbf{J})\mathbf{G}\mathbf{r}+\frac{1}{1-\alpha_{\mathrm{d}}}\mathbf{J}(\mathbf{G}\mathbf{r}-\mathbf{J}\mathbf{c})=\mathbf{M}\mathbf{s}+(\mathbf{I}-\mathbf{J})\mathbf{w}+\mathbf{J}\frac{\mathbf{w}}{1-\alpha_{\mathrm{d}}}. \tag{3.4.30}$$

From the left-hand part of this expression, the recovering model, denoted as $\mathbf{y}$, can be obtained. At the right-hand side, it is possible to see the original signal and the AWGN noise that affects the system.

$$\mathbf{y}=\mathbf{M}\mathbf{s}+(\mathbf{I}-\mathbf{J})\mathbf{w}+\mathbf{J}\frac{\mathbf{w}}{1-\alpha_{\mathrm{d}}}. \tag{3.4.31}$$

Considering that $\mathbf{M}^H\mathbf{M}=\mathbf{I}$ and knowing that the data signal is precoded, the recovered information will be obtained using $\tilde{\mathbf{s}}=\mathbf{M}^H\mathbf{y}$. So, it is possible to say that

$$\tilde{\mathbf{s}}=\mathbf{s}+\mathbf{M}^H(\mathbf{I}-\mathbf{J})\mathbf{w}+\mathbf{M}^H\mathbf{J}\frac{\mathbf{w}}{1-\alpha_{\mathrm{d}}}. \tag{3.4.32}$$

Now, the data detector can be constructed using an iterative loop algorithm being its hard decision as follows $\hat{\mathbf{s}}^0=\lfloor\tilde{\mathbf{s}}\rfloor$, where the minimum-distance detector is represented as $\lfloor . \rfloor$. The soft ith iterations are defined as follows

$$\hat{\mathbf{s}}^i=\lfloor \mathbf{M}^H(\mathbf{I}-\mathbf{J})\mathbf{y}+\mathbf{M}^H\mathbf{J}\mathbf{M}\hat{\mathbf{s}}^{i-1}\rfloor. \tag{3.4.33}$$

Note that the $(\mathbf{I}-\mathbf{J})$ positions of $\mathbf{y}$ were unspread and summed to $\mathbf{J}$ positions values obtained from the last iteration $\hat{\mathbf{s}}^{i-1}$.

3.5 Analysis of the average system capacity

The average system capacity expression, as defined in [63] [65] [66], can be denoted as follows

$$C = \frac{1}{N}\sum_{k=0}^{N-1} E\{\log_2(1+|g|^2\rho_k)\} \tag{3.5.34}$$

where ρ_k corresponds to the SNR applied to the kth subcarrier, and $g\sim(0,1)$ corresponds to a random variable with zero mean and unitary variance. The average system capacity is dependent on the power allocation factor and the interference control factor, β and α_{d}, respectively, and can be represented as

$$C(\alpha_{\mathrm{d}},\beta) = \frac{1}{N}E\left\{\sum_{k\in\mathcal{I}_0} log_2(1+|g|^2\rho_k) + \sum_{k\in\mathcal{I}_0^{\perp}} log_2(1+|g|^2\rho_k)\right\}. \tag{3.5.35}$$

Then, using a similar approximation as in [(22)- [63]], it is possible to say that

$$\begin{aligned} C(\alpha_{\mathrm{d}},\beta) = \; & \frac{N-N_{\mathrm{P}}}{N}E\{log_2(1+|g|^2\rho_{NST})\}+ \\ & \frac{N_{\mathrm{P}}}{N}E\{log_2(1+|g|^2\rho_{ST})\}. \end{aligned} \tag{3.5.36}$$

ρ_k when the $k\in\mathcal{I}_0$ can be recalled as ρ_{NST}, and, ρ_k when $k\in\mathcal{I}_0^{\perp}$ can be represented as ρ_{ST}.

In the case of *pilot-data* subcarriers ($k\in\mathcal{I}_0^{\perp}$), ρ_{ST} can be defined similarly as in [63] as follows

$$\rho_{ST} = \frac{\sigma_H^2 - \sigma_{\Delta_h}^2}{\sigma_{\Delta_h}^2 \frac{E[|\tilde{\mathbf{x}}|^2]+\frac{\beta\mathcal{P}}{N_{\mathrm{P}}}}{E[|\tilde{\mathbf{x}}|^2]} + \frac{\sigma_W^2}{E[|\tilde{\mathbf{x}}|^2]}} \tag{3.5.37}$$

where the expected value $E[|\tilde{\mathbf{x}}|^2]$ and $\sigma_{\Delta_h}^2$ are denoted as in (3.2.14) and (3.3.23), respectively. Using (3.2.14), (3.2.18) and (3.3.23), the channel estimation error as a function of the channel power can be defined as

$$\frac{\sigma_{\Delta_h}^2}{\sigma_H^2} = \frac{L}{\beta K}\left[\frac{(1-\beta)(1-\alpha_{\mathrm{d}})^2}{N-N_{\mathrm{P}}+N_{\mathrm{P}}(1-\alpha_{\mathrm{d}})^2} + \frac{1}{N\rho_{snr}}\right] \tag{3.5.38}$$

Table 3.4: System Parameters

Parameter	Value
Subcarrier number (N)	64, 128, 256
Pilot number (N_{P})	8, 16, 32
Modulation scheme	QPSK, 16QAM
Number of multicarrier symbols (K)	10, 20
Channel distribution	Rayleigh
Taps number (L)	8
CP length	8

and then, the ratio of the noise variance and the channel power can be seen as

$$\frac{\sigma_W^2}{\sigma_H^2}\frac{1}{E[|\tilde{\mathbf{x}}|^2]} = \frac{N - N_{\mathrm{P}} + N_{\mathrm{P}}(1-\alpha_{\mathrm{d}})^2}{\rho_{snr} N(1-\beta)(1-\alpha_{\mathrm{d}})^2}. \tag{3.5.39}$$

Then, taking into account (3.5.37), (3.5.38) and (3.5.39), ρ_{ST} will be expressed as

$$\rho_{ST} = \frac{(1-\alpha_{\mathrm{d}})^2(1-\beta)\left[1-\frac{L}{\beta K}\left(\frac{(1-\beta)(1-\alpha_{\mathrm{d}})^2}{N-N_{\mathrm{P}}+N_{\mathrm{P}}(1-\alpha_{\mathrm{d}})^2}+\frac{1}{N\rho_{snr}}\right)\right]}{\frac{L}{\beta K}\left[(1-\alpha_{\mathrm{d}})^2+\beta(\frac{N}{N_{\mathrm{P}}}-1)\right]\left[\frac{(1-\beta)(1-\alpha_{\mathrm{d}})^2}{N-N_{\mathrm{P}}+N_{\mathrm{P}}(1-\alpha_{\mathrm{d}})^2}+\frac{1}{N\rho_{snr}}\right]+\frac{N-N_{\mathrm{P}}+N_{\mathrm{P}}(1-\alpha_{\mathrm{d}})^2}{\rho_{snr}N}}. \tag{3.5.40}$$

In the case of *data* subcarriers ($k \in \mathcal{I}_0$), from [(27)- [65]] and (3.2.15), ρ_{NST} is represented as

$$\rho_{NST} = \frac{\sigma_H^2 - \sigma_{\Delta_h}^2}{\sigma_{\Delta_h}^2 + \sigma_W^2 \frac{1}{E[|\tilde{\mathbf{x}}|^2]}}. \tag{3.5.41}$$

Now, the ratio $\sigma_W^2/\sigma_H^2 E[|\tilde{\mathbf{x}}|^2]$ in *data* subcarriers is denoted as follows

$$\frac{\sigma_W^2}{\sigma_H^2}\frac{1}{E[|\tilde{\mathbf{x}}|^2]} = \frac{N - N_{\mathrm{P}} + N_{\mathrm{P}}(1-\alpha_{\mathrm{d}})^2}{(1-\beta)N\rho_{snr}}. \tag{3.5.42}$$

Thus, the variance of the channel estimation error is assumed to be the same as in ST subcarriers, and then, the ratio $\sigma_{\Delta_h}^2/\sigma_W^2$ is the same as in (3.5.38). Taking into account (3.5.38), (3.5.41) and(3.5.42), the signal-to-noise ratio in non-ST subcarriers ρ_{NST} will be denoted as

$$\rho_{NST} = \frac{N\rho_{snr}(1-\beta)\left[1-\frac{L}{\beta K}\left(\frac{(1-\beta)(1-\alpha_{\mathrm{d}})^2}{N-N_{\mathrm{P}}+N_{\mathrm{P}}(1-\alpha_{\mathrm{d}})^2}+\frac{1}{N\rho_{snr}}\right)\right]}{\frac{L(1-\beta)}{\beta K}\frac{N\rho_{snr}(1-\beta)(1-\alpha_{\mathrm{d}})^2}{N-N_{\mathrm{P}}+N_{\mathrm{P}}(1-\alpha_{\mathrm{d}})^2}+1+N-N_{\mathrm{P}}+N_{\mathrm{P}}(1-\alpha_{\mathrm{d}})^2}. \tag{3.5.43}$$

The parameters that maximize the average channel capacity α_{d} and β can be reached through a maximum search taking into account (3.5.36), (3.5.40) and (3.5.43).

$$\begin{aligned} \underset{\alpha_{\mathrm{d}},\beta}{\text{maximize}} \quad & C(\alpha_{\mathrm{d}}, \beta), \\ \text{subject to} \quad & 0 < \alpha_{\mathrm{d}} < 1, \qquad 0 < \beta < 1. \end{aligned} \tag{3.5.44}$$

3.6 Complexity analysis of algorithms

3.6.1 Transmitter

It is necessary to find the values that maximize the average channel capacity. In this case, the corresponding values α_{d} and β can be found using exhaustive search of these values in (3.5.44). Now, assuming that the length of the range of values in $0 < \alpha_{\mathrm{d}} < 1$ and $0 < \beta < 1$ is n, n^2 comparisons are needed, then, the complexity will be in the order of $O(n^2)$. Thus, an off-line exhaustive search and a pre-computed table of values can help to reduce the algorithm complexity.

3.6.2 Receiver

As it has been seen in the previous sections at the receiver several steps are necessary to recover the information. The number of complex multiplications (CM) define the complexity of the algorithm in the data detector which can be computed in a similar way as done in [62]. The complexity analysis can be seen in Tables 3.2 and 3.3. At first step, Op. 1, a matrix for the equalization is built consuming N CM, requiring one complex multiplication per each subcarrier. At second step, Op. 2, the model to recover the information expressed in (3.4.30), needs N times to execute Op. 1 for $\mathbf{y}$ to be built. Note that $N - N_{\mathrm{P}}$ CM are required to recover the information of *data* subcarriers, and then, N_{P} CM are needed to obtain data from the subcarriers at *pilot-data* positions. At the end, no CM are required in step Op. 3. It is important to note that the application of selection matrices and zero and one products do not require

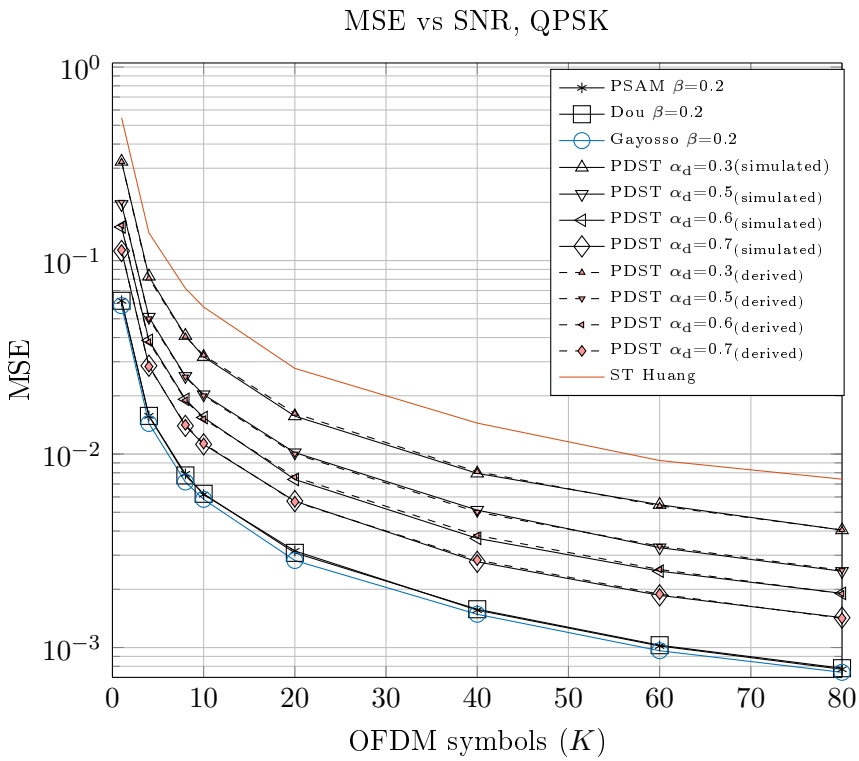

Figure 3-4: MSE for ST and PSAM schemes.

complex operations, then, these ones could be neglected. Thus, $N^2 + N$ complex multiplications are needed at the receiver for PDST algorithm. In Table 3.3, it is shown a comparison of the complexity between several methods. It can be observed that the proposal has a similar complexity than the rest of the algorithms.

3.7 Simulation results

For these scenarios an OFDM transmitter was considered using a subcarrier number of $N = \{64, 128, 256\}$ conveying Quadrature Phase-Shift Keying (QPSK) and Quadrature Amplitude Modulation (16QAM) symbol constellations. For the channel generation it is assumed a Rayleigh distribution taking into account L=8 taps and a power-delay-profile (PDP) of $E[|h_\ell|^2]$=$e^{-\frac{L}{10}\ell}$ [67]. The CP size is considered to be greater or equal to L. The training sequence to be conveyed is chosen to be optimal as in [57–59]. A Hadamard matrix of size $N \times N$ is used as precoder. As it can be seen in the following simulations, this technique has been tested when the channel

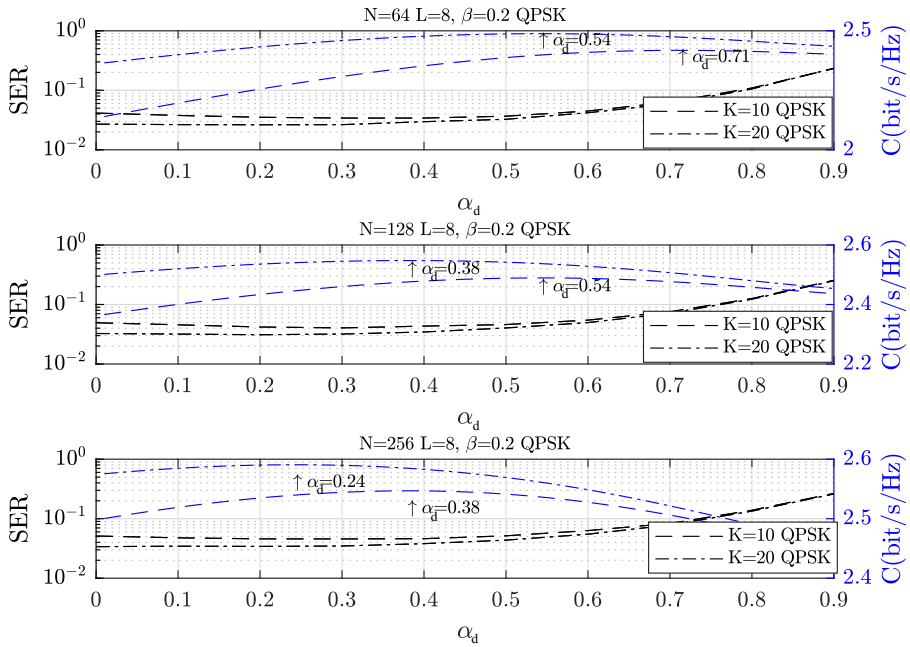

Figure 3-5: Average system capacity and symbol error rate as a function of α_{d} using QPSK and a SNR=10dB.

remains static per K OFDM symbols. Note that parameters of the simulations can be seen in Table 3.4.

3.7.1 Channel estimator performance

As it can be seen in Fig. 3-4, the performance of MSE is presented as a function of the number of multicarrier symbols where the channel remains stationary (K) with a fixed SNR=10dB N=64, N_{P}=8 and β=0.2. Here, it is possible to see that the curves that were analytically derived in (3.3.23) match with the ones obtained through simulations. Several values of α_{d} where used to test and compare this technique with the others in literature. Now, it is possible to see how this proposal can overcome similar approaches from the literature. The obtained gain depends on the interference control factor that was proposed here. Note that PSAM is used as a bound for comparison purposes with other techniques.

It is possible to see that [60] and [59] show a channel estimation performance

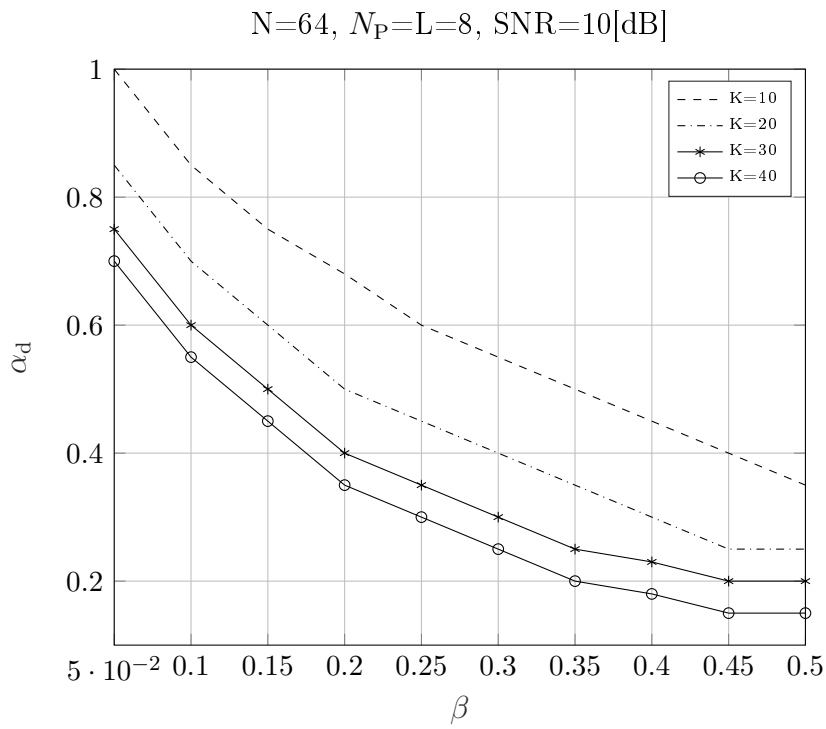

Figure 3-6: Evolution of the interference control factor (α_{d}) as a function of the power allocation factor (β) for different K.

similar to PSAM. PDST channel estimation error equals to PSAM as α_{d} is tuned. And then, SER in PDST proposal is better than [59] and [60] due to the data interference, as it will be illustrated later. Note that SER can be considered as the key parameter rather than MSE for communication systems.

3.7.2 Average capacity performance

For comparison purposes (3.5.36), [(32), (34) [65]] and [(26), (29) [63]] have been considered. The ideal average channel capacity can be denoted as

$$C_{ideal} = \frac{N - N_{\mathrm{P}}}{N} E\{\log_2(1 + \rho_{ideal}|g|^2)\} \tag{3.7.45}$$

where the ideal condition is maintained as N_{P} tends to zero and there is no presence of channel estimation error. Thus, $\rho_{ideal} = \sigma_H^2 \mathcal{P}_S / N\sigma_W^2$ where the data transmission spends the total power.

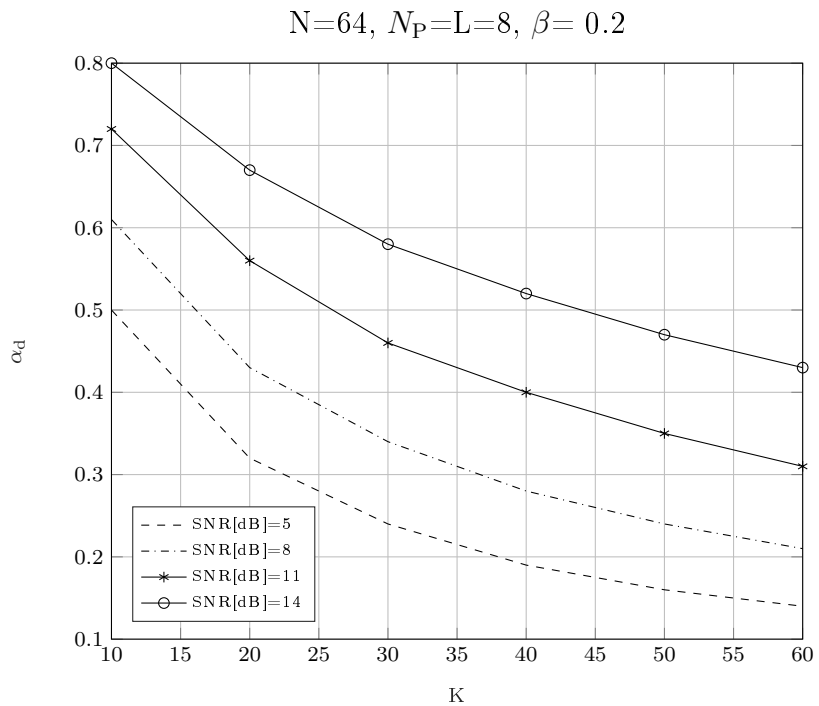

Figure 3-7: Interference control factor (α_d) as a function of K averaged multicarrier symbols

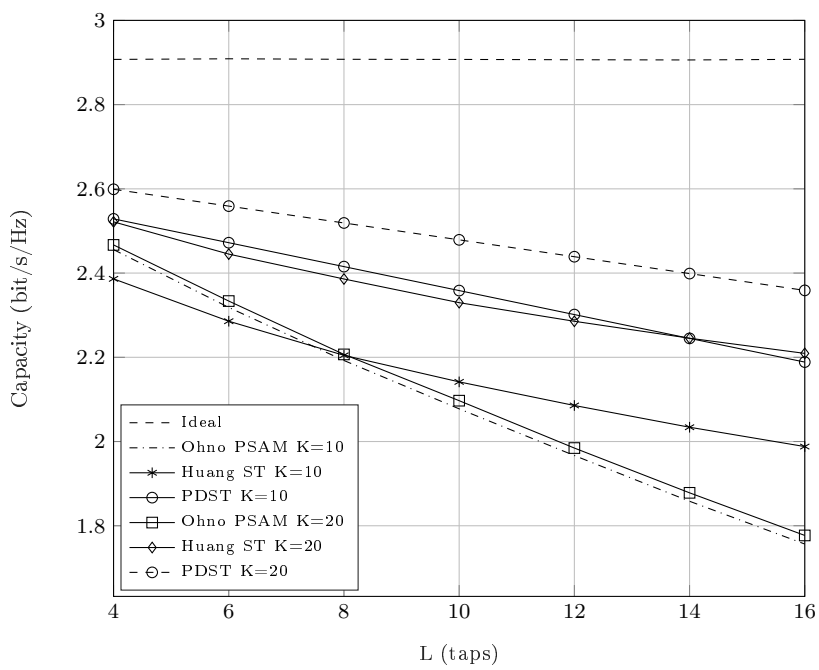

Figure 3-8: Average channel capacity of ST and PSAM considering channels with i.i.d. PDP with $N = 64$ (SNR= $10dB$, $K = 10$ and $K = 20$).

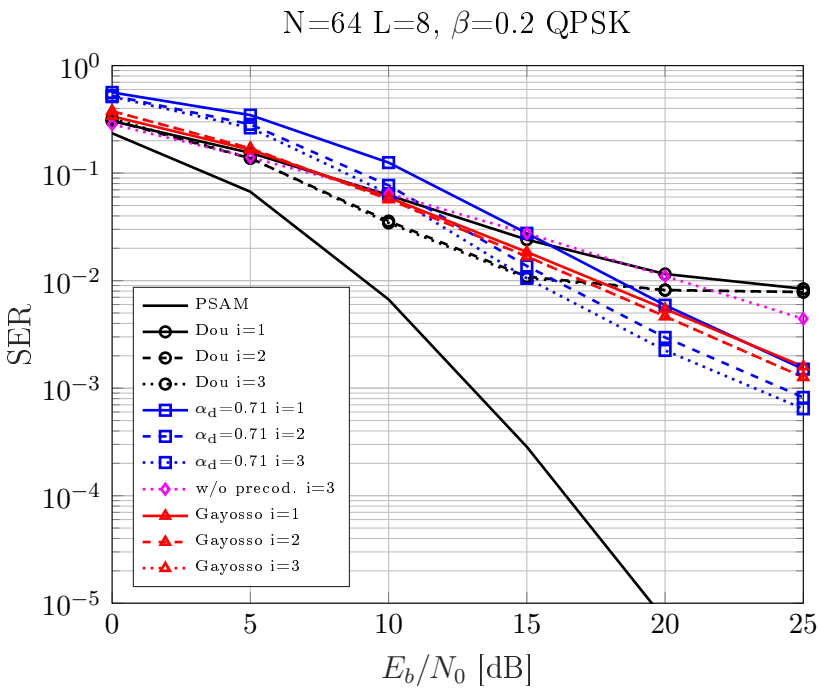

Figure 3-9: Symbol error rate using QPSK modulation and K=10 OFDM symbols with $N = 64$ and $N_{\mathrm{P}} = 8$. The value of $\alpha_{\mathrm{d}} = 0.71$ maximizes the average channel capacity.

In Fig. 3-5, the optimal α_{d} that maximizes (3.5.36) can be found for a fixed β. Then, with these values determined, the SER will be evaluated.

In Fig. 3-5, it is possible to see three subfigures that show the simulation results for N=$\{64, 128, 256\}$, respectively. Here, the subfigures draw curves for K=10 and K=20. It is important to realize that K was chosen as a function of real standards, *e.g.* LTE standardized slots for groups of OFDM symbols as can be seen in [68], and knowing that related works use even larger K as it is explained in [63]. The value of α_{d}, that maximizes the average channel capacity, is highlighted in each subfigure. Note that the values that minimize SER and maximizes the average channel capacity do not coincide exactly because SER considers equalization and data detection steps which modifies the performance and the value of α_{d}. Furthermore, as shown in Fig. 3-5, when K increases the value of α_{d} is reduced.

In Fig. 3-6, it is possible to see the values of α_{d} plotted as a function of β taking into account a SNR=10dB and a range of values of K. It must be noted that the

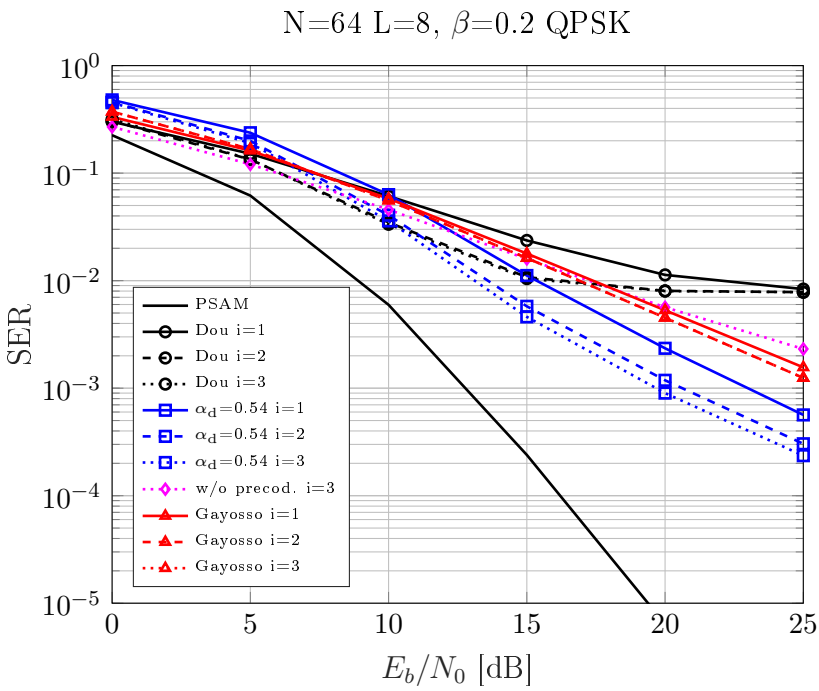

Figure 3-10: Symbol error rate using QPSK modulation and K=20 OFDM symbols with $N = 64$ and $N_{\mathrm{P}} = 8$. The value of $\alpha_{\mathrm{d}} = 0.54$ maximizes the average channel capacity.

more power is assigned to the pilots (β) the better the channel estimation is. Thus, more data could be overlaid in *pilot-data* subcarriers increasing ($1-\alpha_{\mathrm{d}}$).

In Fig. 3-7, we can see that the value of α_{d} decays in the case that K is increased using an specific value of SNR and β. Consequently, with a more static channel, α_{d} reduces or equivalently ($1-\alpha_{\mathrm{d}}$) increases, then a higher quantity of information can be overlaid.

In Fig. 3-8, it is possible to see the average channel capacity for a different channel scenario, considering an independent and identically distributed (i.i.d.) PDP, varying L with $K = 10, 20$. For comparison purposes the average channel capacity is plotted using (3.7.45) for the ideal case, [(32), (34) [65]] for PSAM and [(26), (29) [63]] for ST. Note that each value is obtained using its corresponding α_{d} where $N_{\mathrm{P}} = L$ taps are considered. The performance is evaluated considering a channel that varies every $K = 10, 20$ multicarrier symbols. As it can be seen, PSAM performance curve falls quicker than this proposal because of the influence of the dedicated resources used

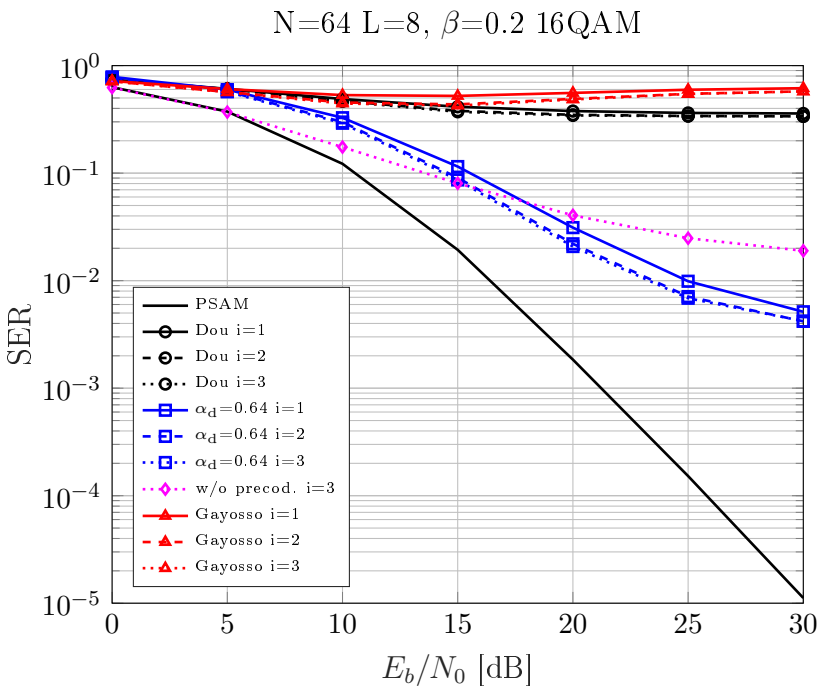

Figure 3-11: Symbol error rate using 16QAM modulation and K=20 OFDM symbols with $N = 64$ and $N_{\mathrm{P}} = 8$. The value of $\alpha_{\mathrm{d}} = 0.64$ maximizes the average channel capacity.

for the pilot transmission. Comparing ST and PDST, it is possible to say that ST is not as good as PDST because the interference generated by the superimposed data is still present for the values of K that were tested. It is important to note that the data-interference of ST, [(26), (29) [63]], can be reduced increasing K. In PDST, the data interference can be controlled by α_{d} and K, what permits to improve the performance at reduced values of K.

3.7.3 Symbol error rate performance

To plot the SER performance of this technique α_{d} was found thought exhaustive search of the value which maximize the average channel capacity as it is explained in (3.5.35). Every compared proposal was simulated considering each iterative detection algorithm proposed for every technique, using 3 iterations and the same quasi-stationarity conditions.

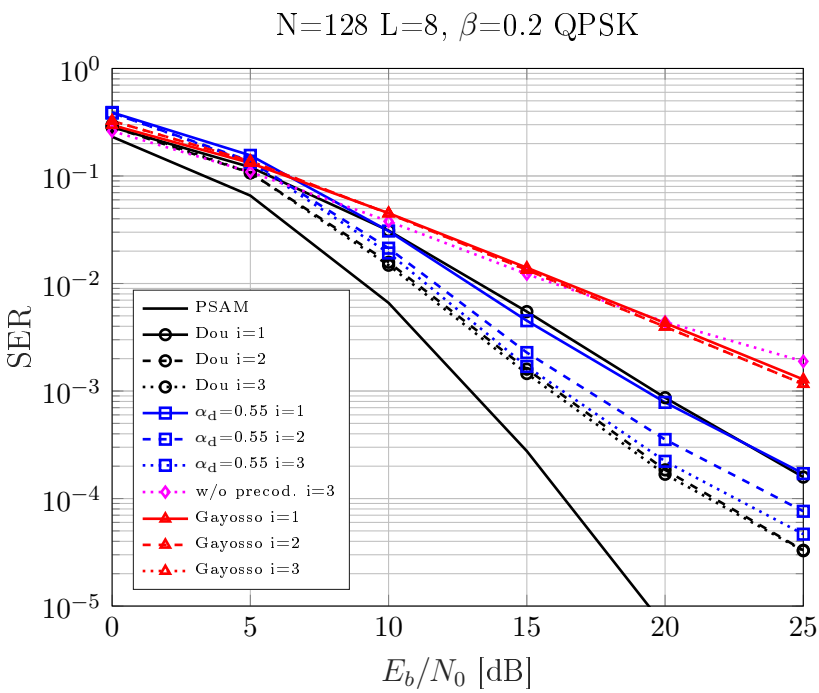

Figure 3-12: Symbol error rate using QPSK modulation and K=20 OFDM symbols with $N = 128$ and $N_{\mathrm{P}} = 8$. The value of $\alpha_{\mathrm{d}} = 0.55$ maximizes the average channel capacity.

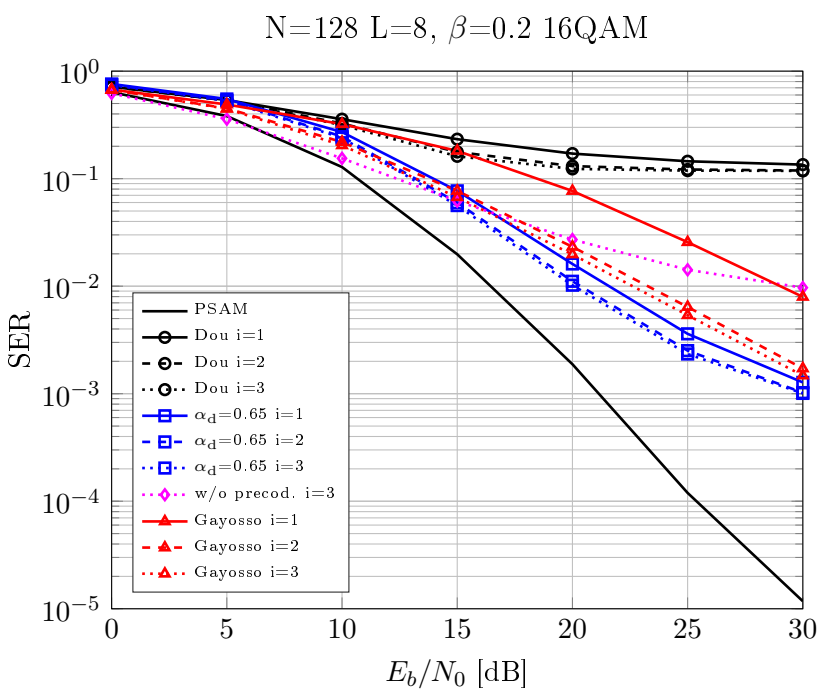

Figure 3-13: Symbol error rate using 16QAM modulation and K=20 OFDM symbols with $N = 128$ and $N_{\mathrm{P}} = 8$. The value of $\alpha_{\mathrm{d}} = 0.65$ maximizes the average channel capacity.

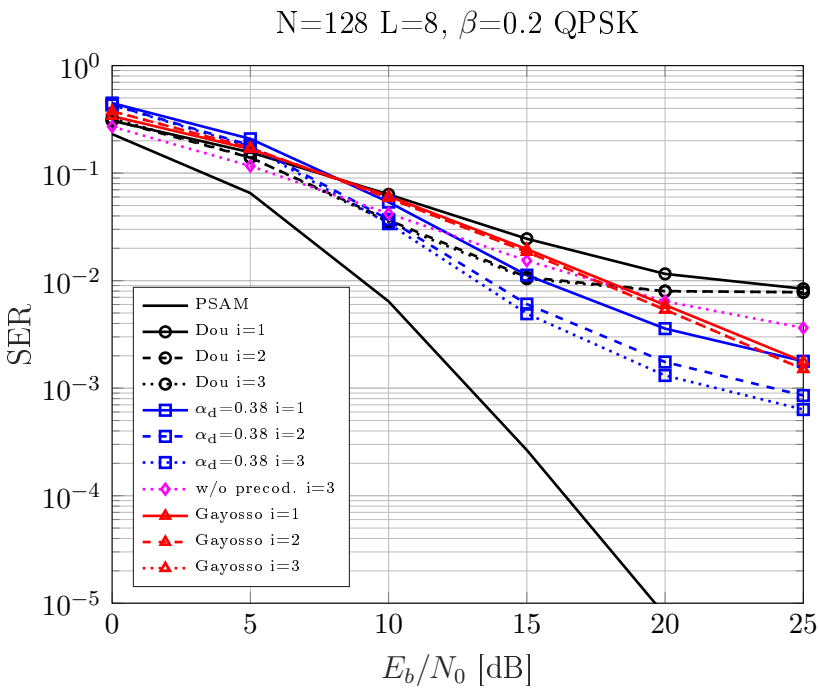

Figure 3-14: Symbol error rate using QPSK modulation and K=20 OFDM symbols with $N = 128$ and $N_{\mathrm{P}} = 16$. The value of $\alpha_{\mathrm{d}} = 0.38$ maximizes the average channel capacity.

As it can be seen in Figs. 3-9-3-17, SER plots using QAM constellation, with $N = \{64, 128, 256\}$ and $K = \{10, 20\}$, are presented. Here, the channel estimation techniques known as SBST [59], DNST [60], PSAM [69] are compared. In Fig. 3-9, it is possible to see the evaluation of the SER performance using K=10, N=64, N_{P}=8 and QPSK constellation symbols, and then, in Fig. 3-10 the SER performance using the same conditions, excepting K=20, is presented. PDST overcomes the other ST proposals in SER performance in these scenarios. Increasing K, it is possible to see that the interference control factor α_{d} is reduced what suggests that a greater data superimposition is permitted.

In Fig. 3-11, the SER performance using a 16QAM constellation with $K = 20$, $N = 64$ and $N_{\mathrm{P}} = 8$ is depicted. Here, it is possible to see that PDST is capable to work with dense constellation as 16QAM showing better results than the other ST techniques.

The SER performance is evaluated in Figs. 3-12 and 3-13, using N=128 and

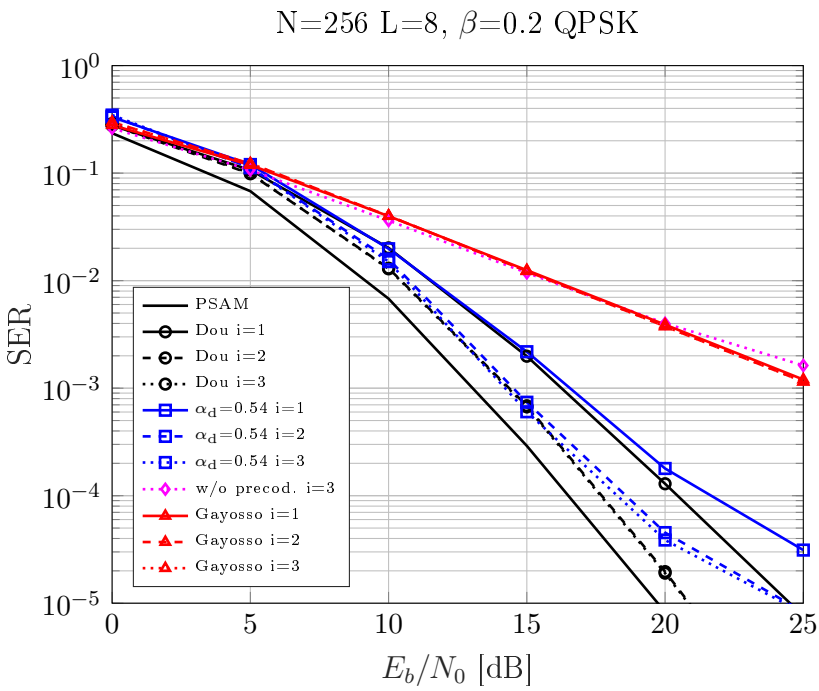

Figure 3-15: Symbol error rate using QPSK modulation and K=20 OFDM symbols with $N = 256$ and $N_{\mathrm{P}} = 8$. The value of $\alpha_{\mathrm{d}} = 0.54$ maximizes the average channel capacity.

$K = 20$, N_{P}=8 with QPSK and 16QAM constellations, respectively. As it can be seen in these figures, DNST can obtain similar results as PDST when transmitting QPSK. Nevertheless, PDST is preferable when conveying a denser constellation as 16QAM. Then, Fig. 3-14 shows the SER performance for N=128 and $K = 20$ with N_{P}=16 using QPSK.

Figs. 3-15 and 3-16 evaluate the SER performance using N=256, N_{P}=8 with QPSK and 16QAM constellations, respectively. From these results it is possible to say that our proposal is robust when employing 16QAM constellations.

Fig. 3-17 shows the SER performance when N=256, N_{P}=32, $K = 20$ and QPSK are used. Comparing previous Figs. 3-14 and 3-17, it is possible to see that PDST has a better performance than [59] and [60] when an increasing number of pilots is used.

The PSAM curve has been included as a bound remembering that it uses dedicated resources to transmit the pilot sequences [70].

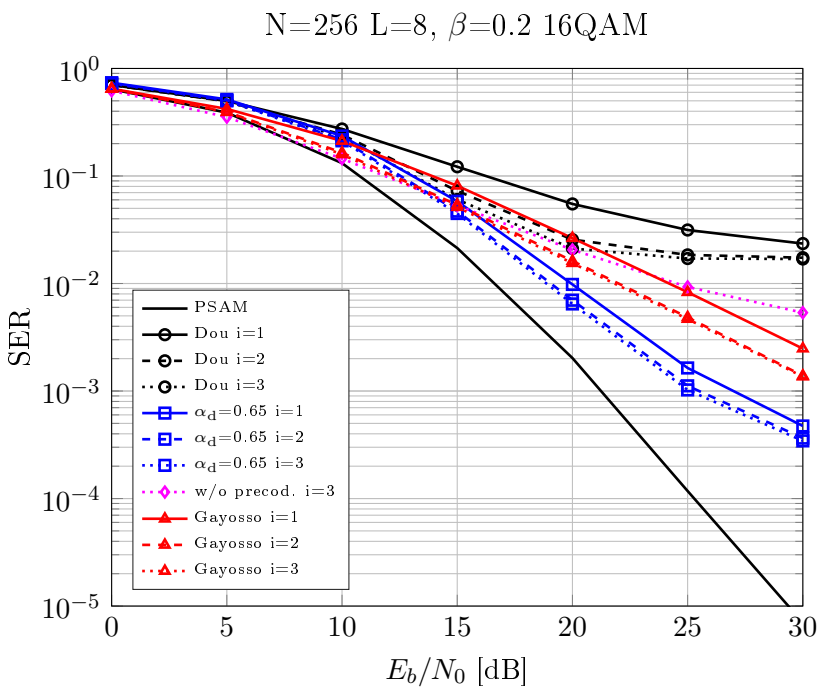

Figure 3-16: Symbol error rate using 16QAM modulation and K=20 OFDM symbols with $N = 256$ and $N_{\mathrm{P}} = 8$. The value of $\alpha_{\mathrm{d}} = 0.65$ maximizes the average channel capacity.

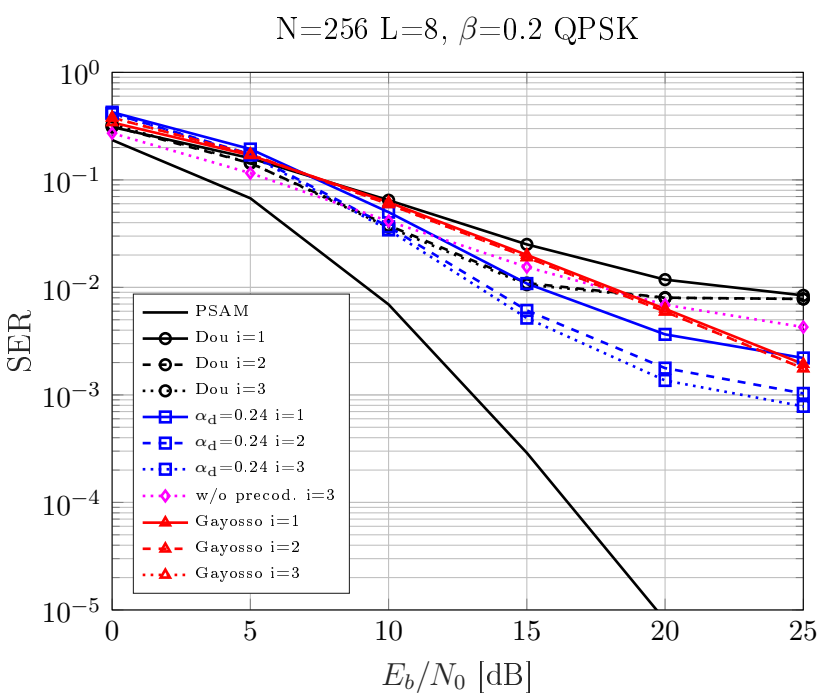

Figure 3-17: Symbol error rate using QPSK modulation and K=20 OFDM symbols with $N = 256$ and $N_{\mathrm{P}} = 32$. The value of $\alpha_{\mathrm{d}} = 0.24$ maximizes the average channel capacity.

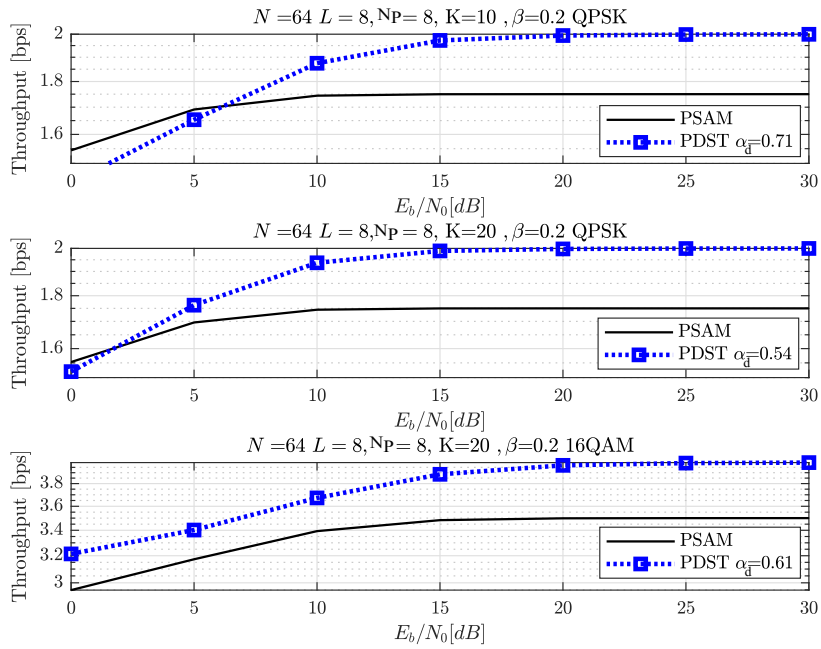

Figure 3-18: Throughput analysis using PSAM and PDST.

As a reference, the PDST technique avoiding the use of precoding has been included. Here, it is possible to see, specially at high SNR, how the SER performance is improved using a precoder.

3.7.4 Throughput Analysis

In order to compare these techniques, the throughput can be used as a metric which can be defined as the number of bits correctly conveyed per unit of time. Thus, as can be seen in [71], it can be represented as

$$R_t = \frac{N - N_{\mathrm{P}}}{N} \frac{N_t \left(1 - \mathrm{BER}\right)}{T}. \tag{3.7.46}$$

Assuming that Gray encoding was used, it can be said that the bit error rate (BER) $\mathrm{BER} \approx \frac{\mathrm{SER}}{N_t}$, where N_t represents the number of bits to be conveyed per complex symbol and T is the transmission time that in this case has been assumed to be $T = 1s$.

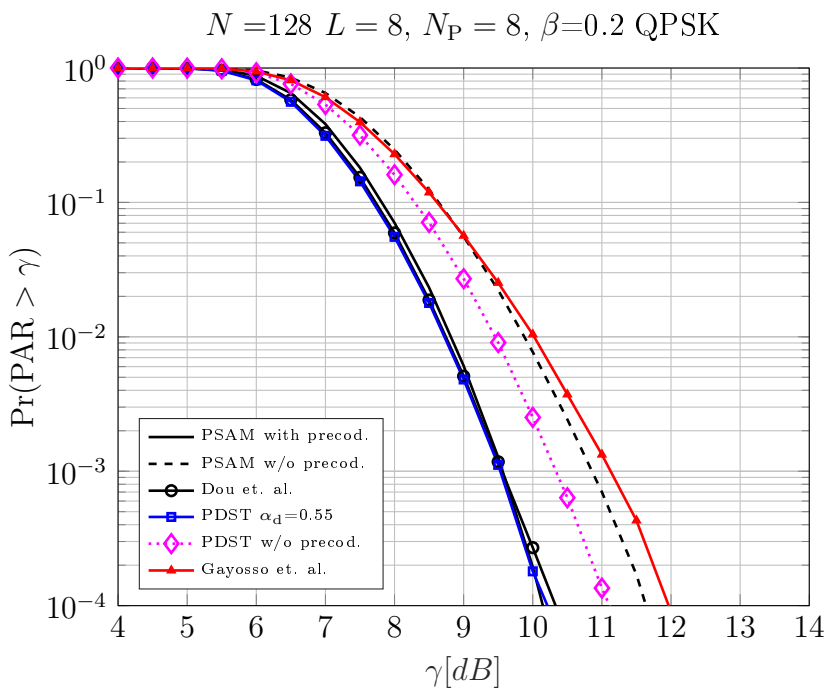

Figure 3-19: Comparison of the PAR performance using its CCDF of ST techniques with $N = 128$ and $N_{\mathrm{P}} = 8$.

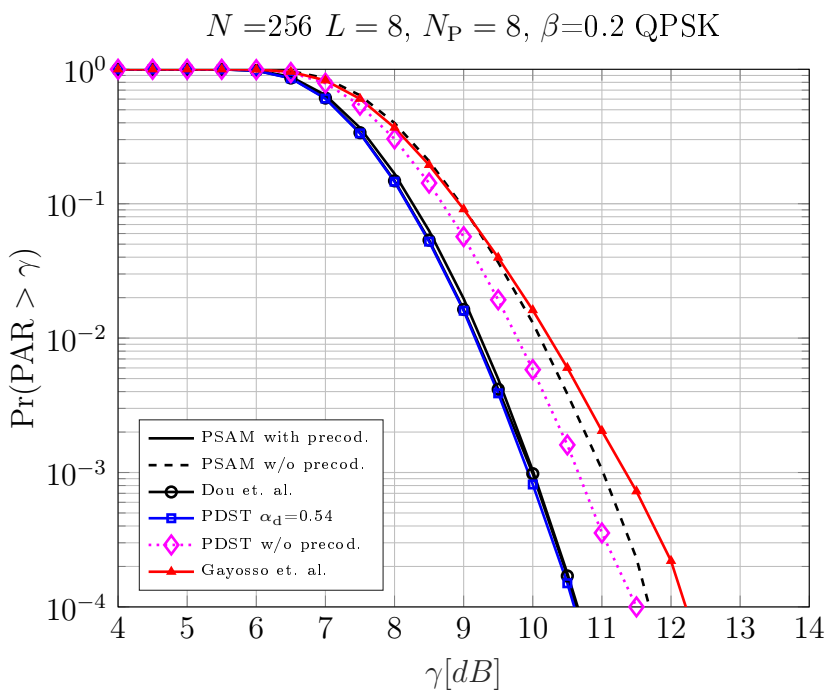

Figure 3-20: Comparison of the PAR performance using its CCDF of ST techniques with $N = 256$ and $N_{\mathrm{P}} = 8$.

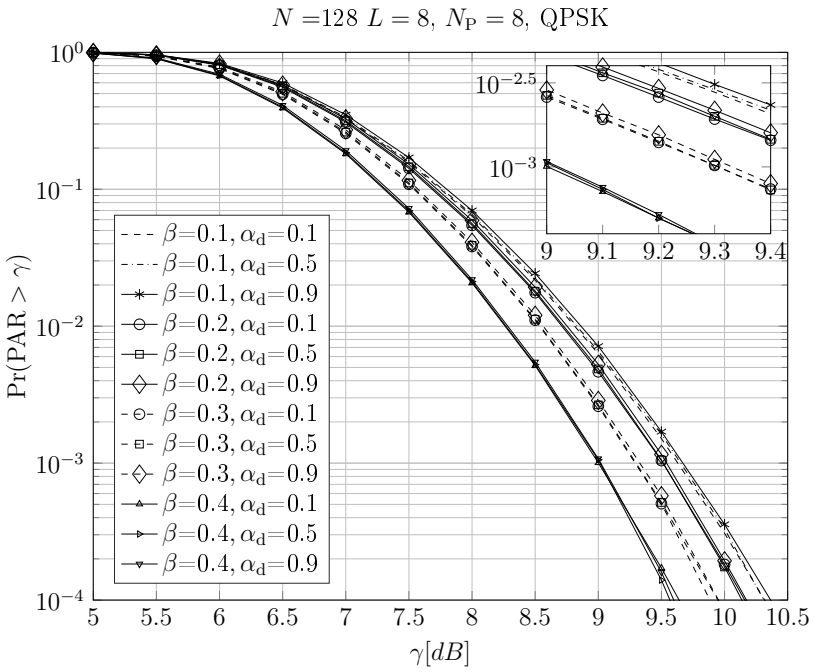

Figure 3-21: Comparison of the PAR performance for PDST using its CCDF changing α_{d} and β with $N = 128$ and $N_{\mathrm{P}} = 8$.

In Fig. 3-18, the subcarrier throughput using $N = 64$ has been depicted. Using QPSK, in the first and second plots, the effects of the stationarity can be seen through the variation of K. If the parameter K is high, a better throughput can be reached.

In the third plot, the throughput is represented using a 16QAM constellation to compare the schemes. It is important to say that in ST schemes, where no dedicated resources were used for pilot transmission, $\frac{N-N_{\mathrm{P}}}{N} = 1$ has to be assumed. In the rest of scenarios, the performance follows a similar behavior as the one in Fig. 3-18.

3.7.5 PAR performance

In this proposal, the complementary cumulative distribution function (CCDF) was used to analyze the PAR in PDST proposal. This can be defined as

$$\mathrm{CCDF}(\gamma) = \Pr(\mathrm{PAR} > \gamma) \tag{3.7.47}$$

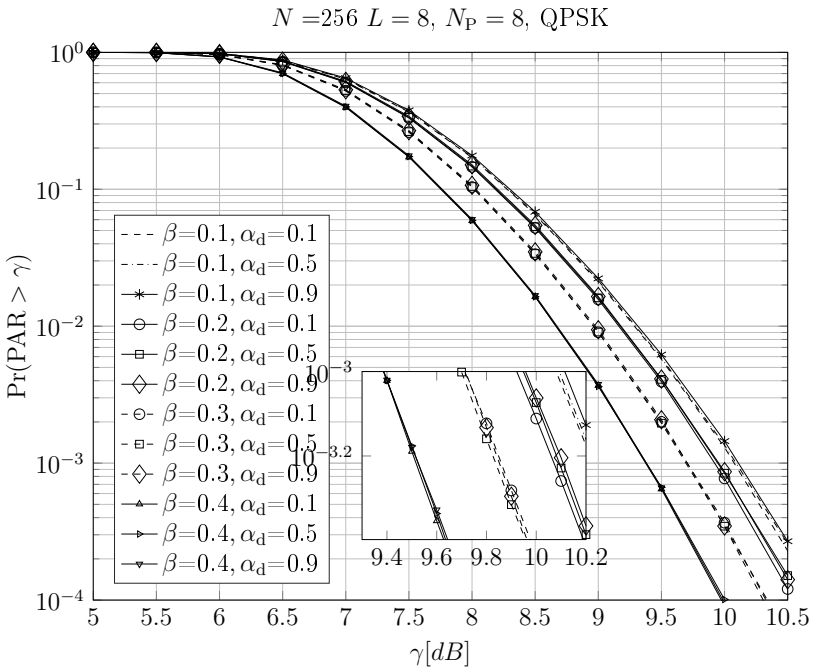

Figure 3-22: Comparison of the PAR performance for PDST using its CCDF changing α_{d} and β with $N = 256$ and $N_{\mathrm{P}} = 8$.

where the definition of PAR can be seen in [72]. Figs. 3-19 and 3-20, compare the PAR performance of ST and PSAM techniques. Here, it is possible to see that the techniques PDST and DNST perform similarly as [59] and PDST without precoding. Note that PAR depends on the nature of the pilot sequence, thus, we have used training sequences that have been designed to avoid high PAR in OFDM transmissions as the ones used in [57].

In Figs. 3-21 and 3-22, it is possible to see that the CCDF for PDST decreases with an increasing β. From the same figures, it can be seen a reduced deterioration with the variation of α_{d} when β takes low values. Thus, increasing power assigned to the training sequence, β, makes the degradation in PAR negligible. Similar results changing β were mentioned in [72].

Chapter 4

Superimposed training in FBMC-based systems

In this chapter, we analyze the application of superimposed training technique (ST) for channel estimation over a new waveform known as filterbank multicarrier offset quadrature amplitude modulation (FBMC-OQAM). As it is explained in previous chapters FBMC-OQAM presents better spectral efficiency than orthogonal frequency division multiplexing (OFDM) due to the fact that it avoids the use of cyclic prefix (CP) using well localized filters which reduce the spectral leakage between subcarriers. The main drawback of this technique consists in the generation of an intrinsic self-interference provoked by the neighboring OQAM symbols. In this case, to avoid the effects of inter-symbol interference this technique transmits longer multicarrier symbols.

The superimposed training improves the spectral efficiency in comparison with pilot symbol assisted modulation (PSAM) techniques given that PSAM technique uses dedicated resources wasting valuable bandwidth. The effects of the interference caused by adding the data over the pilot signal in an FBMC-OQAM scenario will be analyzed in this chapter.

4.1 State of the art

In the literature, there are several proposals for channel estimation in OFDM. However, not every channel estimation in technique can be successfully applied to this new waveform. This is because of the intrinsic interference caused by the prototype filters and data symbols around [47]. Some channel estimation techniques using FBMC-OQAM are proposed in [73] and [74] where scattered and preamble-based pilot techniques are taken into account, respectively.

Some scattered pilot techniques have been proposed in [48–50, 75–77]. The key idea in these techniques implies placing more than one pilot symbol to be conveyed in addition to a processing capacity to counteract the intrinsic self-interference. In this way, the received pilots are free from self-interference, then, the channel state information (CSI) can be obtained in the same way than in any other multicarrier technique. By other side, these techniques have disadvantages related to the greater number of pilots in comparison with OFDM, what affects the spectral efficiency. The techniques that use auxiliary pilots waste energy resources in the added signaling and present an increased peak-to-average power ratio (PAPR). Additional complex operations are required to process the auxiliary pilots and counteract the self-interference.

An interesting investigation is proposed in [78], where the channel capacity in a FBMC-OQAM scenario is presented showing how this multicarrier technique overcomes OFDM. Nevertheless, it is assumed a perfect knowledge of CSI, then, pilots are not considered. Finally, a first approach for ST in FBMC-OQAM is proposed in [29] where some simulation results, but no analytical expressions, are provided to evaluate the channel estimation error.

4.2 System model

In this proposal, the system model studies a point to point communication link using FBMC-OQAM as a multicarrier transmission technique.

In this chapter, let us denote $\mathbf{S}$ as the $N \times K/2$ complex data symbols matrix

transmitted to the receiver. Here, N and K correspond to the subcarriers number and time symbols number, respectively. The complex data symbols are obtained using a QAM constellation powered by $\mathcal{P}_S/N$ where $\mathcal{P}_S$ indicates the information signal power. Then, recalling expressions from Chapter 2, the QAM symbols vector S is transformed to OQAM, where S_o is constructed from the real and imaginary values of S

$$S_o[k, m = 2m'] = \Re(S[k, m']), \tag{4.2.1}$$

$$S_o[k, m = 2m' + 1] = \Im(S[k, m']), \tag{4.2.2}$$

considering that $k = 0 \cdots N - 1$ and $m' = 0 \cdots K/2 - 1$. S_o corresponds to a $N \times K$ symbols matrix.

A discrete-time system model is considered with a $T_S{=}\frac{T}{K}$ sampling period, being T the N-symbols transmission time. Thus, the transmitted signal is denoted as

$$x[n]{=}\sum_{m=0}^{K-1}\sum_{k=0}^{N-1} S_o\left[k, m\right] e^{j\phi[k,m]} g\left[n{-}m\frac{N}{2}\right] e^{j\frac{2\pi}{N}\Delta f k\left(n-m\frac{N}{2}\right)}, \tag{4.2.3}$$

where $g[\cdot]$ is to the prototype filter, $\Delta f{=}\frac{1}{T}$ corresponds to the subcarriers-separation and $\phi[k, m]$ is described by

$$\phi[k, m] = \left\{ \begin{array}{ll} 0, & k + m \text{ even} \\ \frac{\pi}{2}, & k + m \text{ odd} \end{array} \right\}. \tag{4.2.4}$$

The shifted version of the prototype filter is given by $g_k[n] = g[n]e^{j\frac{2\pi}{N}\Delta f k n}$. Then, $x[n]$ is denoted as

$$x[n]{=}\sum_{m=-\infty}^{K-1}\sum_{k=0}^{N-1} S_o[k, m]e^{j\phi[k,m]} g_k\left[n{-}m\frac{N}{2}\right]. \tag{4.2.5}$$

It is important to remember that the filter $g[n]$ and the phase $\phi[k, m]$ have to be implemented in a way that $g_k[n]$ can be orthogonal in real-domain accomplishing

that

$$\Re\left\{< g_k[n], g_{k'}[n] >\right\} = \left\{\begin{matrix} 1, & k = k' \text{ and } n = n' \\ 0 & \text{otherwise} \end{matrix}\right\}. \tag{4.2.6}$$

We can say that the signal model under a frequency selective fading channel at the receiver side can be expressed as

$$y[n] = x[n] \circledast h[\tau, n] + w[n]. \tag{4.2.7}$$

where the circular convolution is represented by $\circledast$. Then, the channel impulse response is

$$h[\tau, n] = \sum_{l=0}^{L-1} h[\tau_l, n]\delta[\tau - \tau_l]. \tag{4.2.8}$$

L represents the number of channel taps and τ_l indicates each l-th tap delay being $l = \{0, 1, ..., L-1\}$. Taking into account frequency-flat channel which remains constant during the filter length as in [74], the received signal will be expressed as

$$R_o[k_0, m_0] = e^{-j\phi[k_0,m_0]} \left(y[n] \circledast g^*_{k_0} \left[m_0 \frac{N}{2} - n \right] \right)_{\downarrow \frac{N}{2}} \tag{4.2.9}$$

where $(\cdot)_{\downarrow \frac{N}{2}}$ represents the sampling period of $N/2$ in OQAM modulation. Now, the information is recovered from the received and filtered signal as can be seen as follows

$$\begin{aligned} & y[n] \circledast g^*_{k_0} \left[m_0 \frac{N}{2} - n \right] = \\ & \left(\sum_{m=0}^{K-1} \sum_{k=0}^{N-1} S_o[k, m] e^{j\phi[k,m]} \sum_{l=0}^{L-1} h[\tau_l, n] g_k \left[n - \tau_l - m \frac{N}{2} \right] \right) \circledast \\ & \circledast g^*_{k_0} \left[m_0 \frac{N}{2} - n \right], \end{aligned} \tag{4.2.10}$$

then, it is possible the say that

$$\begin{aligned} & \left(y[n] * g^*_{k_0} \left[m_0 \frac{N}{2} - n \right] \right)_{\downarrow \frac{N}{2}} = \\ & = \sum_{m=0}^{K-1} \sum_{k=0}^{N-1} S_o[k, m] e^{j\phi[k,m]} H_{k_0,m_0}[k, m], \end{aligned} \tag{4.2.11}$$

where $H_{k_0,m_0}[k,m]$ is represented as

$$H_{k_0,m_0}[k,m]=\Bigg(\sum_{l=0}^{L-1} h[\tau_l,n] \sum_{\eta=-\infty}^{\infty} g_k\left[\eta-\tau_l-m\frac{N}{2}\right]\cdot g^*_{k_0}\left[\eta+n-m_0\frac{N}{2}\right]\Bigg)_{\downarrow\frac{N}{2}}. \tag{4.2.12}$$

Finally, simplifying (4.2.12), the channel in frequency-domain can be represented as

$$H_{k_0,m_0}[k,m]=\sum_{l=0}^{L-1} h[\tau_l,n]D_{k_0,m_0}[k,m,\tau_l]e^{-j\frac{2\pi}{N}\Delta fk\tau_l}, \tag{4.2.13}$$

where $D_{k_0,m_0}[k,m,\tau_l]$ is called ambiguity function and can be represented as

$$D_{k_0,m_0}[k,m,\tau_l]=\sum_{\eta=-\infty}^{\infty} g\left[\eta-\tau_l-\Delta_m\frac{N}{2}\right] g\left[\eta\right]\cdot \cdot e^{j\frac{2\pi}{N}\Delta f\Delta_k\eta}e^{-j\frac{2\pi}{N}\Delta fk\Delta_m\frac{N}{2}} \tag{4.2.14}$$

where $\Delta_k{=}k{-}k_0$ and $\Delta_m{=}m{-}m_0$. The received signal (4.2.9) after the synthesis can be seen as follows

$$R_o[k_0,m_0]=e^{-j\phi[k_0,m_0]}. \cdot\Bigg(\sum_{m=0}^{K-1}\sum_{k=0}^{N-1} S_0[k,m]e^{j\phi[k,m]}H_{k_0,m_0}[k,m]\Bigg). \tag{4.2.15}$$

Finally, simplifying (4.2.15), the expression can be reduced to

$$R_o[k_0,m_0]=\underbrace{H_{k_0,m_0}[k_0,m_0]S_o[k_0,m_0]}_{\text{desired signal}}+W[k_0,m_0]+ \underbrace{+\,e^{-j\phi[k_0,m_0]}\underbrace{\Bigg(\sum_{m=0}^{K-1}\sum_{k=0}^{N-1} S_o[k,m]e^{j\phi[k,m]}H_{k_0,m_0}[k,m]\Bigg)}_{m\neq m_0 \text{ and } k\neq k_0}}_{\text{interference}}, \tag{4.2.16}$$

where $W[k,m]$ represents the additive white Gaussian noise $W \sim \mathcal{CN}(0, \sigma_W^2)$ as is defined in [46]. Then, it is assumed that a unitary gain is assigned to the the prototype filter.

4.2.1 FBMC-OQAM with superimposed training

Taking into account a FBMC-OQAM multicarrier technique, we define a $N \times 1$ vector $\mathbf{q}$ with the pilot training sequence, being the real and imaginary parts the same value. To get the $N \times 2$ vector $\mathbf{q}_{\mathrm{o}}$, we combine (4.2.1) and (4.2.2) as it can be seen as follows. Then, matrix $\mathbf{Q}_{\mathrm{o}}$ containing the pilot sequence matrix is built as

$$\mathbf{Q}_o = \mathbf{q}_o \otimes \mathbf{1}_{1,K/2}. \tag{4.2.17}$$

where the columns of $\mathbf{Q}_{\mathrm{o}}$ have equal value for a specific row. Note that this characteristic is necessary to take advantage of the averaging process in the channel estimation error. Here, the conveyed signal is composed by the data and pilot signals taking into account that $\mathcal{P}$ represents the total power being $\mathcal{P} = \mathcal{P}_{\mathrm{S}} + \mathcal{P}_{\mathrm{P}}$. The power to be spent in data symbols is $\mathcal{P}_{\mathrm{S}} = \alpha\mathcal{P}$, and the power used in the transmission of the pilots is $\mathcal{P}_{\mathrm{P}} = (1-\alpha)\mathcal{P}$ where data power coefficient is α. In the superimposition process of $\mathbf{S}_o$ with $\mathbf{Q}_o$, it is necessary to satisfy the following power constraint

$$\frac{\mathcal{P}}{2N} = \alpha E\left\{\|\mathbf{S}_o\|^2\right\} + (1-\alpha)E\left\{\|\mathbf{Q}_o\|^2\right\}. \tag{4.2.18}$$

where the Euclidean norm is represented by $\|\cdot\|$. Consequently, the pilot-data matrix $\mathbf{T}_o$ can be represented by

$$\mathbf{T}_o = \sqrt{\alpha}\mathbf{S}_o + \sqrt{1-\alpha}\mathbf{Q}_o. \tag{4.2.19}$$

Having the new pilot-data sequence as it can be seen in (4.2.19), it can be conveyed through the baseband model in (4.2.15), being $\mathbf{S}_o$ replaced by $\mathbf{T}_o$.

4.3 Channel estimation error for ST in FBMC-OQAM multicarrier technique

Form the previous proposed signal model, the received signal can be represented as

$$\begin{aligned} R_o[k_0,m_0] = & \sqrt{\alpha} R_o^S[k_0,m_0] + \sqrt{1-\alpha} R_o^Q[k_0,m_0] + \\ & + W[k_0,m_0], \end{aligned} \tag{4.3.20}$$

being $R_o^S[k_0,m_0]$ and $R_o^Q[k_0,m_0]$, the received data and pilot signal, respectively, which were influenced by the channel and filters, as it is explained in (4.2.15),

$$\begin{aligned} R_o^S[k_0,m_0] = & H_{k_0,m_0}[k_0,m_0] S_o[k_0,m_0] + W[k_0,m_0] + \\ & + e^{-j\phi[k_0,m_0]} \underbrace{\left(\sum_{m=0}^{K-1} \sum_{k=0}^{N-1} S_o[k,m] e^{j\phi[k,m]} H_{k_0,m_0}[k,m] \right)}_{k \neq k_0 \text{ and } m \neq m_0}, \\ R_o^Q[k_0,m_0] = & H_{k_0,m_0}[k_0,m_0] Q_o[k_0,m_0] + W[k_0,m_0] + \\ & + e^{-j\phi[k_0,m_0]} \underbrace{\left(\sum_{m=0}^{K-1} \sum_{k=0}^{N-1} Q_o[k,m] e^{j\phi[k,m]} H_{k_0,m_0}[k,m] \right)}_{k \neq k_0 \text{ and } m \neq m_0}, \end{aligned} \tag{4.3.21}$$

Then, considering the pilot sequence described in the previous section, the received signal can be denoted as

$$\begin{aligned} R_o^Q[k_0,m_0] = & \tilde{H}[k_0,m_0] q_o + W[k_0,m_0] + \\ & + q_o e^{-j\phi[k_0,m_0]} \sum_k \sum_m e^{j\phi[m,n]} H_{k_0,m_0}[k,m], \end{aligned} \tag{4.3.22}$$

where, the quasi-stationarity condition is assumed to be met and no Doppler effect is present. Then, it is possible to say that, the channel $h[\tau_l, n] = h[\tau_l]$ and $\tilde{H}[k_0] = H_{k_0,m_0}[k_0, m_0]$. From the multicarrier techniques, it is satisfied that $N \gg \tau_l$ by design, $D_{k_0,m_0}[k, m, \tau_0] \simeq D_{k_0,m_0}[k, m, \tau_{L-1}]$, and $\tilde{H}[k] \simeq \tilde{H}[k \pm \frac{1}{2}]$. Then,

$$\begin{aligned} R_o^Q[k_0, m_0] \simeq & \tilde{H}[k_0] q_o + W[k_0, m_0] + \\ & + q_o e^{-j\phi[k_0,m_0]} \sum_k \tilde{H}[k] \sum_m e^{j\phi[m,n]} D_{k_0,m_0}[k, m] \approx \\ & \approx \tilde{H}[k_0] \left(q_o + j B_q[k_0, m_0] \right), \end{aligned} \tag{4.3.23}$$

where the self-interference produced by the neighboring symbols will be represented by $j\mathbf{B}_q$.

For the channel estimation, the received signal $\mathbf{R}_o$ is averaged over K symbols, $\{m, ..., m + K\}$, per subcarrier k, as follows

$$\begin{aligned} & E_K \{R_o[k, m]\} = E_K \{W[k, m]\} + h[k] \times \\ & \times \Big(\sqrt{\alpha} \left(E_K \{S_o[k, m]\} + j E_K \{B_S[k, m]\} \right) + \\ & + \sqrt{1 - \alpha} \left(E_K \{Q_o[k, m]\} + j E_K \{B_Q[k, m]\} \right) \Big). \end{aligned} \tag{4.3.24}$$

Remembering that the elements of $\mathbf{q}_o$ have the same values, it is possible to say that $q_o[k] = E_K \{Q_o[k, m]\}$ and $b_{\mathrm{q}}[k] = E_K \{B_Q[k, m]\}$, and defining the self-interference and noise value $u[k]$ as

$$\begin{aligned} & u[k] = E_K \{W[k, m]\} + h[k] \times \\ & \times \left(\sqrt{\alpha} \left(E_K \{S_o[k, m]\} + j E_K \{B_S[k, m]\} \right) \right). \end{aligned} \tag{4.3.25}$$

Then, the expression (4.3.24) can be reduced to

$$E_K \{R_o[k, m]\} = h[k] \sqrt{1 - \alpha} \left(q_o[k] + j b_{\mathrm{q}}[k] \right) + u[k]. \tag{4.3.26}$$

It is important to note that the training sequence, also known as pseudo-pilots as

indicated, $q_o[k] + jb_{\mathrm{q}}[k]$ is deterministic and it will improve the channel estimation error as indicated in [77]. The power of $jb_{\mathrm{q}}[k]$ can be calculated as it can be seen in the Appendix section replacing the data sequence instead of the pilot sequence. Note that its vectorized form can be represented as $\mathbf{b}_{\mathrm{q}}$ with a power of $\mathcal{P}_{b_{\mathrm{q}}}$.

The interference and noise variance σ_{u}^2 can be calculated using $E\{\mathbf{u}\mathbf{u}^{\mathrm{H}}\} = \sigma_{\mathrm{u}}^2 \mathbf{I}_N$ where

$$\begin{aligned} E\{\mathbf{u}\mathbf{u}^{\mathrm{H}}\} = & E\Bigg\{ \left(\frac{1}{K}\overline{W} + \frac{\sqrt{\alpha}}{K}\mathbf{h}\left(\overline{S}_{\mathbf{o}} + j\overline{B}_S\right)\right) \times \\ & \times \left(\frac{1}{K}\overline{\mathbf{W}} + \frac{\sqrt{\alpha}}{K}\mathbf{h}\left(\overline{\mathbf{S}}_{\mathbf{o}} + j\overline{\mathbf{B}}_{\mathbf{S}}\right)\right)^{\mathrm{H}} \Bigg\}, \end{aligned} \tag{4.3.27}$$

where the self-interference and noise values in a vectorized form are presented as $\mathbf{S}_{\mathbf{o}}$, $\mathbf{B}_S$ and $\mathbf{W}$, respectively. $\overline{\mathbf{W}}$ is $\overline{\mathbf{W}} = \sum_{i=0}^{K-1} \mathbf{W}^i$. Note that these overlined vectors $\overline{\mathbf{S}}_{\mathbf{o}}$ and $\overline{\mathbf{B}}_S$ represent the same definitions than before.

The power generated by the intrinsic interference is dependent of OQAM symbols. Then, the OQAM power corresponds to one half of the QAM symbol power. Thus, the variance of the intrinsic interference is

$$\sigma_{\mathrm{u}}^2 = \frac{\sigma_{\mathrm{W}}^2}{K} + \frac{\sigma_{\mathrm{H}}^2 \alpha \mathcal{P}}{2NK} + \frac{\sigma_{\mathrm{H}}^2 \alpha \mathcal{P}}{2NK}\frac{\sigma_{\mathrm{v}}^2}{K}, \tag{4.3.28}$$

then, reordering, it is possible to obtain that

$$\sigma_{\mathrm{u}}^2 = \frac{1}{K}\left(\sigma_{\mathrm{W}}^2 + \frac{\sigma_{\mathrm{H}}^2 \alpha \mathcal{P}}{2N}\left(1 + \frac{\sigma_{\mathrm{v}}^2}{K}\right)\right). \tag{4.3.29}$$

Analyzing the previous equation, the first term consists in the AWGN noise, the second term is data interference and the last term is composed by the intrinsic self-interference. This final term is composed by the accumulative effect of the surrounding symbols of the analyzed OQAM symbol, the data signal power and channel effects. The power from the intrinsic interference (σ_{v}^2) can be deduced as it is done in the Appendix. The quasi-stationary condition is considered and the number of multicarrier symbols where the channel does not vary is K multicarrier symbols. Then, if this coherence time increases a better averaging will be done which will reduce the noise

and interference signal σ_{u}^2 even more as it can be seen in (4.3.29).

In (4.3.26), a least squares (LS) channel estimator can be applied so it is possible to say that

$$\begin{aligned}\hat{h}[k]=&\left(\sqrt{1-\alpha}(q_{\mathrm{o}}[k]+jb_{\mathrm{q}}[k])\right)^{-1} E_K\left\{R_o\right\}[k]\\ =&h[k]+\left(\sqrt{1-\alpha}(q_{\mathrm{o}}[k]+jb_{\mathrm{q}}[k])\right)^{-1} u[k].\end{aligned} \tag{4.3.30}$$

Now, the channel estimation error may be expressed as

$$\begin{aligned}\Delta h[k]=&\hat{h}[k]-h[k]\\ =&\left(\sqrt{1-\alpha}(q_{\mathrm{o}}[k]+jb_{\mathrm{q}}[k])\right)^{-1}u[k].\end{aligned} \tag{4.3.31}$$

Its variance can be represented as

$$\begin{aligned}\sigma_{\Delta_{\mathrm{h}}}^2 = \quad & E\left(\left(\sqrt{1-\alpha}\,(q_{\mathrm{o}}[k]+jb_{\mathrm{q}}[k])\right)^{-1} u[k]\right.\\ & \left.\left(\left(\sqrt{1-\alpha}(q_{\mathrm{o}}[k]+jb_{\mathrm{q}}[k])\right)^{-1} u[k]\right)^{\mathrm{H}}\right) =\\ & = N\frac{\sigma_{\mathrm{u}}^2}{(1-\alpha)\mathcal{P}}\mathbf{I}_N.\end{aligned} \tag{4.3.32}$$

Then, after removing the pilot sequences from the received symbols, it is possible to recover the original information and joining the OQAM parts as follows

$$\begin{aligned}\tilde{S}[k_0,m_0'] =&\Re\left(R_o[k_0,m_0=2m_0']\right)+\\ &+j\Re\left(R_o[k_0,m_0=2m_0'+1]\right).\end{aligned} \tag{4.3.33}$$

Hence, for a given m-th subcarrier the complex symbols recovered at the receiver

can be represented as

$$\begin{aligned}
\tilde{S}[k,m'] = & \Re\left\{\sqrt{\alpha}\cdot H[k,2m']\left(S_o[k,2m']+jB_S[k,2m']\right)\right. \\
& \left.+\sqrt{1-\alpha}\cdot\Delta H[k,m]\left(Q_o[k,2m']+jB_Q[k,2m']\right)+W[k,2m']\right\} \\
& +j\Re\left\{\sqrt{\alpha}\cdot H[k,m]\left(S_o[k,2m'+1]+jB_S[k,2m'+1]\right)\right. \\
& +\sqrt{1-\alpha}\cdot\left\{\Delta H[k,m]\left(Q_o[k,2m'+1]+jB_Q[k,2m'+1]\right)\right\} \\
& \left.+W[k,2m'+1]\right\}. \qquad (4.3.34)
\end{aligned}$$

The signal-to-noise ratio (SNR) per subcarrier at the receiver side can be defined as

$$\gamma_{\mathrm{SNR}} = \frac{\mathcal{P}\sigma_{\mathrm{H}}^2}{2N\sigma_{\mathrm{W}}^2}, \qquad (4.3.35)$$

where the channel variance can be expressed as $\sigma_{\mathrm{H}}^2 = \sum_{l=0}^{L-1} {\sigma_{h_l}}^2$.

4.4 Analysis of the average system capacity

The average system capacity can be denoted as in [63] [65] and can be expressed as

$$\mathrm{C}=A\cdot E\{\log_2(1+\overline{\gamma})\} \approx A\cdot\log_2(1+\overline{\gamma}), \qquad (4.4.36)$$

where the signal-to-interference noise ratio (SINR) is represented as $\overline{\gamma}$ being $A = \frac{N-N_{\mathrm{P}}}{N}$ in PSAM and unitary in ST.

N_{P} is defined, in PSAM schemes, as the number of pilots dedicated to channel estimation. Here, the channel can be obtained almost perfectly estimated assuming that the interference and noise are zero having equispaced and equipowered pilots. A minimum interpolation error can be guaranteed assuming $N_{\mathrm{P}} \geq L$ as can be seen in [63] and [65]. In this chapter, it is assumed that the minimum number of pilots is lower bounded by $N_{\mathrm{P}} = L$ taps for a channel acquisition ensured. Transmitting the minimum number of pilots, the maximum number of resources are obtained ,

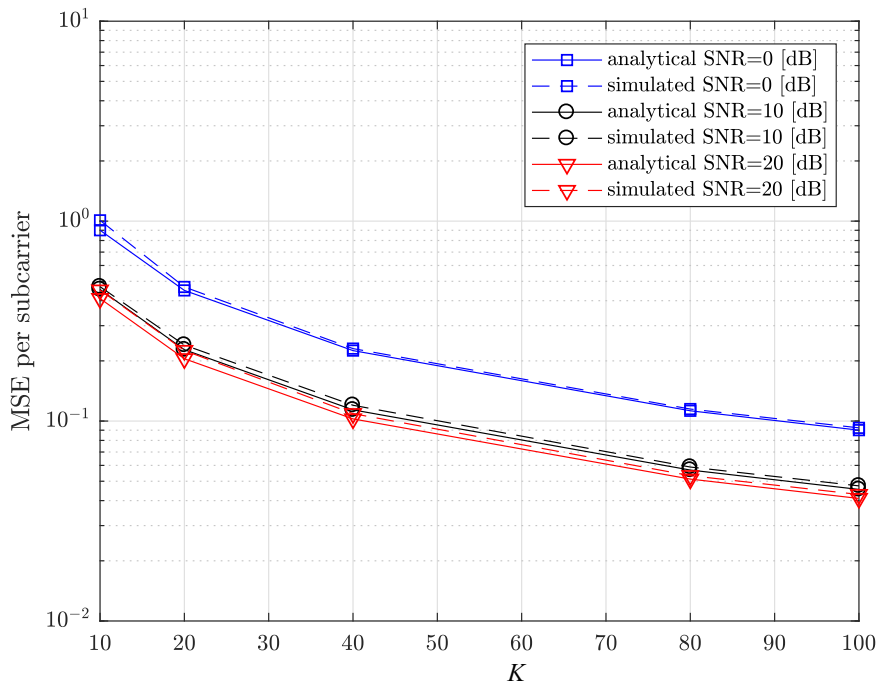

Figure 4-1: Average mean squared error as a function of K multicarrier symbols using γ_{SNR}=$\{0, 10, 20\}$ $[dB]$.

i.e. $(N - L)$. Furthermore, the maximum ratio of data symbols over the subcarrier number is $\frac{N-L}{N}$. Thus, the maximum α can be denoted as α_{max}=$1 - L/N$. In this section, for comparison purposes, N_{P} can be calculated as N_{P}=$\lceil (1-\alpha)\, N \rceil$, i. e. the number resulted from rounding up the product of the pilot power allocation by the subcarrier number. For ST techniques, the condition $(L \leq N_{\text{P}})$ is always satisfied due to it is assumed that a pilot symbol is transmitted in every subcarrier.

The CP length influences the signal-to-noise ratio applied over a multicarrier symbol, thus, it affects the average channel capacity. For that reason, γ_{SNR} is penalized in each case.

4.4.1 Average channel capacity for PSAM-FBMC

Considering the representation of capacity in previous section, the average channel capacity for PSAM-FBMC can be denoted as

$$\begin{aligned} \mathrm{C}_{\mathrm{PSAM}}^{\mathrm{FBMC}} &= \frac{N-N_{\mathrm{P}}}{N} E\{\log_2\left\{1+\overline{\gamma}_{\mathrm{PSAM}}^{\mathrm{FBMC}}\right\}\} \\ &\approx \frac{N-N_{\mathrm{P}}}{N} \log_2\left\{1+\overline{\gamma}_{\mathrm{PSAM}}^{\mathrm{FBMC}}\right\}, \end{aligned} \tag{4.4.37}$$

being $\overline{\gamma}_{\mathrm{PSAM}}^{\mathrm{FBMC}}$ the SINR in PSAM-FBMC. Assuming that the pilot symbol strategy cancels the interference, the variance of the channel estimation error, using (4.3.32), can be seen as follows

$$\begin{aligned} \sigma_{\Delta\mathrm{h}}^2 &= N \frac{1}{(1-\alpha)\mathcal{P}} \frac{1}{K} \left(\sigma_{\mathrm{W}}^2 + \frac{\alpha \mathcal{P} \sigma_{\mathrm{H}}^2}{2N} \sigma_{\mathrm{v}}^2\right) \\ &\approx N \frac{1}{(1-\alpha)\mathcal{P}} \frac{1}{K} \left(\sigma_{\mathrm{W}}^2\right). \end{aligned} \tag{4.4.38}$$

Now, considering (4.4.38) as in [65], $\overline{\gamma}_{PSAM}^{\mathrm{FBMC}}$ can be denoted as

$$\overline{\gamma}_{\mathrm{PSAM}}^{\mathrm{FBMC}} = \frac{\sigma_{\mathrm{H}}^2 \frac{\mathcal{P}_{\mathrm{S}}}{K}}{\sigma_{\Delta_{\mathrm{h}}}^2 \frac{\mathcal{P}_{\mathrm{S}}}{K} + \sigma_{\mathrm{W}}^2}, \tag{4.4.39}$$

where, simplifying the formulation it is possible to say that

$$\overline{\gamma}_{\mathrm{PSAM}}^{\mathrm{FBMC}} = \frac{\alpha}{\alpha \frac{\sigma_{\Delta\mathrm{h}}^2}{\sigma_{\mathrm{H}}^2} + \frac{K}{\mathcal{P}} \frac{\sigma_{\mathrm{W}}^2}{\sigma_{\mathrm{H}}^2}}, \tag{4.4.40}$$

and $\sigma_{\Delta\mathrm{h}}^2/\sigma_{\mathrm{H}}^2$ is obtained from (4.4.38)

$$\frac{\sigma_{\Delta\mathrm{h}}^2}{\sigma_{\mathrm{H}}^2} = N \frac{1}{(1-\alpha)\mathcal{P}} \frac{1}{K} \left(\frac{\sigma_{\mathrm{W}}^2}{\sigma_{\mathrm{H}}^2}\right). \tag{4.4.41}$$

Finally, the signal-to-interference noise ratio can be represented similarly to PSAM-OFDM that is different from PSAM-FBMC in the addition of CP. Thus, $\overline{\gamma}_{\mathrm{PSAM}}^{\mathrm{FBMC}}$ can be seen

as

$$\overline{\gamma}_{\mathrm{PSAM}}^{\mathrm{FBMC}}=\frac{\alpha(1-\alpha)NK}{\frac{1}{\gamma_{\mathrm{SNR}}^{\mathrm{FBMC}}}\left(N+NK(1-\alpha)\right)}, \tag{4.4.42}$$

where $\gamma_{\mathrm{SNR}}^{\mathrm{FBMC}}=\gamma_{\mathrm{SNR}}$ because no CP is present in this case.

4.4.2 Average channel capacity for ST-FBMC

In the case of ST, the average channel capacity for FBMC can be denoted as follows

$$\mathrm{C}_{\mathrm{ST}}^{\mathrm{FBMC}}=E\{\log_2\left\{1+\overline{\gamma}_{\mathrm{ST}}^{\mathrm{FBMC}}\right\}\}\approx\log_2\left\{1+\overline{\gamma}_{\mathrm{ST}}^{\mathrm{FBMC}}\right\}. \tag{4.4.43}$$

Taking into account (4.3.34), applying (23)- [63], and assuming the OQAM power constrains, $\overline{\gamma}_{ST}^{\mathrm{FBMC}}$ will be given by

$$\overline{\gamma}_{\mathrm{ST}}^{\mathrm{FBMC}}=\frac{\sigma_{\mathrm{H}}^2\frac{\mathcal{P}_{\mathrm{S}}}{K}}{\sigma_{\Delta_{\mathrm{h}}}^2\frac{\mathcal{P}_{\mathrm{S}}}{K}+\sigma_{\Delta_{\mathrm{h}}}^2\frac{\mathcal{P}_{\mathrm{P}}}{K}+\sigma_{\mathrm{W}}^2}. \tag{4.4.44}$$

Then, after some arithmetic simplifications, it is possible to say that

$$\overline{\gamma}_{\mathrm{ST}}^{\mathrm{FBMC}}=\frac{\alpha}{\frac{\sigma_{\Delta\mathrm{h}}^2}{\sigma_{\mathrm{H}}^2}+\frac{K}{\mathcal{P}}\frac{\sigma_{\mathrm{W}}^2}{\sigma_{\mathrm{H}}^2}}, \tag{4.4.45}$$

where the ratio between the channel estimation error and the channel power $\sigma_{\Delta\mathrm{h}}^2/\sigma_{\mathrm{H}}^2$ can be obtained combining (4.3.29) in (4.3.32) as follows

$$\frac{\sigma_{\Delta\mathrm{h}}^2}{\sigma_{\mathrm{H}}^2}=N\frac{1}{(1-\alpha)\mathcal{P}}\frac{1}{K}\left(\frac{\sigma_{\mathrm{W}}^2}{\sigma_{\mathrm{H}}^2}+\frac{\alpha\mathcal{P}}{2N}\left(1+\sigma_{\mathrm{v}}^2\right)\right), \tag{4.4.46}$$

and the ratio between the noise variance and the channel power $\sigma_{\mathrm{W}}^2/\sigma_{\mathrm{H}}^2$ can be deduced from (4.3.35). Thus, (4.4.45) can be reduced to

$$\overline{\gamma}_{\mathrm{ST}}^{\mathrm{FBMC}}=\frac{\alpha\left(1-\alpha\right)NK}{\alpha\frac{N}{2}\left(1+\sigma_{\mathrm{v}}^2\right)+\frac{1}{\gamma_{\mathrm{SNR}}^{\mathrm{FBMC}}}\left(N+NK(1-\alpha)\right)}. \tag{4.4.47}$$

where $\gamma_{\mathrm{SNR}}^{\mathrm{FBMC}}=\gamma_{\mathrm{SNR}}$, because no CP was used.

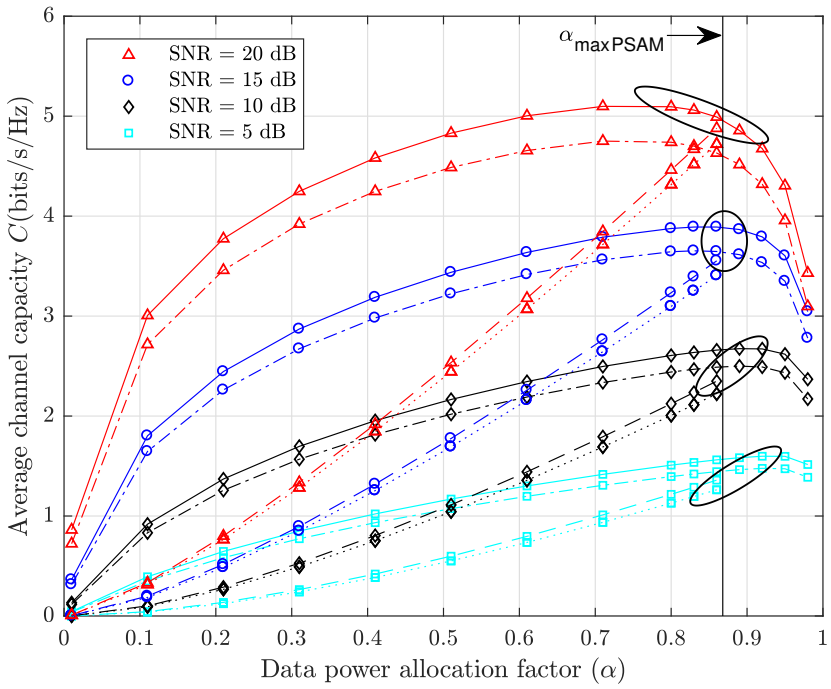

Figure 4-2: Average capacity for OFDM using PSAM (dashed) and ST (dot dashed), and FBMC using AuP (dotted) and ST (solid-line) as a function of the power allocation factor α.

4.5 Analysis of the power allocation

The ratio between the power assigned to the data will be called data power allocation factor α. The average channel capacity is dependent on this parameter. Then, it is possible to show that this expression is concave where its optimal values can be obtained.

4.5.1 FBMC using PSAM

In FBMC technique using PSAM as a channel estimation method, the average channel capacity can be deduced replacing (4.4.42) in (4.4.37). The data power allocation value, that maximizes the average channel capacity, can be obtained deriving

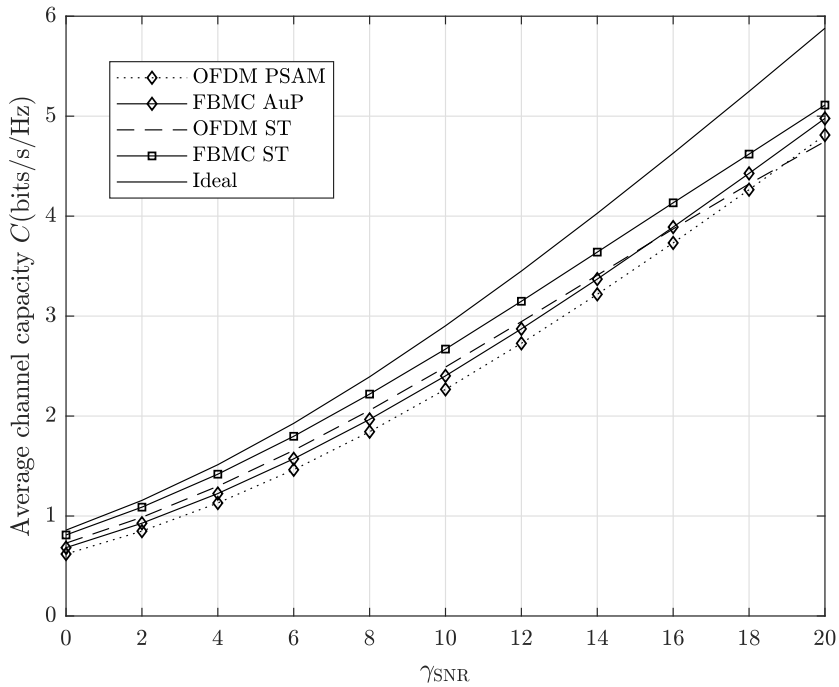

Figure 4-3: Average capacity of OFDM and FBMC multicarrier techniques using ST and PSAM as a function of SNR.

$\partial \mathrm{C}_{\mathrm{PSAM}}/\partial\alpha$=0. Then, $\alpha_{\text{opt}}^{\text{PSAM-FBMC}}$ can be represented as

$$\begin{aligned}\alpha_{\text{opt}}^{\text{PSAM-FBMC}} &= \alpha : -\log_2\left(1+\overline{\gamma}_{\text{AuP}}^{\text{FBMC}}\right)\\ &= \frac{1}{\ln(2)}\frac{(1-2\alpha)(1+K(1-\alpha))+K\alpha(1-\alpha)}{(1+K(1-\alpha))\,(1-\alpha)}\end{aligned} \tag{4.5.48}$$

where $\overline{\gamma}_{\text{AuP}}^{\text{FBMC}}$ corresponds to the SINR from FBMC-OQAM using auxiliary-pilots (AuP) for channel estimation. Here, α has to be chosen selecting between the maximum value and the derived optimal one. If $\alpha_{\text{opt}} \leq \alpha_{\text{max}}$, α_{opt} can be selected. In the case $\alpha_{\text{opt}} \geq \alpha_{\text{max}}$, α_{max} will be selected since a bigger α could not ensure the condition of channel identifiability.

4.5.2 FBMC using ST

In the case of combining the multicarrier technique FBMC with ST, the average channel capacity can be deduced from (4.4.47) and (4.4.43). The α value that max-

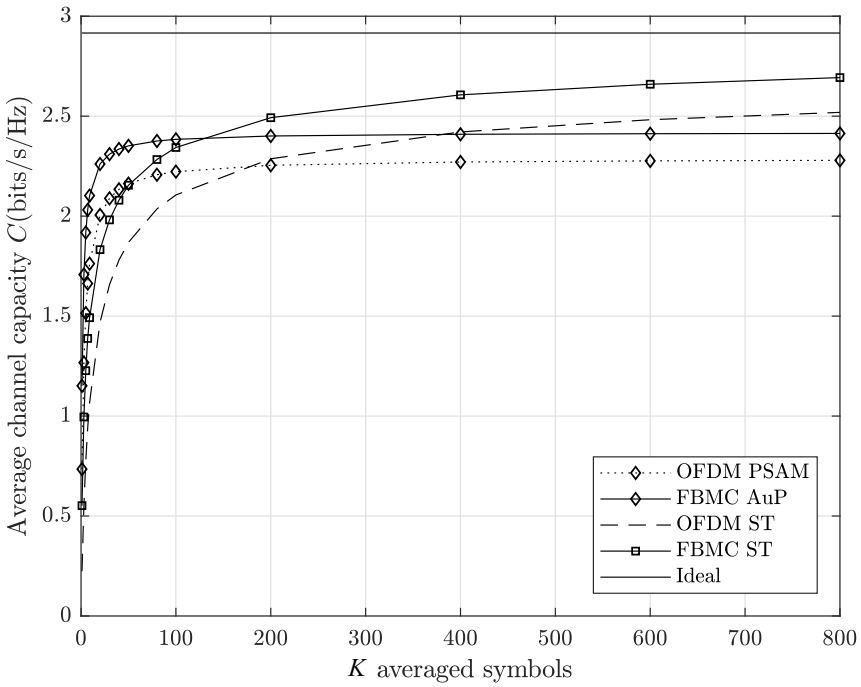

Figure 4-4: Average capacity of OFDM and FBMC multicarrier techniques using ST and PSAM as a function of K with a fixed SNR=10 dB.

imizes the average channel capacity can be obtained through $\partial \mathrm{C}_{\mathrm{ST}}^{\mathrm{FBMC}}/\partial\alpha$=0. Then, $\alpha^2\left(NK-\frac{N}{2}\left(1+\sigma_{\mathrm{v}}^2\right)\gamma_{\mathrm{SNR}}\right)-2\alpha N\left(1+K\right)+N\left(1+K\right)=0$, thus,

$$\alpha_{\mathrm{opt}}^{\text{ST-FBMC}}=\frac{2N\left(1+K\right)-\sqrt{4N^2\left(1+K\right)^2-4\mathrm{A}\left(N+NK\right)}}{2\mathrm{A}}, \tag{4.5.49}$$

where $\mathrm{A}=NK-\frac{N}{2}\left(1+\sigma_{\mathrm{v}}^2\right)\gamma_{\mathrm{SNR}}$.

4.6 Simulation results

In this section, ST and PSAM channel estimation techniques using OFDM and FBMC are compared. In the case of FBMC-OQAM, a PHYDYAS filter is used for its implementation. Note that for comparison purposes, the power assigned to data and pilot symbols is the same in all multicarrier systems being K=64.

It is assumed that the channel follows a Rayleigh distribution with a power delay profile having $L = 8$ taps and $E\{|h_l|^2\} = e^{-\frac{L}{10}l}$. The length of the CP will be equal to L in OFDM to guarantee an ISI/ICI free scenario.

The channel estimation error is presented in Fig. 4-1 for γ_{SNR}=$\{0, 10, 20\}$ [dB] and α=0.8, being the pilot symbols overlaid with QPSK constellation data. The mean squared error (MSE) curves product of simulations match with the curves of the analytical MSE expression obtained in (4.3.32). In Fig. 4-2, it is possible to see the average channel capacity as a function of the data power allocation factor. The value of α that maximizes the average channel capacity can be obtained through (4.5.49) which coincides with the α found through exhaustive search using simulations. Note, highlighted in circles, that ST schemes overcome to the PSAM strategies, in average channel capacity, using OFDM and FBMC multicarrier techniques. The stationarity of the system is set to 100 slots, with 7 multicarrier symbols per slot.

In Fig. 4-3, it is possible to see ST and PSAM strategies versus SNR for different multicarrier techniques. Note that in case of low and medium SNR, FBMC using ST overcomes dedicated pilot techniques. This happens when the data interference generated by the superimposition and by the self-interference are lower than the AWGN noise, i.e. for low and medium SNR.

Fig. 4-4 shows the performance of the channel capacity as a function of the number of multicarrier symbols K with a fixed SNR. Here, ST is better than PSAM techniques using OFDM and FBMC. Furthermore, ST-FBMC outperforms to ST-OFDM when channel presents a certain level of stationarity. This makes ST-FBMC an interesting technique to be used for channel estimation in next generation communication systems.

Appendix

Let us assume an $N_f \times K_f$ self-interference matrix $\mathcal{V}$=$\sum_{m=-\infty}^{K-1} \sum_{k=0}^{N-1} S_o[k,m] e^{j\phi[k,m]}$, which was previously developed using a similar technique in [79]. N_f and K_f are the number of subcarriers and the time samples that are influenced by the filters,

Table 4.1: Intrinsic self-interference that affects the data at $[k_0, m_0]$ position using a PHYDYAS prototype filter.

	m_0-3	m_0-2	m_0-1	m_0	m_0+1	m_0+2	m_0+3
k_0-1	$-j0.0429$	0.125	$j0.2058$	0.2393	$-j0.2058$	-0.125	$j0.0429$
k_0	-0.0668	0	0.5644	1	0.5644	0	-0.0668
k_0+1	$j0.0429$	-0.125	$-j0.2058$	0.2393	$j0.2058$	0.125	$-j0.0429$

respectively. The self-interference is calculated, using an extended matrix form, in a k-th subcarrier and for K consecutive multicarrier symbols as

$$\mathcal{V}_{e_{\left[K\times(N_f\times L_T)\right]}}=\left[\mathcal{V}_{1[K\times L_T]},\mathcal{V}_{2[K\times L_T]},...\mathcal{V}_{N_f[K\times L_T]}\right] \tag{4.6.50}$$

being $L_T = K_f + K - 1$.

$$\mathcal{V}_{S[N_f\times L_T)\times 1]}=\mathcal{V}_e^{\mathrm{T}}\mathbf{1}_{[K\times 1]}. \tag{4.6.51}$$

Then, the self-interference intrinsic power in K consecutive multicarrier symbols can be represented as

$$\sigma_{\mathrm{v}}^2=E\left\{\mathcal{V}_S\mathcal{V}_S^{\mathrm{H}}\right\}. \tag{4.6.52}$$

In Table 4.1, it is possible to see $\mathcal{V}[m,n]$ which represents the PHYDYAS filter coefficients.

Chapter 5

Superimposed training in VLC scenarios based on DCO-OFDM

In this chapter, the contribution made by the authors in [28] is analyzed. Here, the combination of visible light communication (VLC) applying superimposed training (ST) technique for channel estimation is investigated, considering a multiple input single output (MISO) system configuration which is very common in VLC. In this case, ST cannot be easily applied to VLC, then, an analysis of this combination is carried out. Here, an analytical expression of the mean squared error (MSE) using a least squares (LS) estimator which matches with the MSE obtained with simulations is obtained. Additionally, spectral efficiency expressions are obtained to compare the performance of PSAM and ST techniques in this scenario. Furthermore, the optimal values for the maximum spectral efficiency are provided. Finally, simulation results are presented at the end of the chapter.

5.1 State of the art

VLC is considered a promising technology that can satisfy the users demand which is exponentially growing to provide higher data rates in mobile communications. This technology permits to provide and transmit information using a light emitting diode (LED), and at the receiver through a photo diode (PD) the information is converted

from optical to electrical. It is possible in the near future that VLC and radio frequency (RF) work together configuring an hybrid technology [80].

Some multicarrier techniques like direct current biased optical orthogonal frequency division multiplexing (DCO-OFDM), asymmetrically clipped optical OFDM (ACO-OFDM) or unipolar OFDM (U-OFDM) have been built to work in optics [51].

Multiple input multiple output (MIMO) has been widely analyzed in RF. Nevertheless, the correlation between channels in MIMO-VLC are significantly different than in RF, then, the MIMO multiplexing gain cannot be obtained easily. Consequently, larger arrays must be constructed through channel matrices with full rank properties [81] [82] [83]. Considering an indoor scenario for illumination and conveying information, multiple LEDS are necessary. Then, MISO can be considered for VLC transmission in a real scenario as can be seen in [84] [85]. Furthermore, MISO has been used by its diversity and multiplexity as described in [86] [87]. Here, the obtained channel state information (CSI) can serve for equalization at the receiver or precoding at the transmitter. In VLC, the use of pilot symbol assisted modulation (PSAM) for channel estimation has been proposed in [88] [89] for MISO configurations where the channel is assumed quasi-stationary, then it does not change until a specific number of multicarrier symbols have been transmitted.

A Bayesian approximation for channel estimation is presented in [90] for VLC using PSAM. As it has been explained, dedicated pilot-based channel estimation schemes reduce the spectral efficiency since they waste resources due to dedicated transmission of pilots. By other way, ST, as explained before, arithmetically add pilot signal to the data signal sharing the available resources unlike PSAM. A first approach to VLC using ST for channel estimation, in a single input single output configuration, was proposed in [27].

5.2 System model

In this section, a MISO DCO-OFDM system is evaluated where N_{t} and N are the number of transmission LEDs and subcarriers to be considered, respectively. In VLC,

DCO-OFDM is the most common multicarrier configuration to be taken into account thanks to its adaptability and gain in spectral efficiency. Then, this multicarrier technique will be used to discuss this scenario. Note that this analysis can be taken into account in other version of OFDM-based multicarrier techniques as ACO-OFDM.

As state before, MISO is an available technology to be used in illumination and to convey information in VLC.

The signal to be transmitted in frequency-domain is represented by the $(N-2)\times 1$ vector $\mathbf{x}$ and it is a composition of pilot and data symbols $\mathbf{x}=\mathbf{p}+\mathbf{d}$, where $\mathbf{p}$ corresponds to the pilot and data signal in frequency-domain, respectively. These signals consist of $(N-2)\times 1$ vectors which values are $p(k)$ and $d(k)$. Taking into account that DCO-OFDM is used, the subcarrier index is defined as $k=\{1,...,N/2-1\}\cup\{N/2+1,...,N-1\}$. Then, the symbols with the subcarrier index equals to $\{N/2+1,...,N-1\}$ corresponds to the Hermitian symmetric transformation of the symbols with subcarrier index $k=\{1,...,N/2-1\}$. From this, it is possible to say that one half of the useful subcarriers are used in transmission of redundant information. Additionally, the subcarriers with indexes 0-th and $N/2$-th do not carry information. This Hermitian symmetric operation is performed in order to guarantee a real value output signal after the fast Fourier transform. Recalling the signal model for DCO-OFDM, that was already introduced in Chapter 2, the multicarrier symbol DCO-OFDM in frequency-domain can be described as follows

$$\mathbf{x}=\begin{bmatrix}0 & \mathbf{x}_{\mathrm{C}}^{\mathrm{T}}[1,...,N/2-1] & 0 & \mathbf{x}_{\mathrm{C}}^{\mathrm{T}}[N/2,...,N-2]\end{bmatrix}^{\mathrm{T}}, \tag{5.2.1}$$

being $\mathbf{x}_{\mathrm{C}}$ a $(N/2-1)$-column vector and $\mathbf{x}_{\mathrm{C}}[N/2,...,N-2]=\left\{\mathbf{x}_{\mathrm{C}}^{\mathrm{T}}[1,...,N/2-1]\right\}^{\mathrm{H}}=\mathbf{x}_{\mathrm{half}}$. Here, $(\cdot)^{\mathrm{T}}$ and $(\cdot)^{\mathrm{H}}$ correspond to the transpose and Hermitian transpose operators, respectively.

The 0-th subcarrier is used for the DC-bias value which is equal to 0. This parameter is used to trace the signal into the LED dynamic range. This range controls the clipping level of the signal leading to clipping Gaussian noise as a function of the central limit and Bussbang theorems as can be seen in [91]. Considering that an

additive white Gaussian noise (AWGN) is considered in the chapter, the analysis of these parameters can be avoided [92]. Other ones, as the shot and thermal noise, are also modeled as AWGN as can be seen in [93]. Thus, the noises power usually are represented by a combination of their variances as can be seen in [88] [90] and it could indicate the user location in a specific scenario.

For this chapter, $\mathcal{P}$ represents the available electrical power defined as $\mathcal{P}=\mathcal{P}_{\mathrm{S}}+\mathcal{P}_{\mathrm{P}}$, where $\mathcal{P}_{\mathrm{S}}$ and $\mathcal{P}_{\mathrm{P}}$ represent the data signal power and the pilot signal power, respectively, being $\mathcal{P}_{\mathrm{S}}=\mathrm{E}\left[\mathbf{d}^{\mathrm{H}}\mathbf{d}\right]=\alpha\mathcal{P}$ and $\mathcal{P}_{\mathrm{P}}=\mathrm{E}\left[\mathbf{p}^{\mathrm{H}}\mathbf{p}\right]=(1-\alpha)\mathcal{P}$. The data power allocation factor, α, consists in the ratio between the data symbol power and the total power in the range of $0<\alpha<1$, and, $\mathrm{E}[\cdot]$ represents the statistical expectation. Note that it is assumed that the power is equally distributed between the $N-2$ subcarriers used for multicarrier transmission. Then, the power assigned for transmission of data and pilots using ST can be expressed as $\mathrm{E}\left[|d_{\mathrm{ST}}(k)|^2\right]=\frac{\mathcal{P}_{\mathrm{S}}}{N-2}\quad\forall k, \mathrm{E}\left[|p_{\mathrm{ST}}(k)|^2\right]=\frac{\mathcal{P}_{\mathrm{P}}}{N-2}\quad\forall k$, and in PSAM are $\mathrm{E}\left[|d_{\mathrm{PSAM}}(k)|^2\right]=\frac{\mathcal{P}_{\mathrm{S}}}{N-N_{\mathrm{P}}-2}\quad k\in\mathcal{K}_{\mathrm{D}}$, $\mathrm{E}\left[|p_{\mathrm{PSAM}}(k)|^2\right]=\frac{\mathcal{P}_{\mathrm{P}}}{N_{\mathrm{P}}}\quad k\in\mathcal{K}_{\mathrm{P}}$, where $\mathcal{K}_{\mathrm{D}}$ and $\mathcal{K}_{\mathrm{P}}$ represent the subcarrier sets of data and pilot symbols in PSAM techniques, respectively. Then, the cardinality of pilot set is N_{P}, where $N_{\mathrm{P}}=|\mathcal{K}_{\mathrm{P}}|$. It is important to note that using ST, all the subcarriers transmit at the same time equipowered data and pilot symbols at N_{P} ($N_{\mathrm{P}}=N-2$) positions. In the case of a SISO scenario, the received signal can be denoted as

$$y(k)=R_{\mathrm{pd}}H(k)x(k)+w(k), \tag{5.2.2}$$

where R_{pd} denotes the responsivity of the PD, $H(k)$ corresponds to the k-th subcarrier channel gain from the transmitter to the receiver, $x(k)$ is the transmitted symbol and $w(k)$ is the AWGN at the k-th subcarrier.

In a MISO configuration, taking into account N_{t} LEDs for transmission, the signal at the receiver can be seen as

$$y(k)=R_{\mathrm{pd}}\sum_{i=1}^{N_{\mathrm{t}}}H_i(k)x_i(k)+w(k), \tag{5.2.3}$$

where $H_{\mathrm{i}}(k)$ corresponds to the VLC channel gain from the i-th LED to the receiver

PD, and, $x_i(k)$ represents the transmitted symbol at the i-th LED, in the k-th subcarrier. The signal at the receiver can be denoted as

$$\mathbf{y} = R_{\mathrm{pd}} \sum_{i=1}^{N_{\mathrm{t}}} \mathbf{D}_i \mathbf{h}_{\mathrm{i}}^{\mathrm{f}} + \mathbf{w}, \tag{5.2.4}$$

where $\mathbf{y}$ is the $(N-2)\times 1$ vector that represents the received signal , $\mathbf{w}$ is the $(N-2)\times 1$ AWGN vector, and $\mathbf{h}_{\mathrm{i}}^{\mathrm{f}}$ is the $(N-2)\times 1$ vector that describe the i-th VLC channel gain from the i-th LED to the PD in frequency-domain. In addition, $\mathbf{D}_i$=diag $(\mathbf{x}_{\mathrm{C}_i})$ is a diagonal matrix of size $(N-2)\times(N-2)$ whose elements are $\mathbf{x}_{\mathrm{C}_i}$, and these consist of the useful transmitted symbols by the i-th LED. In this case, the channel $\mathbf{h}_i^{\mathrm{f}}$, in frequency-domain, can be denoted by the product of $\mathbf{F}\mathbf{h}_i$, being $\mathbf{F}$ the $(N-2)\times L$ DFT matrix. Its values are described by $[\mathbf{F}]_{k,l}=\mathbf{e}^{\frac{-j2\pi kl}{N}}$ where k and l denote the row and column indices, respectively. The L-tapped channel impulse response (CIR), at the i-th LED, can be described by $\mathbf{h}_i$. Knowing that the transmitted symbols by the i-th LED are defined by $\mathbf{x}_i=\mathbf{d}_i+\mathbf{p}_i$, the signal at the receiver can be denoted as

$$\mathbf{y} = R_{\mathrm{pd}}\mathbf{D}_{\mathrm{DF}}\mathbf{h} + R_{\mathrm{pd}}\mathbf{D}_{\mathrm{PF}}\mathbf{h} + \mathbf{w}. \tag{5.2.5}$$

Here, $\mathbf{D}_{\mathrm{DF}} = [\mathbf{D}_{\mathrm{d}_1}\mathbf{F}, \mathbf{D}_{\mathrm{d}_2}\mathbf{F}, ..., \mathbf{D}_{\mathrm{d}_{N_{\mathrm{t}}}}\mathbf{F}]$ and $\mathbf{D}_{\mathrm{PF}} = [\mathbf{D}_{\mathrm{p}_1}\mathbf{F}, \mathbf{D}_{\mathrm{p}_2}\mathbf{F}, ..., \mathbf{D}_{\mathrm{p}_{N_{\mathrm{t}}}}\mathbf{F}]$, where $\mathbf{D}_{\mathrm{d_i}}$ and $\mathbf{D}_{\mathrm{p}_i}$ are described as $(N-2)\times(N-2)$ diagonal matrices of $\mathbf{d}_i$ and $\mathbf{p}_i$, respectively. Note that spatial diversity is considered, $\mathbf{d}_i = \mathbf{d}$. The channel vector in time-domain can be denoted as $\mathbf{h} = [\mathbf{h}_1^{\mathrm{T}}, \mathbf{h}_2^{\mathrm{T}}, ..., \mathbf{h}_{N_{\mathrm{t}}}^{\mathrm{T}}]^{\mathrm{T}}$. Now, $\mathbf{y}^{(\mathrm{P})}$ is defined as the $N_{\mathrm{P}} \times 1$ vector which contains the pilot positions of the received signal $\mathbf{y}$. Knowing that by the quasi-stationary condition assumed in this case, the channel does not change until K OFDM symbols have been transmitted. Then, it is possible to obtain the pilot information as

$$\widetilde{\mathbf{y}}^{(\mathrm{P})} = R_{\mathrm{pd}}\mathbf{D}_{\mathrm{PF}}^{(\mathrm{P})}\mathbf{h} + \frac{1}{K}R_{\mathrm{pd}} \sum_{\mathrm{m}=1}^{K} \{\mathbf{D}_{\mathrm{DF}}^{(\mathrm{P})}\}_{\mathrm{m}}\mathbf{h} + \frac{1}{K}\sum_{\mathrm{m}=1}^{K} \mathbf{w}_{\mathrm{m}}^{(\mathrm{P})} \tag{5.2.6}$$

where the K-averaged received signal at the pilot positions is represented by the $N_{\mathrm{P}}\times 1$ vector $\widetilde{\mathbf{y}}^{(\mathrm{P})}$. $\mathbf{D}_{\mathrm{PF}}^{(\mathrm{P})}$ and $\left\{\mathbf{D}_{\mathrm{DF}}^{(\mathrm{P})}\right\}_{\mathrm{m}}$ describe the data and pilot $N_{\mathrm{P}}\times LN_{\mathrm{t}}$ matrices,

respectively. $\mathbf{w}_{\mathrm{m}}^{(\mathrm{P})}$ is a $N_{\mathrm{P}} \times 1$ noise vector at the pilot positions and m-th OFDM symbol, being $m \in \{1, ..., K\}$.

5.3 Channel estimation

The construction of a ST-based channel estimator for a VLC scenario in a MISO system is provided in this section. By its simplicity and effectiveness, the LS channel estimator is formulated. Furthermore, no additional information is required avoiding high complexity in the construction of the estimator.

5.3.1 LS channel estimation

Considering the construction of the LS channel estimator in [94], it is possible to say that

$$\hat{\mathbf{h}} = \frac{1}{R_{\mathrm{pd}}} \left(\left\{ \mathbf{D}_{\mathrm{PF}}^{(\mathrm{P})} \right\}^{\mathrm{H}} \mathbf{D}_{\mathrm{PF}}^{(\mathrm{P})} \right)^{-1} \left\{ \mathbf{D}_{\mathrm{PF}}^{(\mathrm{P})} \right\}^{\mathrm{H}} \widetilde{\mathbf{y}}^{(\mathrm{P})}. \tag{5.3.7}$$

Then, combining (5.2.6) with (5.3.7), the time-domain channel estimator can be expressed as

$$\begin{aligned} \hat{\mathbf{h}} = & \mathbf{h} + \frac{1}{K} \left(\left\{ \mathbf{D}_{\mathrm{PF}}^{(\mathrm{P})} \right\}^{\mathrm{H}} \mathbf{D}_{\mathrm{PF}}^{(\mathrm{P})} \right)^{-1} \left\{ \mathbf{D}_{\mathrm{PF}}^{(\mathrm{P})} \right\}^{\mathrm{H}} \\ & \cdot \left(\sum_{\mathrm{m}=1}^{K} \left\{ \mathbf{D}_{\mathrm{DF}}^{(\mathrm{P})} \right\}_{\mathrm{m}} \mathbf{h} + \frac{1}{R_{\mathrm{pd}}} \sum_{\mathrm{m}=1}^{K} \mathbf{w}_{\mathrm{m}}^{(\mathrm{P})} \right) \\ = & \mathbf{h} + \underbrace{\frac{1}{K} \left(\left\{ \mathbf{D}_{\mathrm{PF}}^{(\mathrm{P})} \right\}^{\mathrm{H}} \mathbf{D}_{\mathrm{PF}}^{(\mathrm{P})} \right)^{-1} \left\{ \mathbf{D}_{\mathrm{PF}}^{(\mathrm{P})} \right\}^{\mathrm{H}} \left(\overline{\mathbf{D}}_{\mathrm{DF}}^{(\mathrm{P})} \mathbf{h} + \frac{1}{R_{\mathrm{pd}}} \overline{\mathbf{w}}^{(\mathrm{P})} \right)}_{\mathbf{\Phi}} \end{aligned} \tag{5.3.8}$$

where $\overline{\mathbf{D}}_{\mathrm{DF}}^{(\mathrm{P})} = \sum_{\mathrm{m}=1}^{K} \left\{ \mathbf{D}_{\mathrm{DF}}^{(\mathrm{P})} \right\}_{\mathrm{m}}$, $\overline{\mathbf{w}}^{(\mathrm{P})} = \sum_{\mathrm{m}=1}^{K} \mathbf{w}_{\mathrm{m}}^{(\mathrm{P})}$ and $\mathbf{\Phi}$ corresponds to the $N_{\mathrm{t}} L \times 1$ channel estimation error. The variance of the channel estimation error σ_{LS}^2 can be derived as in [95] as follows

$$\begin{aligned} \sigma_{\mathrm{LS}}^2 &= \mathrm{E}\left[\mathrm{tr}\left[\mathbf{\Phi} \mathbf{\Phi}^{\mathrm{H}} \right] \right] = \mathrm{E}\{ ||\hat{\mathbf{h}} - \mathbf{h}||^2 \} \\ &= \sigma_{\mathrm{deg}}^2 \mathrm{tr} \left[\left(\left\{ \mathbf{D}_{\mathrm{PF}}^{(\mathrm{P})} \right\}^{\mathrm{H}} \mathbf{D}_{\mathrm{PF}}^{(\mathrm{P})} \right)^{-1} \right]. \end{aligned} \tag{5.3.9}$$

Note that $\mathrm{tr}\left[\cdot\right]$ indicates the trace operation of a matrix, and σ^2_{deg} represents the variance of the signal degradation composed of the interference of data and the AWGN. Then, assuming that the pilot and data symbols are equipowered and equispaced, thus

$$\sigma^2_{\mathrm{LS}} = \sigma^2_{\mathrm{deg}} \cdot \frac{LN_{\mathrm{t}}}{(1-\alpha)\,\mathcal{P}}. \tag{5.3.10}$$

The power of the signal degradation can be expressed through its variance σ^2_{deg}, and can be denoted as

$$\sigma^2_{\mathrm{deg}}=\frac{1}{K^2}\mathrm{E}\left[\overline{\mathbf{D}}^{(\mathrm{P})}_{\mathrm{DF}}\mathbf{h}\left\{\overline{\mathbf{D}}^{(\mathrm{P})}_{\mathrm{DF}}\mathbf{h}\right\}^{\mathrm{H}}\right]+\frac{1}{R^2_{\mathrm{pd}}K^2}\mathrm{E}\left[\overline{\mathbf{w}}^{(\mathrm{P})}\left\{\overline{\mathbf{w}}^{(\mathrm{P})}\right\}^{\mathrm{H}}\right]. \tag{5.3.11}$$

In the case that PSAM is implemented, $\mathbf{D}^{(\mathrm{P})}_{\mathrm{DF}} = \mathbf{0}$, being $\mathbf{0}$ an $N_{\mathrm{P}} \times LN_{\mathrm{t}}$ matrix of zero values. By other way, in the case ST is used, pilot and data signals will be transmitted in the same subcarriers, producing data interference denoted as follows $\mathbf{D}^{(\mathrm{P})}_{\mathrm{DF}} \neq \mathbf{0}$. Here, if the stationarity, represented by K, is long enough, the values of $\overline{\mathbf{D}}^{(\mathrm{P})}_{\mathrm{DF}} = \sum_{\mathrm{m}=1}^{K}\left\{\mathbf{D}^{(\mathrm{P})}_{\mathrm{DF}}\right\}_{\mathrm{m}}$ and $\overline{\mathbf{w}}^{(\mathrm{P})} = \sum_{\mathrm{m}=1}^{K}\mathbf{w}^{(\mathrm{P})}_{\mathrm{m}}$ can be described as a zero-mean Gaussian variable, as in [63], with variance $K\mathcal{P}_{\mathrm{S}}/(N-2)$ and $K\sigma^2_{\mathrm{w}}$, respectively. From this, it is possible to deduce the variance of the signal degradation at PSAM and ST as follows

$$\sigma^2_{\mathrm{deg,PSAM}} = \frac{1}{R^2_{\mathrm{pd}}K}\sigma^2_{\mathrm{w}} \tag{5.3.12}$$

and

$$\sigma^2_{\mathrm{deg,ST}} = \frac{\mathcal{P}_{\mathrm{S}}}{(N-2)\,K}\sigma^2_{\mathrm{H}} + \frac{1}{R^2_{\mathrm{pd}}K}\sigma^2_{\mathrm{w}}, \tag{5.3.13}$$

respectively, where $\sigma^2_{\mathrm{H}}=\sum_{\mathrm{i}=1}^{N_{\mathrm{t}}}\sum_{l=0}^{L-1}h^2_{\mathrm{i}}(l)=\sum_{i=1}^{N_{\mathrm{t}}}\sigma^2_{\mathrm{H_i}}$ is the power of the channel.

5.3.2 Description of the pilot sequences and pilot tones

The pilot sequence is formed by $N-2$ pilot symbols or tones which can be designed to be optimal. In ST and PSAM, the minimum MSE is obtained with an interval of $N_{\mathrm{I}} = N/\left(N_{\mathrm{P}}/2\right)$ and an optimal sequence of pilots as defined in [88]. It can be generated as follows

$$\left[\mathbf{p}_{i\mathrm{half}}\right]_v = p_i(v) = e^{-j\frac{2\pi}{N_{\mathrm{P}}/2}\mu_i v}, v \in \left[1, N_{\mathrm{P}}/2\right], \tag{5.3.14}$$

being

$$\mathbf{p}_i = \left[\mathbf{p}_{i\mathrm{half}} \quad \left\{\mathbf{p}_{i\mathrm{half}}^{\mathrm{T}}\right\}^{\mathrm{H}}\right]^{\mathrm{T}}, \tag{5.3.15}$$

where $\mu_i \in \{0, 1, ..., N_{\mathrm{P}}/2 - 1\}$ consists in an integer value associated with the i-th diode. Furthermore, the condition $\frac{\mu_{\mathrm{i}} - \mu_{\mathrm{j}} + q - l}{N_{\mathrm{P}}/2} \notin \mathbb{Z}$ has to be satisfied $\forall\, q, l \in \{1, ..., L\}$ and $i \neq j$, in order to ensure orthogonality between the conveyed pilot sequences from different LEDs, i. e. $\mu_i = (i-1)L + 1$.

It is important to mention that perfect synchronization has been assumed. Also, it is considered that, for channel estimation, orthogonal sequences transmitted and the cochannel interference can be assumed as null. The interference and noise signal generated can be reduced by averaging over K multicarrier symbols in a quasi-stationarity scenario.

5.4 Analysis of the spectral efficiency

Taking into account the transmission electrical power $\mathrm{E}\left[\mathbf{x}^{\mathrm{H}}\mathbf{x}\right] = \mathcal{P}$ and $\mathbf{w}$, the signal-to-noise ratio (SNR) is defined as

$$\overline{\gamma} = \frac{R_{\mathrm{pd}}^2 \mathcal{P} \sum_{\mathrm{i}=1}^{N_{\mathrm{t}}} \sigma_{\mathrm{H_i}}^2}{(N-2) \cdot \sigma_{\mathrm{w}}^2}. \tag{5.4.16}$$

In PSAM and ST techniques, the signal at the receiver can be denoted as $\mathbf{y}_{\mathrm{PSAM}}^{(\mathrm{D})}$

and $\mathbf{y}_{\mathrm{ST}}^{(\mathrm{D})}$, whose sizes are $(N{-}2{-}N_{\mathrm{P}}) \times 1$ and $(N{-}2) \times 1$, respectively, considering the index set of data symbols. For PSAM, the symbols of data can be obtained as

$$\begin{aligned}\mathbf{y}_{\mathrm{PSAM}}^{(\mathrm{D})}&{=}R_{\mathrm{pd}} \cdot \mathbf{D}_{\mathrm{DF}}^{(\mathrm{D})}\mathbf{h}{+}\mathbf{w}^{(\mathrm{D})}\\ &{=}R_{\mathrm{pd}} \cdot \mathbf{D}_{\mathrm{DF}}^{(\mathrm{D})}\left(\hat{\mathbf{h}} - \mathbf{\Phi}\right) + \mathbf{w}^{(\mathrm{D})},\end{aligned} \tag{5.4.17}$$

being $\mathbf{D}_{\mathrm{DF}}^{(\mathrm{D})}$ and $\mathbf{w}^{(\mathrm{D})}$ the $(N{-}N_{\mathrm{P}}{-}2) \times LN_{\mathrm{t}}$ matrix and $(N{-}N_{\mathrm{P}}{-}2) \times 1$ vector at data positions, respectively. By other side, in ST, the pilots can be eliminated through a subtraction as follows

$$\begin{aligned}\mathbf{y}_{\mathrm{ST}}^{(\mathrm{D})}&{=}R_{\mathrm{pd}} \cdot (\mathbf{D}_{\mathrm{DF}}{+}\mathbf{D}_{\mathrm{PF}})\,\mathbf{h}{-}R_{\mathrm{pd}}\mathbf{D}_{\mathrm{PF}}\hat{\mathbf{h}}{+}\mathbf{w}\\ &{=}R_{\mathrm{pd}} \cdot \mathbf{D}_{\mathrm{DF}}\hat{\mathbf{h}}{-}R_{\mathrm{pd}}\,(\mathbf{D}_{\mathrm{DF}}{+}\mathbf{D}_{\mathrm{PF}})\,\mathbf{\Phi}{+}\mathbf{w}.\end{aligned} \tag{5.4.18}$$

In ST, at the receiver, the data signal is affected by the pilot tones considering that pilot and data signals share the same resources. Thus, the signal-to-interference and noise ratio in each channel estimation technique can be expressed as

$$\overline{\gamma}_{\mathrm{PSAM}}{=}\frac{R_{\mathrm{pd}}^2 \frac{\mathcal{P}_{\mathrm{S}}}{N{-}N_{\mathrm{P}}{-}2} \cdot \sum\limits_{\mathrm{i}=1}^{N_{\mathrm{t}}} \sigma_{\mathrm{H_i}}^2}{R_{\mathrm{pd}}^2 \cdot \sigma_{\mathrm{LS}}^2 \cdot \left(\frac{\mathcal{P}_{\mathrm{S}}}{N{-}N_{\mathrm{P}}{-}2}\right) + \sigma_{\mathrm{w}}^2}, \tag{5.4.19}$$

and

$$\overline{\gamma}_{\mathrm{ST}} = \frac{R_{\mathrm{pd}}^2 \frac{\mathcal{P}_{\mathrm{S}}}{N{-}2} \cdot \sum\limits_{\mathrm{i}=1}^{N_{\mathrm{t}}} \sigma_{\mathrm{H_i}}^2}{R_{\mathrm{pd}}^2 \cdot \sigma_{\mathrm{LS}}^2 \cdot \left(\frac{\mathcal{P}_{\mathrm{S}}}{N{-}2} + \frac{\mathcal{P}_{\mathrm{P}}}{N{-}2}\right) + \sigma_{\mathrm{w}}^2}. \tag{5.4.20}$$

Joining the expressions of data and pilot power, the variance of the channel estimation error (5.3.10), the variance of the degradation signal (5.3.12) and (5.3.13) in PSAM (5.4.19) and ST (5.4.20), the corresponding SINR can be denoted as

$$\overline{\gamma}_{\mathrm{PSAM}}{=}\frac{(N{-}2) \cdot (1{-}\alpha) \cdot K}{\frac{1}{\overline{\gamma}}\left(L \cdot N_{\mathrm{t}} + K \cdot (N-2) \cdot (1-\alpha)\right)}, \tag{5.4.21}$$

and

$$\overline{\gamma}_{\mathrm{ST}} = \frac{\alpha \cdot (N-2) \cdot (1-\alpha) \cdot K}{L \cdot N_{\mathrm{t}} \cdot \left(\alpha + \frac{1}{\overline{\gamma}}\right) + (1-\alpha) \cdot K \cdot (N-2)\frac{1}{\overline{\gamma}}}. \tag{5.4.22}$$

A Gaussian random variable g with zero mean and unitary variance is introduced into the spectral efficiency expression obtained from Shannon proposal [66]. Then, assuming an idealistic case, the spectral efficiency can be expressed as

$$C_{\mathrm{Ideal}} = \frac{1}{N} \sum_{k=1}^{N/2-1} \mathrm{E}\left\{\log_2\left[1 + \overline{\gamma} \cdot |g|^2\right]\right\}, \tag{5.4.23}$$

where the CSI is assumed to be known, and, all the DCO-OFDM usable subcarriers are available to convey information considering $\mathcal{P}$ power. For PSAM and ST techniques, the spectral efficiency lower bound can be represented as

$$C_{\mathrm{PSAM}} = \frac{1}{N} \sum_{k \in \mathcal{K}_{\mathrm{D}} \cap \{1,\ldots,N/2-1\}} \mathrm{E}\left\{\log_2\left[1 + \overline{\gamma}_{\mathrm{PSAM}} \cdot |g|^2\right]\right\}, \tag{5.4.24}$$

and

$$C_{\mathrm{ST}} = \frac{1}{N} \sum_{k=1}^{N/2-1} \mathrm{E}\left\{\log_2\left[1 + \overline{\gamma}_{\mathrm{ST}} \cdot |g|^2\right]\right\}. \tag{5.4.25}$$

These expressions will be used for comparison purposes with the ideal case of (C_{Ideal}).

In PSAM, the CSI can be perfectly obtained with absence of noise if equipowered and equispaced pilots are used and if the condition $N_{\mathrm{P}} \geq N_{\mathrm{t}}L$ is accomplished [96]. Given that, in PSAM, N_{P} can be calculated as $N_{\mathrm{P}} = \lceil (1-\alpha)(N-2) \rceil$ ($\lceil \cdot \rceil$ means round to the next integer), for N_{t} number of antennas, L taps and N subcarriers, the maximum parameter α can be computed as

$$\alpha_{\mathrm{maxPSAM}} = 1 - \frac{N_{\mathrm{t}}L}{N-2}. \tag{5.4.26}$$

Table 5.1: Optical parameters

Parameter	Value	Unit
Room size	5x5x4	m
PD height	1	m
Detector area	1	cm^2
Semiangle at half optical power	60	deg.
Optical filter gain	1	-
Field of view at receiver	85	deg.
Refractive index of optical concentrator	1.5	-
PD responsivity, R_{pd}	0.54	A/W
Individual reflectivities	0.8	-

Then, an optimal α, for PSAM, can be computed as follows

$$\begin{aligned}\alpha_{\mathrm{opt}_{\mathrm{PSAM}}} &= \underset{\alpha\in(0,\alpha_{\mathrm{maxPSAM}}]}{\arg\max}\ C_{\mathrm{PSAM}}(\alpha)\\ &= \max\big(0,\min(\alpha'_{\mathrm{PSAM}},\alpha_{\mathrm{maxPSAM}})\big),\end{aligned} \tag{5.4.27}$$

being α'_{PSAM} obtained through $\frac{\partial C_{\mathrm{PSAM}}}{\partial\alpha}=0$, yielding

$$\begin{aligned}\alpha'_{\mathrm{PSAM}} &= \alpha\ :\ \log_2\left[1+\overline{\gamma}_{\mathrm{PSAM}}(\alpha)\right]\\ &= \frac{K(N-2)LN_{\mathrm{t}}}{\ln(2)\cdot\left(\frac{1}{\overline{\gamma}}\left(LN_{\mathrm{t}}+\mathrm{A}(\alpha)\right)+\mathrm{A}(\alpha)\right)\cdot\left(LN_{\mathrm{t}}+\mathrm{A}(\alpha)\right)}\end{aligned} \tag{5.4.28}$$

where $\mathrm{A}(\alpha)=K(N-2)(1-\alpha)$.

In ST, all usable subcarriers ($N_{\mathrm{P}}=N-2$) convey pilot tones, where the parameter α controls its power varying its value within the $0<\alpha<1$ range. The α value can be derived analytically as follows

$$\alpha_{\mathrm{opt}_{\mathrm{ST}}} = \underset{\alpha\in(0,1)}{\arg\max}\ C_{\mathrm{ST}}(\alpha) = \max\big(0,\min(\alpha'_{\mathrm{ST}},1)\big), \tag{5.4.29}$$

being α'_{ST} derived from $\frac{\partial C_{\mathrm{ST}}}{\partial\alpha}=0$, yielding

$$\alpha'_{\mathrm{ST}} = \frac{K(N-2)+LN_{\mathrm{t}}-\sqrt{LN_{\mathrm{t}}\left(\overline{\gamma}+1\right)\left(LN_{\mathrm{t}}+K(N-2)\right)}}{K(N-2)-LN_{\mathrm{t}}\overline{\gamma}}. \tag{5.4.30}$$

It is important to note that at higher SNR $\overline{\gamma}$ the lower α'_{ST} is obtained. This implies that to obtain the maximum spectral efficiency in a low noise scenario, the power assigned to data should be reduced since the data interference in ST techniques becomes more significant in comparison with the noise. Then, the data interference creates a noise floor that can be reduced decreasing the power assigned to data power. Note that it is possible to say that $\lim_{K\to\infty} \alpha'_{\mathrm{ST}} = 1$. This is due to the fact that when the stationarity tends to ∞, K tends to ∞, thus, the channel estimation error tends to 0. In this case, the maximum spectral efficiency can be achieved assigning all the power to the data symbols.

Finally, the channel variations can influence the spectral efficiency. Any change in the channel stationarity, the channel dispersion or SNR (which depends on the channel power) (5.4.16), influences the computation of K, L or $\overline{\gamma}$, respectively.

5.5 Simulation results

The DCO-OFDM multicarrier technique is used with $N = 256$ subcarriers and a sampling rate of 500 MHz in this section. In this scenario, the channel samples are generated by a ray-tracing algorithm [96] in a room and LED locations described in Table 5.1 and Fig. 5-1. The max-tap-delay is assumed to be equal to 30 ns which corresponds to L=16 taps. The corresponding cyclic prefix (CP) is configured to 16.

In Fig. 5-2, it is possible to see the time continuous CIR to be discretized for three different user positions, U1, U2 and U3, established in Fig. 5-1. Note that as the user becomes closer to the building walls the reflections become stronger. Having the CIR discretized, the sampling period takes the first tap as a reference point.

Fig. 5-3 shows the MSE of the channel estimation in this VLC scenario an $\alpha = 0.8$ and SNR $\overline{\gamma} = 10\,\mathrm{dB}$. The analytical expressions obtained in (5.3.10) fits the perfor-

Table 5.2: CPU time (s) in MSE computation

K	0	20	40	60	80	100
Random pilots	0.1299	0.1877	0.2515	0.3136	0.3752	0.4394
Optimal pilots	0.1294	0.1858	0.2483	0.3096	0.3691	0.4317

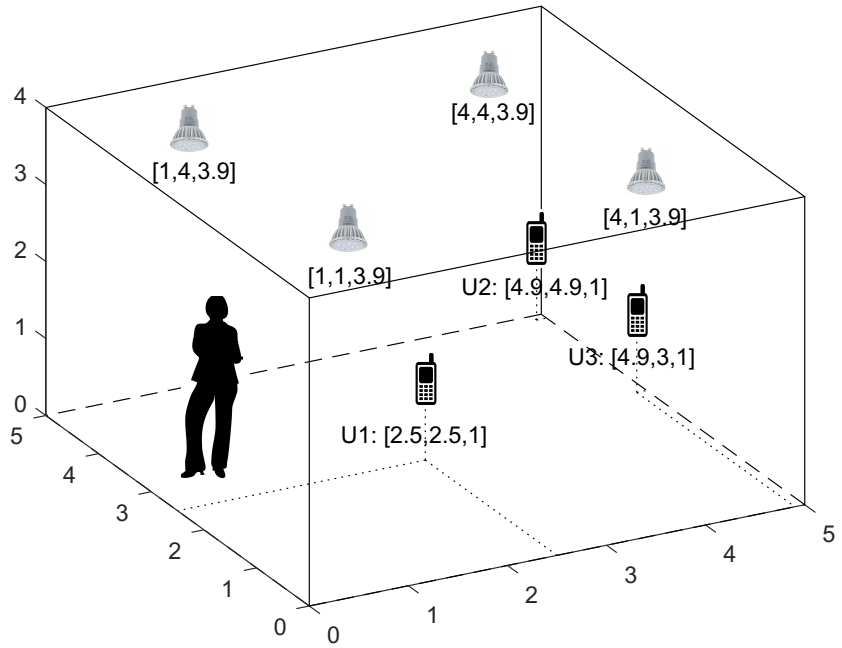

Figure 5-1: VLC scenario. (Coordinates in meters.)

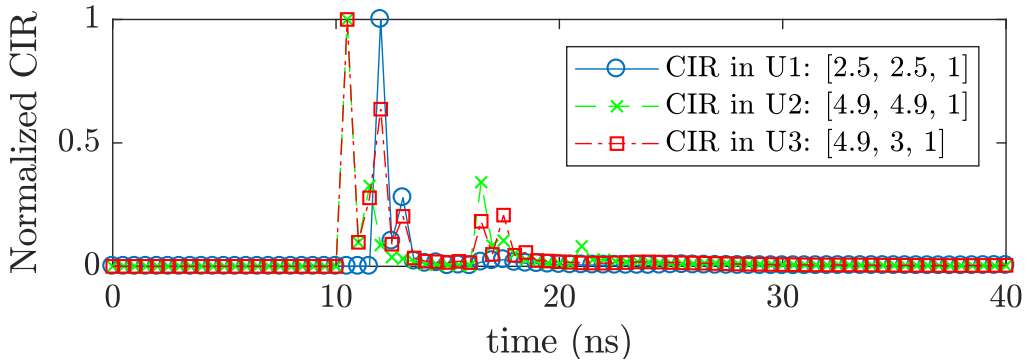

Figure 5-2: CIR for three different user locations.

mance of simulations, thus, this validates the study presented here. It is important to note that the MSE is reduced when the averaging increases and optimal pilots are used.

The CPU time as a function of the number of OFDM symbols used for averaging (K) the channel estimation is showed in Table 5.2, using both random and optimal pilots. For the time calculation an Intel Core i5 4440 3.10GHz processor, Microsoft Windows 7 and Matlab 2017(a) were used.

The spectral efficiency as a function of α is plotted in Fig. 5-4. For a fixed SNR the optimal data power allocation is pointed out, and it was analytically derived for

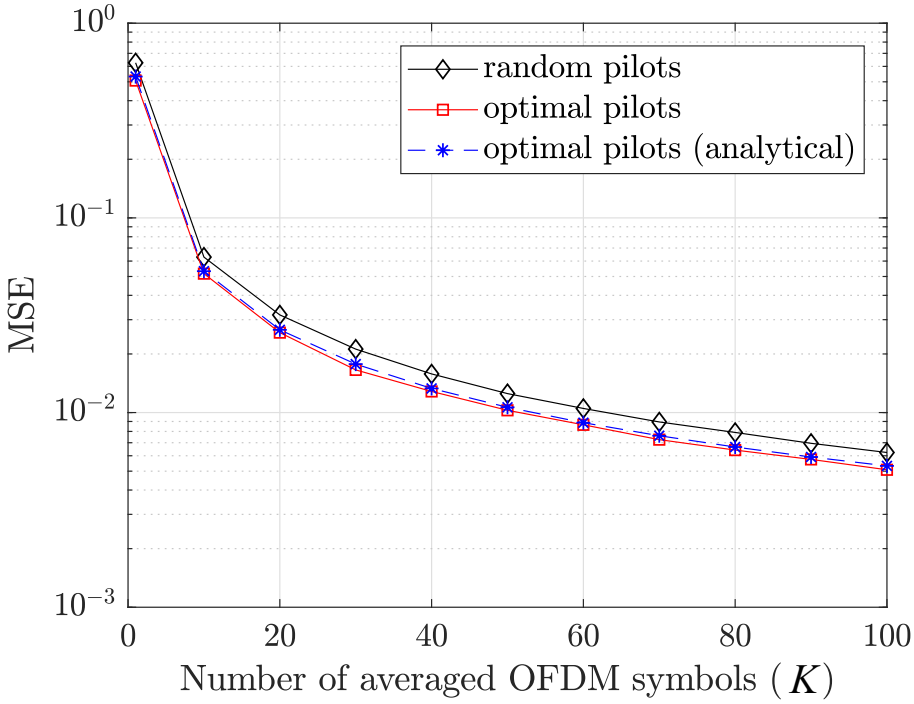

Figure 5-3: MSE using ST as a function of the number of averaged OFDM symbols, SNR $\overline{\gamma} = 10\,\text{dB}$ and $\alpha = 0.8$.

PSAM and ST in (5.4.27) and (5.4.29), respectively.

Note that when α tends to 0 or 1, the spectral efficiency C_{ST} could decrease since too much power is spent in pilot or data symbols, respectively. In the case of ST techniques, the range of α is [0, 1] and allows the system to reach higher values of spectral efficiency than PSAM as can be seen in Fig. 5-4. Note the higher spectral efficiency for ST instead of PSAM, for every SNR, as can be seen within the ellipses.

As it is expected, ST overcomes PSAM in a range of SNR from low to medium values. It is possible to say that the spectral efficiency reduces at high SNR, and, this is because when noise decreases the signal interference depends exclusively on the superimposed data. In the case of PSAM, there is no data interference, then, such interference is not present. Additionally, the Shannon spectral efficiency curves are presented for the ideal case, ST and PSAM schemes applying the optimal value of α.

In Fig. 5-6, the spectral efficiency is depicted as a function of the channel stationarity. The stationarity is defined by the number of OFDM symbols (K) that fits in a

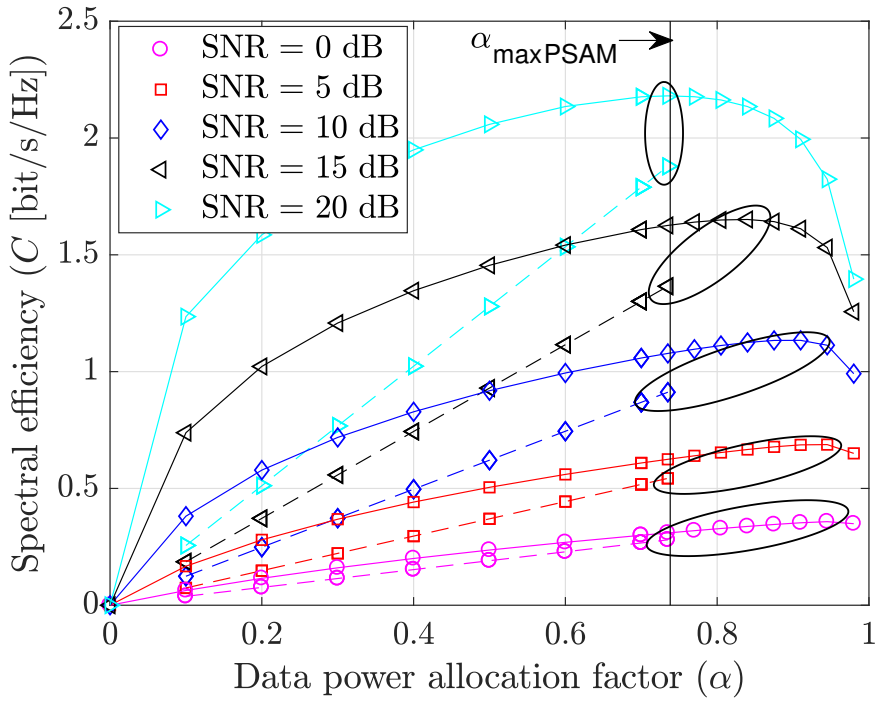

Figure 5-4: Spectral efficiency as a function of the data power allocation α for ST (solid line) and PSAM (dashed line), for $K = 200$ and several SNR $\overline{\gamma}$.

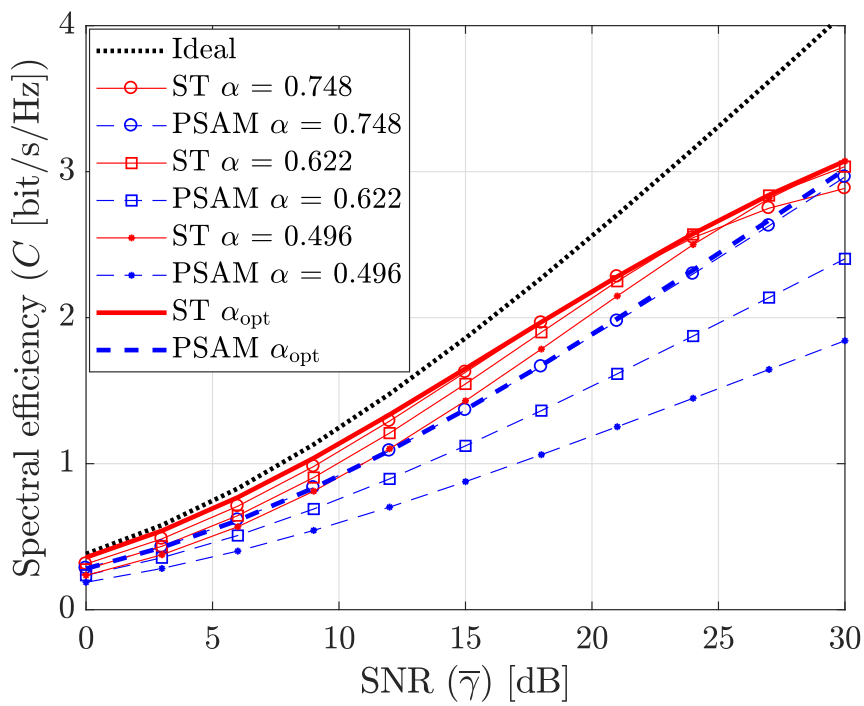

Figure 5-5: Spectral efficiency (ideal, ST and PSAM) as a function of SNR for a range of α values and a $K = 200$.

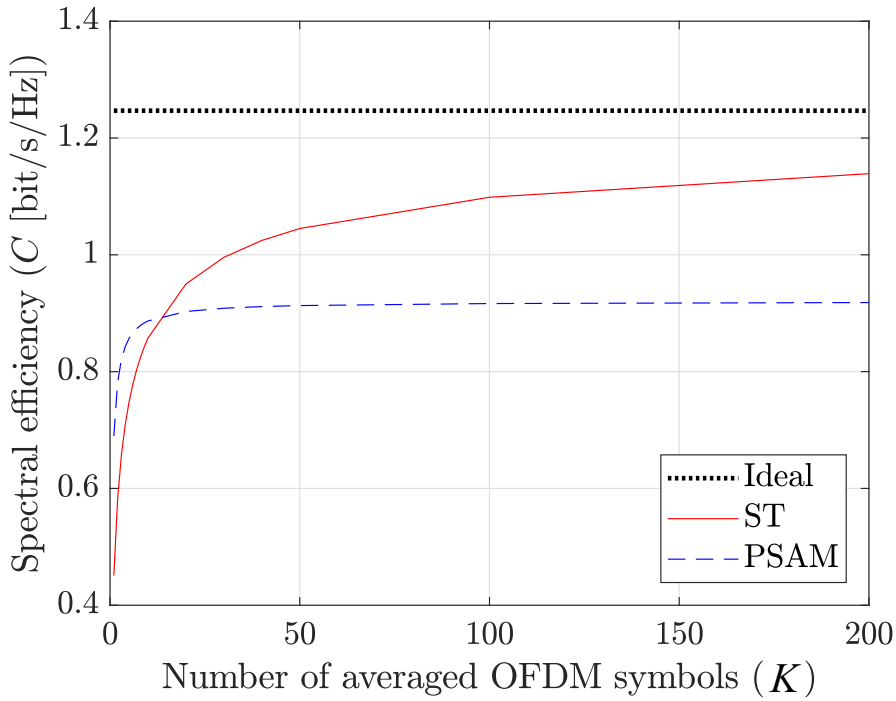

Figure 5-6: Spectral efficiency (ideal, ST and PSAM) as a function of K for a fixed α=α_{opt} and $\overline{\gamma}$=10 dB.

coherence time, and, the value of α that is considered is the optimal one.

In Fig. 5-7, the spectral efficiency is depicted as a function of the number of taps L for ST and PSAM using a fixed SNR $\overline{\gamma}$=10 dB and α=α_{opt}. It is possible to say that when L is increased the spectral efficiency decreases. The more the channel dispersion, the lower the spectral efficiency is. Nevertheless, the performance of ST decays more slowly than PSAM since ST is more robust than PSAM to dispersive channels.

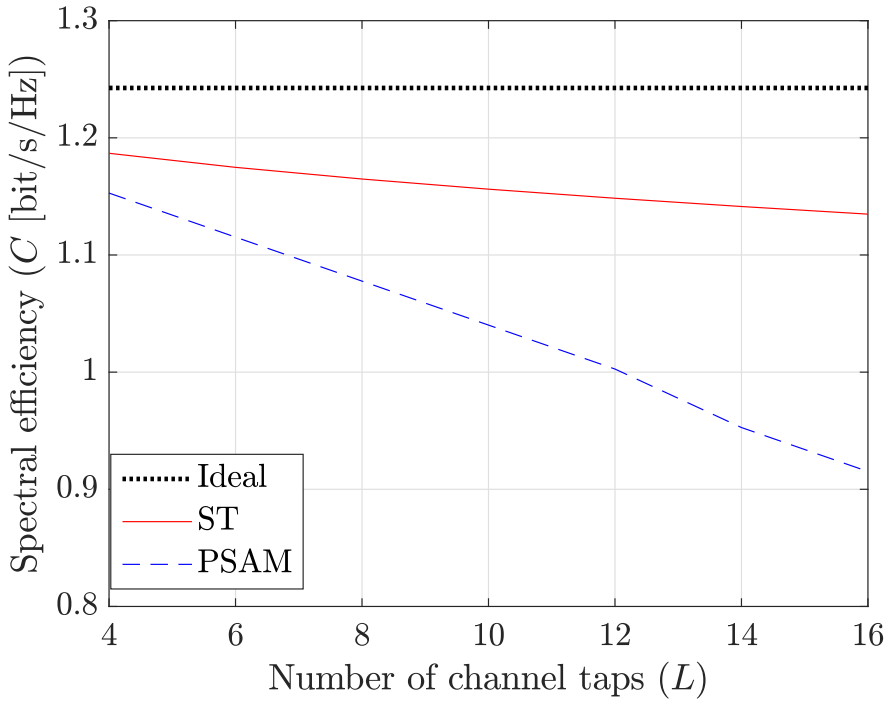

Figure 5-7: Spectral efficiency (ideal, ST and PSAM) as a function of the number of channel taps L for a fixed SNR $\overline{\gamma}$=10 dB, K=200 and α=α_{opt}.

Chapter 6

Conclusions and future lines of research

6.1 Conclusions

In this thesis, we have described several novel ST-based channel estimation techniques for 5G and beyond technologies.

A new ST approach denoted as partial data superimposed training (PDST) has been analyzed where an interference control factor is introduced to face the degradation produced by the data overlaid. Some analytical expressions from the channel estimation error and the average channel capacity were analyzed. The analysis of PDST was validated though simulations.

Another interesting approach for channel estimation in FBMC-OQAM was presented. The channel estimation using ST over a promising multicarrier waveform known as FBMC-OQAM was introduced. The analytical expression of the channel estimation error and the average channel capacity are deduced and validated through simulations.

Finally, the use of ST over visible light communications (VLC) was analyzed. ST-based channel estimation using visible light parameters was tested over DCO-OFDM. The channel estimation error and spectral efficiency is analytically derived. The analysis is validated using simulation results.

In all cases, ST schemes overcome PSAM techniques in low and medium SNRs, being PSAM the best option in high SNRs scenarios. For this reason, hybrid schemes, considering at the same time ST and PSAM, may be considered for analysis when the SNR continuously change.

It is possible to say that from the formulation provided in ST cases, the channel estimation error is composed by the noise, the data interference and additional interferences depending on the tested scenario e.g. intrinsic interference if apply.

6.2 Future lines

Millimeter wave is a promising technology that have recently attracted attention from the scientific community because of the great bandwidth that is offered by the frequencies that involve this technology. The influence of superimposed training over millimeter waves could be measured and modeled and its results reported to know if the advantages maintain in this scenario.

Also, hybrid channel estimation is a promising technique that have been studied using massive MIMO, as it can be seen in [3]. This mechanism uses part of the resources to estimate the channel dynamically using PSAM and ST techniques, simultaneously. Thus, the changes of the channel estimation mechanism are controlled using optimization. This study can be extended to different scenarios using new multicarrier techniques e. g. FBMC-OQAM or even in 5G and beyond scenarios e.g. millimeter waves. Also, visible light communication (VLC) consists in a promising technique where the channel estimation is currently analyzed. Hybrid channel estimation could be an interesting technique to be considered in VLC.

The power allocation strategies, which consist in different ways to efficiently distribute the pilot and data power in communication systems, have attracted much interest. Using adequate cost functions and mathematical tools, it is possible to find the best power ratio that accomplish energy-efficient transmission assuming limited power.

Nowadays, energy harvesting is a hot topic that has gained much interest. Several

proposals have been presented with the objective of effectively use the energy, as it can be seen in [97]. These ideas can be easily applied to superimposed training in several new scenarios.

Bibliography

[1] T. S. Rappaport. *Wireless Communications: Principles and Practice.* Second Edition, Prentice Hall, 2002.

[2] X. Li, A. Gani, R. Salleh, and O. Zakaria. The future of mobile wireless communication networks. In *2009 International Conference on Communication Software and Networks*, pages 554–557, Feb 2009.

[3] K. Upadhya, S. A. Vorobyov, and M. Vehkapera. Superimposed pilots are superior for mitigating pilot contamination in massive MIMO. *IEEE Trans. Signal Process.*, 65(11):2917–2932, June 2017.

[4] J. Ma, C. Liang, C. Xu, and L. Ping. On orthogonal and superimposed pilot schemes in massive MIMO NOMA systems. *IEEE J. Sel. Areas Commun.*, 35(12):2696–2707, Dec 2017.

[5] T. S. Rappaport, S. Sun, R. Mayzus, H. Zhao, Y. Azar, K. Wang, G. N. Wong, J. K. Schulz, M. Samimi, and F. Gutierrez. Millimeter wave mobile communications for 5g cellular: It will work! *IEEE Access*, 1:335–349, 2013.

[6] S. Geng, J. Kivinen, X. Zhao, and P. Vainikainen. Millimeter-wave propagation channel characterization for short-range wireless communications. *IEEE Transactions on Vehicular Technology*, 58(1):3–13, Jan 2009.

[7] M. Shafi, A. F. Molisch, P. J. Smith, T. Haustein, P. Zhu, P. De Silva, F. Tufvesson, A. Benjebbour, and G. Wunder. 5g: A tutorial overview of standards, trials, challenges, deployment, and practice. *IEEE Journal on Selected Areas in Communications*, 35(6):1201–1221, June 2017.

[8] P. Guan, D. Wu, T. Tian, J. Zhou, X. Zhang, L. Gu, A. Benjebbour, M. Iwabuchi, and Y. Kishiyama. 5g field trials: Ofdm-based waveforms and mixed numerologies. *IEEE Journal on Selected Areas in Communications*, 35(6):1234–1243, June 2017.

[9] Y. Medjahdi, S. Traverso, R. Gerzaguet, H. Shaïek, R. Zayani, D. Demmer, R. Zakaria, J. Doré, M. Ben Mabrouk, D. Le Ruyet, Y. Louët, and D. Roviras. On the road to 5g: Comparative study of physical layer in mtc context. *IEEE Access*, 5:26556–26581, 2017.

[10] H. Lin. Flexible configured ofdm for 5g air interface. *IEEE Access*, 3:1861–1870, 2015.

[11] P. H. Pathak, X. Feng, P. Hu, and P. Mohapatra. Visible light communication, networking, and sensing: A survey, potential and challenges. *IEEE Communications Surveys Tutorials*, 17(4):2047–2077, Fourthquarter 2015.

[12] S. Abdallah and I. N. Psaromiligkos. Semi-blind channel estimation with superimposed training for ofdm-based af two-way relaying. *IEEE Transactions on Wireless Communications*, 13(5):2468–2467, May 2014.

[13] Malihe Ahmadi and Aryan Saadat Mehr. Superimposed training aided carrier frequency offset estimation in ofdm systems. In *2007 IEEE International Conference on Electro/Information Technology*, pages 296–299, May 2007.

[14] E. Alameda-Hernandez, D. C. McLernon, A. G. Orozco-Lugo, M. M. Lara, and M. Ghogho. Frame/Training sequence synchronization and DC-offset removal for (data-dependent) superimposed training based channel estimation. *IEEE Trans. Signal Process.*, 55(6):2557–2569, June 2007.

[15] X. Xu, J. Wu, S. Ren, X. Luan, and H. Xiang. Superimposed training and channel estimation for two-way relay networks. In *16th International Conference on Advanced Communication Technology*, pages 1050–1054, Feb 2014.

[16] G. Wang, F. Gao, and C. Tellambura. Superimposed pilot based joint cfo and channel estimation for cp-ofdm modulated two-way relay networks. In *2010 IEEE Global Telecommunications Conference GLOBECOM 2010*, pages 1–5, Dec 2010.

[17] C. W. R. Chiong, Y. Rong, and Y. Xiang. Superimposed channel training algorithm for time-varying mimo relay systems. In *2015 24th Wireless and Optical Communication Conference (WOCC)*, pages 24–28, Oct 2015.

[18] X. Xie, M. Peng, F. Gao, and W. Wang. Superimposed training based channel estimation for uplink multiple access relay networks. *IEEE Transactions on Wireless Communications*, 14(8):4439–4453, Aug 2015.

[19] C. W. R. Chiong, Y. Rong, and Y. Xiang. Channel estimation for time-varying mimo relay systems. *IEEE Transactions on Wireless Communications*, 14(12):6752–6762, Dec 2015.

[20] C. Chiang and C. C. Fung. Robust training sequence design for spatially correlated mimo channel estimation. *IEEE Transactions on Vehicular Technology*, 60(7):2882–2894, Sep. 2011.

[21] F. Gao, B. Jiang, X. Gao, and X. Zhang. Superimposed training based channel estimation for ofdm modulated af relay networks. In *2011 IEEE International Conference on Communications (ICC)*, pages 1–5, June 2011.

[22] R. Luo, X. Wu, and Y. Dang. An improved slm scheme with superimposed training sequence for papr reduction in ofdm system. In *2011 7th International Conference on Wireless Communications, Networking and Mobile Computing*, pages 1–4, Sep. 2011.

[23] G. Tan, Z. Li, J. Su, and H. Zhang. Superimposed training for pts-papr reduction in ofdm: A side information free data recovery scheme. In *2013 8th International Conference on Communications and Networking in China (CHINACOM)*, pages 694–698, Aug 2013.

[24] T. Levanen, J. Talvitie, and M. Renfors. Performance evaluation of a ddst based simo sc system with papr reduction. In *2010 6th International Symposium on Turbo Codes Iterative Information Processing*, pages 186–190, Sep. 2010.

[25] J. C. Estrada-Jiménez and M. J. Fernández-Getino García. Partial-data superimposed training with data precoding for ofdm systems. *IEEE Transactions on Broadcasting*, 65(2):234–244, June 2019.

[26] J. C. Estrada-Jiménez, K. Chen-Hu, M. J. F. García, and A. García Armada. Power allocation and capacity analysis for fbmc-oqam with superimposed training. *IEEE Access*, 7:46968–46976, 2019.

[27] J. C. Estrada-Jimenez, B. Genoves Guzman, M. J. Fernandez-Getino Garcia, and V. P. Gil Jimenez. Superimposed training-based channel estimation for visible light communications. In *Proc. Int. Wireless Commun. Mobile Comput. Conf.*, pages 240–245, Valencia, Spain, June 2017.

[28] J. C. Estrada-Jiménez, B. G. Guzmán, M. J. Fernández-Getino García, and V. P. G. Jiménez. Superimposed training-based channel estimation for miso optical-ofdm vlc. *IEEE Transactions on Vehicular Technology*, 68(6):6161–6166, June 2019.

[29] Kun Chen-Hu, Juan Carlos Estrada-Jiménez, M. Julia Fernández-Getino García and Ana García Armada. Superimposed training channel estimation in FBMC-OQAM. *Proc. IEEE Int. Veh. Technol. Conf.*, 28(3):92–112, October 2017.

[30] J. C. Estrada-Jimenez, B. Genoves Guzman, M. J. Fernandez-Getino Garcia, and V. P. Gil Jimenez. Comparativa de técnicas de estimación de canal para VLC en interiores. In *Proc. of XXXII Simposio de la Unión Científica de Radio (URSI)*, Granada, Spain, September 2018.

[31] D. Gregoratti and X. Mestre. Uplink fbmc/oqam-based multiple access channel: Distortion analysis under strong frequency selectivity. *IEEE Transactions on Signal Processing*, 64(16):4260–4272, Aug 2016.

[32] E. Kofidis. Preamble-based estimation of highly frequency selective channels in fbmc/oqam systems. *IEEE Transactions on Signal Processing*, 65(7):1855–1868, April 2017.

[33] R. T. Kamurthi and S. R. chopra. Review of ufmc technique in 5g. In *2018 International Conference on Intelligent Circuits and Systems (ICICS)*, pages 115–120, April 2018.

[34] P. N. Rani and C. S. Rani. Ufmc: The 5g modulation technique. In *2016 IEEE International Conference on Computational Intelligence and Computing Research (ICCIC)*, pages 1–3, Dec 2016.

[35] N. Michailow, M. Matthé, I. S. Gaspar, A. N. Caldevilla, L. L. Mendes, A. Festag, and G. Fettweis. Generalized frequency division multiplexing for 5th generation cellular networks. *IEEE Transactions on Communications*, 62(9):3045–3061, Sep. 2014.

[36] Y. Medjahdi, S. Traverso, R. Gerzaguet, H. Shaïek, R. Zayani, D. Demmer, R. Zakaria, J. Doré, M. Ben Mabrouk, D. Le Ruyet, Y. Louët, and D. Roviras. On the road to 5g: Comparative study of physical layer in mtc context. *IEEE Access*, 5:26556–26581, 2017.

[37] R. Mesleh, H. Elgala, and H. Haas. On the performance of different ofdm based optical wireless communication systems. *IEEE/OSA Journal of Optical Communications and Networking*, 3(8):620–628, August 2011.

[38] H. Chen, S. Hu, J. Ding, S. Bian, H. Wu, P. Hua, S. You, X. Li, Q. Yang, and M. Luo. Performance comparison of visible light communication systems based on aco-ofdm, dco-ofdm and ado-ofdm. In *2017 16th International Conference on Optical Communications and Networks (ICOCN)*, pages 1–3, Aug 2017.

[39] J. Zhou, Y. Qiao, Z. Cai, and Y. Ji. Asymmetrically clipped optical fast ofdm based on discrete cosine transform for im/dd systems. *Journal of Lightwave Technology*, 33(9):1920–1927, May 2015.

[40] IEEE 802.11: Wireless lan medium access control (MAC) and physical layer (PHY) specifications, 2012.

[41] Base station (BS) radio transmission and reception, 2017.

[42] T. Hwang, C. Yang, G. Wu, S. Li, and G. Y. Li. OFDM and its wireless applications: A survey. *IEEE Trans. Veh. Technol.*, 58(4):1673–1694, May. 2009.

[43] J. Wang, H. Yu, Y. Wu, F. Shu, J. Wang, R. Chen, and J. Li. Pilot optimization and power allocation for OFDM-based full-duplex relay networks with IQ-imbalances. *IEEE Access*, 5:24344–24352, 2017.

[44] B. Farhang-Boroujeny and H. Moradi. Ofdm inspired waveforms for 5g. *IEEE Communications Surveys Tutorials*, 18(4):2474–2492, Fourthquarter 2016.

[45] Y. Cai, Z. Qin, F. Cui, G. Y. Li, and J. A. McCann. Modulation and multiple access for 5g networks. *IEEE Communications Surveys Tutorials*, 20(1):629–646, Firstquarter 2018.

[46] L. Zhang, P. Xiao, A. Zafar, A. ul Quddus, and R. Tafazolli. FBMC system: an insight into doubly dispersive channel impact. *IEEE Trans. Veh. Technol.*, 66(5):3942–3956, May. 2017.

[47] Q. Bodinier, F. Bader, and J. Palicot. On spectral coexistence of CP-OFDM and FB-MC waveforms in 5G networks. *IEEE Access*, 5:13883–13900, 2017.

[48] V. Savaux, F. Bader, and Y. Louet. A joint MMSE channel and noise variance estimation for OFDM/OQAM modulation. *IEEE Trans. Commun.*, 63(11):4254–4266, Nov 2015.

[49] B. Yu, S. Hu, P. Sun, S. Chai, C. Qian, and C. Sun. Channel estimation using dual-dependent pilots in FBMC/OQAM systems. *IEEE Commun. Lett.*, 20(11):2157–2160, Nov 2016.

[50] C. Lele, P. Siohan, R. Legouable, and J. P. Javaudin. Preamble-based channel estimation techniques for OFDM/OQAM over the powerline. In *Proc. IEEE Int. Symp. on Power Line Commun. and Its Appl.*, pages 59–64, Mar. 2007.

[51] Zhaocheng Wang, Qi Wang, Wei Huang, and Zhengyuan Xu. *Visible Light Communications: Modulation and Signal Processing.* Wiley-IEEE Press, 2018.

[52] S. D. Dissanayake and J. Armstrong. Comparison of aco-ofdm, dco-ofdm and ado-ofdm in im/dd systems. *Journal of Lightwave Technology*, 31(7):1063–1072, April 2013.

[53] G. Fettweis, M. Krondorf, and S. Bittner. Gfdm - generalized frequency division multiplexing. In *VTC Spring 2009 - IEEE 69th Vehicular Technology Conference*, pages 1–4, April 2009.

[54] Eleftherios Kofidis Markku Renfors, Xavier Mestre and Faouzi Bader. *Orthogonal Waveforms and Filter Banks for Future Communication Systems.* Academic Press, London, UK, 2017.

[55] I. B. F. de Almeida, L. L. Mendes, J. J. P. C. Rodrigues, and M. A. A. da Cruz. 5g waveforms for iot applications. *IEEE Communications Surveys Tutorials*, pages 1–1, 2019.

[56] X. He, F. Wang, X. Chen, D. Miao, and Z. Zhao. Non-orthogonal waveforms for machine type communication. In *2017 XXXIInd General Assembly and Scientific Symposium of the International Union of Radio Science (URSI GASS)*, pages 1–4, Aug 2017.

[57] M. Ghogho, D. McLernon, E. Alameda-Hernandez, and A. Swami. Channel estimation and symbol detection for block transmission using data-dependent superimposed training. *IEEE Signal Process. Lett.*, 12(3):226–229, March 2005.

[58] M. Ghogho, D. McLernon, E. Alameda-Hemandez, and A. Swami. SISO and MIMO channel estimation and symbol detection using data-dependent superimposed training. In *Proceedings. (ICASSP '05). IEEE International Conference on Acoustics, Speech, and Signal Processing*, volume 3, pages 461–464, March 2005.

[59] E. Gayosso-Rios, M. M. Lara, A. G. Orozco-Lugo, and D. McLernon. Symbol-Blanking Superimposed Training for Orthogonal Frequency Division Multiplexing systems. In *2010 7th International Symposium on Wireless Communication Systems*, pages 204–208, Sept 2010.

[60] G. Dou, C. He, C. Li, and J. Gao. Channel estimation and symbol detection for OFDM systems using data-nulling superimposed pilots. *Electronics Letters*, 50(3):179–180, January 2014.

[61] G. Dou, X. He, R. Deng, J. Gao, and Q. Wang. Individual channel estimation for amplify-and-forward relay networks using in-band superimposed training. *IET Communications*, 12(9):1141–1147, 2018.

[62] F. Zaarour, E. Simon, M. Zwingelstein-Colin, and I. Dayoub. A low complexity turbo receiver for data nulling superimposed pilots in OFDM. In *2015 Fifth International Conference on Digital Information and Communication Technology and its Applications*, pages 32–37, April 2015.

[63] W. C. Huang, C. P. Li, and H. J. Li. On the Power Allocation and System Capacity of OFDM Systems Using Superimposed Training Schemes. *IEEE Trans. Veh. Technol.*, 58(4):1731–1740, May 2009.

[64] S. M. Kay. *Fundamentals of statistical signal processing.* Englewood Cliffs, NJ: Prentice Hall, 1993.

[65] Shuichi Ohno and G. B. Giannakis. Capacity maximizing MMSE-optimal pilots for wireless OFDM over frequency-selective block Rayleigh-fading channels. *IEEE Trans. Inf. Theory*, 50(9):2138–2145, Sept 2004.

[66] M. Medard. The effect upon channel capacity in wireless communications of perfect and imperfect knowledge of the channel. *IEEE Trans. Inf. Theory*, 46(3):933–946, May 2000.

[67] Y.S.Cho and J. Kim. *MIMO-OFDM Wireless Communications with MATLAB.* Singapore, John Wiley & Sons (Asia) Pte Ltd, 2 Clementi Loop, #02-01, 1993.

[68] 3GPP TS. *Evolved Universal Terrestrial Radio Access (E-UTRA); Physical channels and modulation*, 1 2011. 36.211 version 10.0.0 Release 10.

[69] Tao Cui and C. Tellambura. Pilot symbols for channel estimation in OFDM systems. In *GLOBECOM '05. IEEE Global Telecommunications Conference*, volume 4, pages 2229–2233, Dec 2005.

[70] N. Bonello, S. Chen, and L. Hanzo. Pilot symbol assisted coding. *Electronics Letters*, 45(10):518–519, May 2009.

[71] D. Tse and P. Viswanath. *Fundamentals of Wireless Communications*. Cambridge Univ. Press, Cambridge, U.K., 2005.

[72] Ning Chen and G. T. Zhou. Superimposed training for OFDM: a peak-to-average power ratio analysis. *IEEE Trans. Signal Process.*, 54(6):2277–2287, June 2006.

[73] M. Fuhrwerk, S. Moghaddamnia, and J. Peissig. Scattered pilot-based channel estimation for channel adaptive FBMC-OQAM systems. *IEEE Trans. Wireless Commun.*, 16(3):1687–1702, March 2017.

[74] E. Kofidis and D. Katselis. Improved interference approximation method for preamble-based channel estimation in FBMC/OQAM. In *Eur. Signal Process. Conf*, pages 1603–1607, Aug 2011.

[75] C. Lele, R. Legouable, and P. Siohan. Channel estimation with scattered pilots in OFDM/OQAM. In *Proc. IEEE Workshop on Signal Process. Advances in Wireless Commun.*, pages 286–290, Jul. 2008.

[76] Z. Zhao, N. Vucic, and M. Schellmann. A simplified scattered pilot for FBMC/OQAM in highly frequency selective channels. In *Proc. IEEE Int. Symp. on Wireless Commun. Syst. (ISWCS)*, pages 819–823, Aug 2014.

[77] J. M. Choi, Y. Oh, H. Lee, and J. S. Seo. Interference-dependent pair of pilots for channel estimation in FBMC systems. In *Proc. IEEE Int. Symp. on Broadband Multimedia Syst. and Broadcasting (BMSB)*, pages 1–4, Jun. 2016.

[78] A. RezazadehReyhani and B. Farhang-Boroujeny. Capacity analysis of FBMC-OQAM systems. *IEEE Commun. Lett.*, 21(5):999–1002, May 2017.

[79] Kun Chen-Hu, Juan Carlos Estrada-Jiménez, M. J. Fernández-Getino García and Ana García Armada. Continuous and burst pilot sequences for channel estimation in FBMC-OQAM. *IEEE Trans. Veh. Technol.*, 67(10):9711–9720, Oct 2018.

[80] J. Wang, C. Jiang, H. Zhang, X. Zhang, V. C. M. Leung, and L. Hanzo. Learning-aided network association for hybrid indoor LiFi-WiFi systems. *IEEE Trans. Veh. Technol.*, 67(4):3561–3574, Apr. 2018.

[81] L. Zeng, D. C. O'Brien, H. L. Minh, G. E. Faulkner, K. Lee, D. Jung, Y. Oh, and E. T. Won. High data rate multiple input multiple output (MIMO) optical wireless communications using white LED lighting. *IEEE J. Sel. Areas Commun.*, 27(9):1654–1662, Dec. 2009.

[82] K. Ying, H. Qian, R. J. Baxley, and G. T. Zhou. Mimo transceiver design in dynamic-range-limited vlc systems. *IEEE Photonics Technology Letters*, 28(22):2593–2596, Nov 2016.

[83] K. Ying, H. Qian, R. J. Baxley, and S. Yao. Joint optimization of precoder and equalizer in mimo vlc systems. *IEEE Journal on Selected Areas in Communications*, 33(9):1949–1958, Sep. 2015.

[84] Z. G. Sun, H. Y. Yu, W. C. Li, Z. J. Tian, and Y. J. Zhu. Power-efficient linear precoding for MU-MISO VLC systems with channel uncertainty. *IEEE Photon. Technol. Lett.*, 30(7):626–629, Apr. 2018.

[85] Y. J. Zhu, Z. G. Sun, J. K. Zhang, Y. Y. Zhang, and J. Zhang. Training receivers for repetition-coded MISO outdoor visible light communications. *IEEE Trans. Veh. Technol.*, 66(1):529–540, Jan. 2017.

[86] R. Mesleh, R. Mehmood, H. Elgala, and H. Haas. Indoor MIMO optical wireless communication using spatial modulation. In *Proc. IEEE Int. Conf. Commun.*, pages 1–5, Cape Town, South Africa, May 2010.

[87] W. Wang, Y. Zhu, Y. Zhang, and J. Zhang. An optimal power allocation for multi-led phase-shifted-based miso vlc systems. *IEEE Photonics Technology Letters*, 27(22):2391–2394, Nov 2015.

[88] L. Wu, J. Cheng, Z. Zhang, J. Dang, and H. Liu. Channel estimation for optical-OFDM-based multiuser MISO visible light communication. *IEEE Photon. Technol. Lett.*, 29(20):1727–1730, Oct. 2017.

[89] Z. Sun, H. Yu, Z. Tian, and Y. Zhu. Linear precoding for mu-miso vlc systems with noisy channel state information. *IEEE Communications Letters*, 22(4):732–735, April 2018.

[90] X. Chen and M. Jiang. Adaptive statistical Bayesian MMSE channel estimation for visible light communication. *IEEE Trans. Signal Process.*, 65(5):1287–1299, Mar. 2017.

[91] S. Dimitrov, S. Sinanovic, and H. Haas. Clipping noise in OFDM-Based optical wireless communication systems. *IEEE Trans. Commun.*, 60(4):1072–1081, Apr. 2012.

[92] X. Ling, J. Wang, Z. Ding, C. Zhao, and X. Gao. Efficient OFDMA for LiFi downlink. *J. Lightw. Technol*, 36(10):1928–1943, May 2018.

[93] C. Chen, D. A. Basnayaka, and H. Haas. Downlink performance of optical attocell networks. *J. Lightw. Technol.*, 34(1):137–156, Jan. 2016.

[94] Steven M. Kay. *Fundamentals of Statistical Signal Processing: Estimation Theory.* 1993.

[95] I. Barhumi, G. Leus, and M. Moonen. Optimal training design for MIMO OFDM systems in mobile wireless channels. *IEEE Trans. Signal Process.*, 51(6):1615–1624, June 2003.

[96] J. R. Barry, J. M. Kahn, W. J. Krause, E. A. Lee, and D. G. Messerschmitt. Simulation of multipath impulse response for indoor wireless optical channels. *IEEE J. Sel. Areas Commun.*, 11(3):367–379, Apr. 1993.

[97] J. Li, H. Zhang, D. Li, and H. Chen. On the performance of wireless-energy-transfer-enabled massive mimo systems with superimposed pilot-aided channel estimation. *IEEE Access*, 3:2014–2027, 2015.